UNIVERSITÀ DEGLI STUDI DI PADOVA

UNIVERSITA' DEGLI STUDI DI PADOVA

Dipartimento di Ingegneria Industriale DII

Master Degree in Aerospace Engineering

AERODYNAMIC MODELING OF SUPERSONIC PARACHUTES FOR TRAJECTORY SIMULATION OF A PLANETARY PROBE

Thesis advisor: Prof. Francesco Picano
Thesis co-advisor: Dr. Alessio Aboudan
Thesis co-advisor: Dr. Luca Placco

Candidate: Simone Calgaro
1238966

Academic Year 2022/2023.

ABSTRACT

The purpose of this master thesis is to study, simulate and examine the descent phase of a spacecraft into an extraterrestrial atmosphere (Mars and/or other planets in the solar system).
The paper includes an initial introductory part in which the descent phase is described in a general way along with a brief discussion of each characterizing event. In describing it, special attention will be paid to the parachute opening event. After a presentation of the main types and respective characteristics of parachutes used on Mars, some examples of past missions from which to derive information for the simulative part of the thesis are briefly illustrated.The type of supersonic parachute for the simulations in this study is selected based on the analysis of past missions.
The first step concerning the simulation aspect involves a preliminary one-dimensional descent study where the descent phase with the capsule alone and the descent phase with the additional action of the supersonic parachute are simulated. Then a more detailed code is proposed with the objective of evaluating and studying over time characteristic parameters of the parachute along with atmospheric parameters related to the trajectory.
In this second part of the simulations, the concept of bidimensionality and the notion of verticalization are introduced through the study of the variation of the angle between the capsule-parachute system and the horizon. Perturbative phenomena such as atmospheric velocity, parameter variations during the inflation phase, and the area oscillation phenomenon of the parachute are also considered. All of these factors contribute to making the simulation as realistic as possible.
The final part of the thesis presents the results from the simulations following the assumptions and design choices made during the initial selection phase.In particular, the thesis analyzes the main aspects and parameters that influence the descent phase of the capsule decelerated by the supersonic parachute.
The study concludes with the presentation of possible and necessary future steps and implementations for the code used, in order to further improve the study of descent with a supersonic parachute in the Martian and non-Martian atmospheres.

RIASSUNTO

Lo scopo di questa tesi di laurea magistrale è studiare, simulare ed esaminare la fase di discesa di un veicolo spaziale in atmosfera extraterrestre (Marte e/o altri pianeti del sistema solare).
Il lavoro include una parte introduttiva in cui la fase di discesa viene descritta in modo generale, insieme a una breve discussione di ciascun evento caratterizzante. Nella descrizione, verrà prestata particolare attenzione all'evento di apertura del paracadute supersonico. Dopo una presentazione delle principali caratteristiche e tipologie dei paracadute supersonici per applicazioni di esplorazione spaziale, vengono brevemente illustrati alcuni esempi di missioni passate da cui trarre informazioni per la parte simulativa della tesi. In particolare, il tipo di paracadute supersonico utilizzato nele simulazioni svolte in questo studio viene selezionato in base all'analisi di missioni passate.
Il primo passo riguardante l'aspetto della simulazione prevede uno studio preliminare di discesa unidimensionale, in cui viene simulata la fase di discesa con la sola capsula e la fase con l'azione aggiuntiva del paracadute supersonico. Successivamente viene proposto un codice più dettagliato con l'obiettivo di valutare e studiare nel tempo i parametri caratteristici del paracadute insieme ai parametri atmosferici legati alla traiettoria.
In questa seconda parte simulativa, viene introdotto il concetto di bidimensionalità e la nozione di verticalizzazione attraverso lo studio della variazione dell'angolo tra il sistema capsula-paracadute e l'orizzonte. Vengono inoltre considerati fenomeni perturbativi come la velocità atmosferica, le variazioni dei parametri durante la fase di inflazione e il fenomeno dell'oscillazione dell'area del paracadute. Tutti questi fattori contribuiscono a rendere la simulazione il più realistica possibile.
La parte finale della tesi presenta i risultati delle simulazioni seguendo le ipotesi e le scelte di progettazione fatte durante la fase iniziale di selezione. In particolare, la tesi analizza gli aspetti principali e i parametri che influenzano la fase di discesa della capsula decelerata dal paracadute supersonico.
Lo studio si conclude con la presentazione di possibili e necessari passi futuri e implementazioni per il codice utilizzato, al fine di migliorare ulteriormente lo studio della discesa con un paracadute supersonico nelle atmosfere marziane e non.

Contents

List of Figures

List of Tables

1 INTRODUCTION

1.1 MARS ATMOSPHERIC RE-ENTRY

The pioneering phase of space exploration is encapsulated in twenty years of history, from 1957 to 1977, from the Sputnik satellites to the Voyager probes. It was an important period, which allowed the space agencies of the major countries involved (Soviet Union and the United States) to learn how to build reliable space systems and paved the way for the highly important subsequent phase, that of the systematic exploration of the Solar System coordinated internationally.
The first important target of the space exploration, after the missions around Earth, was the Moon. The exploration of the Moon lasted, with automatic probes, for more than a decade by the two superpowers.In particular the most famous space programm fro Moon exploration was the Apollo program developed by NASA which led to landing a man on the moon on July 21st, 1969.
During the 1960s, in addition to the development of Apollo, NASA began to design an exploration program for the two closest planets, Mars and Venus. It was initially an experimental activity in the fields of missile technology, celestial dynamics, and mission reliability: a phase that can be defined as 'heroic' and typically characterizes the first stage of a new era.
So, therefore since the beginning of the space exploration era, Mars has represented the main target of robotic exploration by world space agencies. At the basis of this scientific and strategic interest lies mainly the opportunity to provide answers to fundamental questions, including the origin and evolution of life. In particular, the Red Planet has focused on itself the main efforts of human interplanetary exploration for other important reasons listed below:

- rappresents the most similar planet to Earth in the solar system,
- among the planets in the solar system, Mars represents a key target of space exploration for the search of extraterrestrial life, as it is believed to have possibly hosted indigenous forms of life besides Earth,
- It will likely be the first extraterrestrial planet visited by humans.

The exploration of Mars began in the 1960s with the missions of the NASA Mariner program and those of the Soviet space agency, both with the goal of sending unmanned automatic probes, including orbiters, lander, and rovers, to collect data and answer questions about the red planet and its past. The answers could lead to discoveries about the past and future of Earth. After numerous failures, in 1965 NASA's Mariner 4 probe executed the first flyby of Mars and sent the first photos of the red planet. The same NASA program succeeded in 1971 with the Mariner 9 mission, which brought the first orbiter around Mars. In the following years, Soviet and US missions followed until the historic success of 1976 when NASA, with the twin Viking 1 and Viking 2 missions, managed to land two landers on the Martian surface whose objective was to take high-resolution photos of the planet, characterize the composition of the atmosphere and the surface of Mars, and search for signs of evidence of life. The great value of the Viking missions, in addition to the success of the mission, is that they still represent today a fundamental reference point for the design and planning of missions to Mars, especially regarding the atmospheric reentry phase.

Some of the principal martian exploration mission: Talking about Mars exploration missions, the re-entry

Table 1: Mars robotic exploration missions

Mission name	**Entry year**	**Agency/ Country**	**Parachute type and diameter [m]**	**Deployment Mach number**	**Landing ourcome**
Viking 1, 2	1976	NASA	DGB, 16.2	2.1	Succesful
MPF	1997	NASA	DGB, 12.7	1.71	Succesful
MPL	1999	NASA	DGB, 12.7	1.85	Failed
Beagle 2	2003	ESA	DGB, 3.2	1.5	Failed
MER	2004	NASA	DGB, 14.1	1.9	Succesful
Phoenix	2008	NASA	DGB, 11.7	1.74	Succesful
MSL	2010	NASA	DGB, 21.4	1.75	Succesful
Exomars	2016	ESA/Russia	DGB, 12.0	1.8	Failed
Insignt	2018	NASA	DGB, 11.8	1.49	Succesful

phase represents one of the most important and critical part for the success of the entire mission and all the sacrifices made over the years by the team leading it.

After a journey lasting between six and nine months, NASA's Mars exploration missions conclude with the famous "seven minutes of terror", which are the minutes between the spacecraft's entry into the Martian atmosphere and the rover's touchdown on the planet's surface. This phase is called the Entry, Descent, and Landing (EDL) phase.

1.2 ENTRY, DESCENT AND LANDING SEQUENCE

The entry, descent and landing phase of a Mars exploration mission is one of the most difficult engineering challenges in the design process. One of the most famous failures during this phase occurred with the European Space Agency's (ESA) ExoMars mission, in which the Schiaparelli lander crashed onto the Martian surface due to a measurement system error that caused the thrusters to malfunction during descent.
In general, this phase consists of a sequence of programmed events that occur when the spacecraft reaches certain values of variables such as spacecraft velocity, distance from Mars, altitude above the Martian surface, and so on. Over the years and with the experience gained from past missions, the EDL phase has undergone updates, while maintaining a basic structure. These differences mainly concern the last phase, that of landing on the Martian surface. Therefore, for both NASA and ESA, the main events of EDL are common. Taking NASA's 2020 "Perseverance" mission as a reference, the atmospheric entry phase involves the following steps:

1.2.1 FINAL PREPARATIONS

During this first phase the spacraft separates from propulsion stage that brought it to Mars using solar panel and propellant tank. Before entering the martian atmopsphere, the thrusters of the attitude control system adjust spacecraft orientation to ensure that the heat shield protects the rover during the entry phase (figura 1).

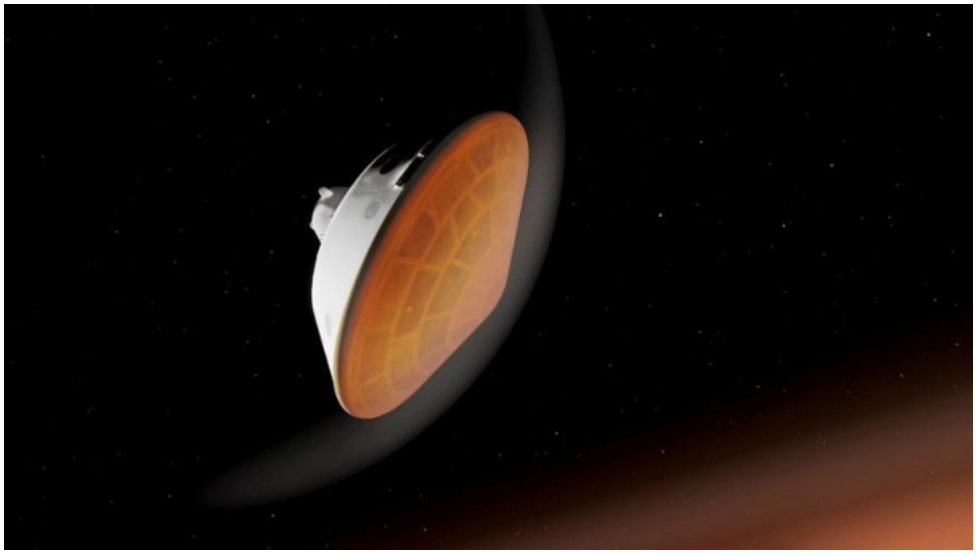

Figure 1: Capsule approach to martian atmosphere

1.2.2 MARTIAN ATMOSPHERIC ENTRY

This second part involves the spacecraft entering the atmosphere (figura 2). The resistance generated in this phase causes a drastic slowdown and a sudden increase in temperatures on the protective heat shield. This descent through the different density layers of the atmosphere can push the spacecraft off course. This possible drift is compensated for by using small thrusters placed on the back shell that regulate the angle and direction of lift, keeping the spacecraft on the designated trajectory.

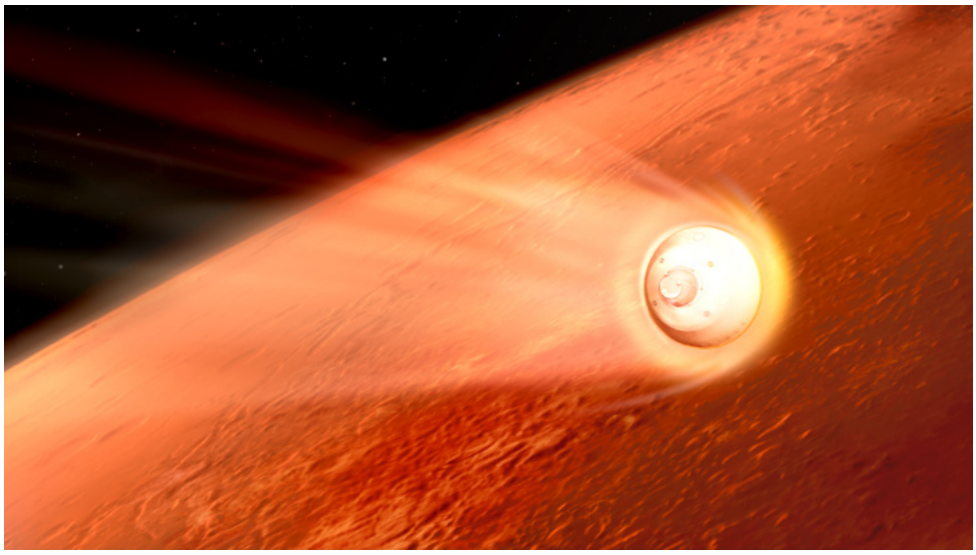

Figure 2: Re-entry of the Perseverance rover into the martian atmosphere (illustration)

1.2.3 PARACHUTE DEPLOYMENT

The action of the heat shield allows the spacecraft to slow down to a "safe" descent speed (M $\simeq$ 2), at which point the supersonic parachute is deployed (figura 3) to slow down the capsule to a subsonic speed. There are different types of supersonic parachutes for space applications, which can be used in single parachute configurations or in some cases in double parachute configurations. This topic will be discussed in more detail in the next paragraph.

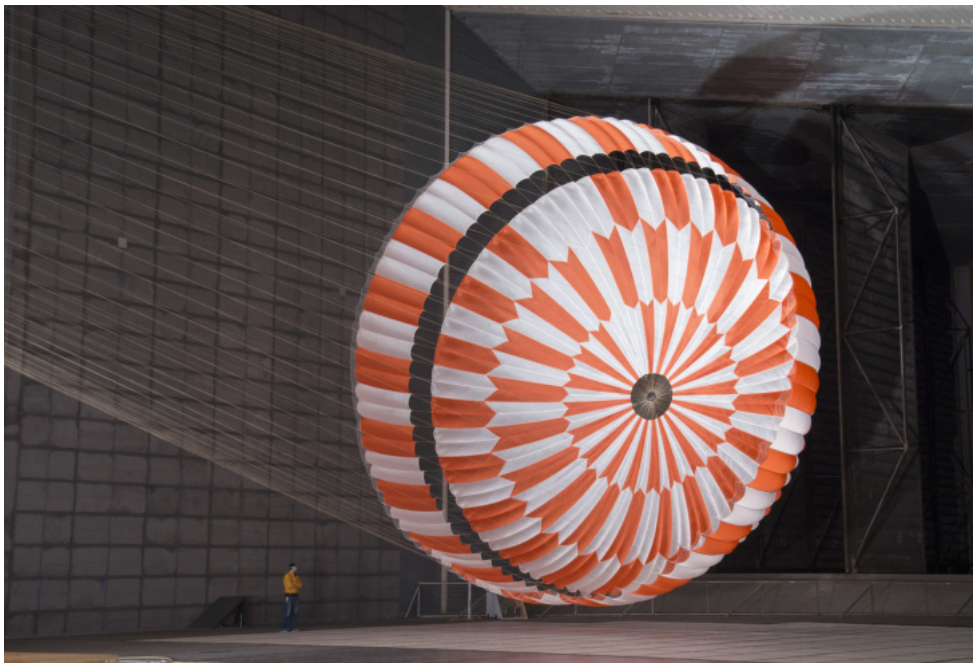

Figure 3: Perseverance test parachute

1.2.4 ZEROING IN ON LANDING

This phase occurs 20 seconds after the parachute deployment, and with it, the heat shield separates from the spacecraft, leaving the rover exposed to the Martian atmosphere for the first time. Thanks to this action, the main cameras and instrumentation are activated and begin to collect the first information about the Martian surface.

1.2.5 POWERED DESCENT

In the thinnest part of the Martian atmosphere, the parachute is able to slow down the spacecraft to about 360 km/h. To safely reach the surface, auxiliary rocket thrusters are activated to guide and slow down the rover during the final part of the descent (figura 4) . The rocket system (8 for the Perseverance mission) is located above the rover inside the rear shell and is activated at around 2100 meters altitude when separation from the rear shell occurs.

Figure 4: Powered descent system

1.2.6 SKYCRANE MANEUVER

This is the final maneuver before the contact with the Martian ground, which occurs when the descent module's speed is about 2.7 km/h. At about 20 meters from the Martian surface, the descent module releases the rover using a set of cables, and at the same time, the mobility system deploys, locking the legs and wheels in the landing position (figura 5).
Once the wheels make contact with the Martian soil, the cables connecting the rover to the descent module are cut, and the module flies away to land uncontrollably in an area far from that of the rover.

Figure 5: Perseverance skycrane manuever

All these events are depicted in the following figura 6, which provides an overview of the Perseverance mission's EDL phase:

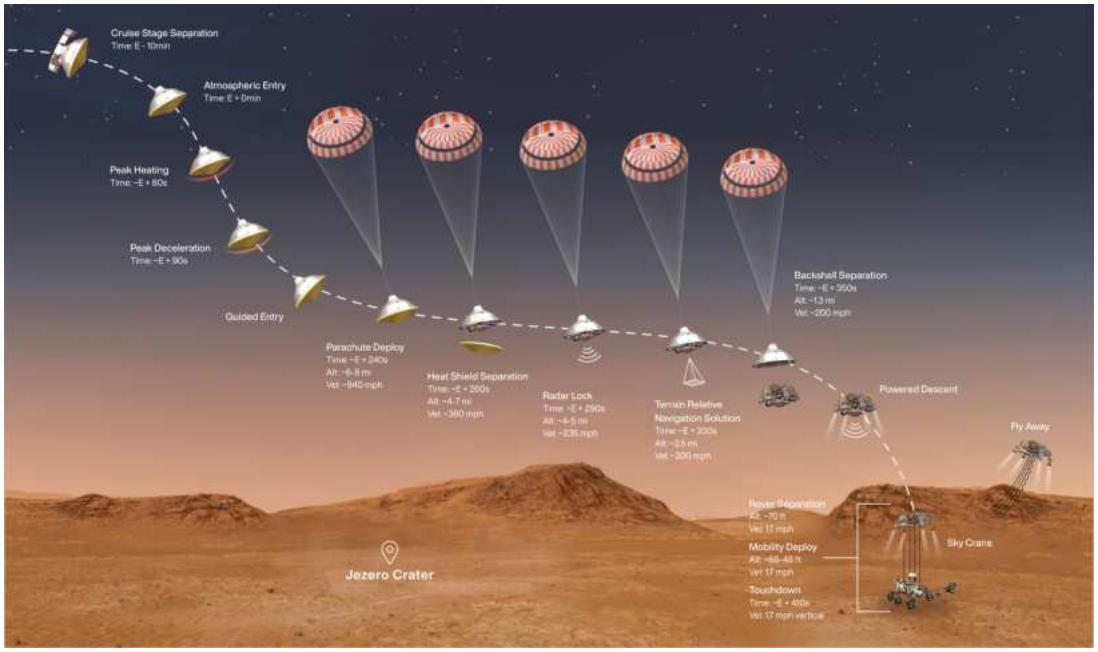

Figure 6: EDL of Perseverance mission (NASA)

The study over the years and the design of the EDL sequence for a Mars exploration mission represents an important reference for other solar system planets exploration missions.
In fact, since the focus on martian exploration increased in the mid-1990s, most of the familiarity with the sequence of entry, descent, and landing (EDL) of lander and rovers on the surface of other planets has taken place against the backdrop of Mars.
An example is the "Dragonfly" project, a NASA mission to Saturn's largest moon Titan scheduled to launch in 2027.

1.3 PARACHUTE SYSTEMS FOR INTERPLANETARY MISSIONS

During the first phase of the martian atmospheric re-entry the first component of the capsule that works is the heat shield. It has the double function of protection of the rover or lander, inside the capsule, from the hight temperatures and to decellerate the capsule thanks to its blunt shape [12].

	Viking 1/2	Pathfinder	MER A/B	Phoenix	MSL
Diameter, m	3.5	2.65	2.65	2.65	4.5
Entry Mass, kg	930	585	840	602	> 3000
Landed Mass, kg	603	360	539	364	> 1700
Landing Altitude, km	-3.5	-1.5	-1.3	-3.5	+1.0
Landing Ellipse, km	420 x 200	100 x 50	80 x 20	75 x 20	< 10 x 10
Relative Entry Vel., km/s	4.5/4.42	7.6	5.5	5.9	> 5.5
Relative Entry FPA, deg	-17.6	-13.8	-11.5	-13	-15.2
$m/(C_DA)$, kg/m^2	63.7	62.3	89.8	65	> 140
Turbulent at Peak Heating?	No	No	No	No	Yes
Peak Heat Flux, W/cm^2	24	115	54	56	> 200
Hypersonic α, deg	-11.2	0	0	0	-15.5
Hypersonic L/D	0.18	0	0	0	0.24
Control	3-axis	Spinning	Spinning	3-axis	3-axis
Guidance	No	No	No	No	Yes

(a) *NASA martian capsules comparison [12]*

(b) *Components of Mars exploration capsule [1]*

Figure 7: Mars exploration capsules

However, due to its poor drag area, it is not able to safely bring the spacecraft onto the Martian surface. Therefore, to achieve a controlled and safe landing, the use of the supersonic parachute comes into play. Supersonic parachutes have been used in all Mars exploration missions due to their reliability given by the high value of the ratio between drag coefficient and mass.
The opening of the supersonic parachute is a critical and fundamental event of the EDL sequence; in fact, for stability and material resistance reasons, it usually occurs when the Mach number is around 2, and slows down the capsule to a subsonic speed ($M \simeq 0.1$).
The supersonic parachute is the key for the rover landing success because it has some vital functions:

- decelerates the capsule from supersonic to subsonic speed;
- allows a controlled descent capable of obtaining scientific measurements required by the mission;
- guarantees stability allowing an excellent functioning of the instrumentation avoiding malfunctions;
- in some configurations it serves for the deployment of an additional slowdown system (pilot function);
- allows you to reach the height and time needed to complete the EDL sequence.

To perform these important functions, the design of the supersonic parachute must also take into account the turbulent wake that forms behind the capsule and that consequently tends to destabilize and cause the parachute to oscillate (see figura 8 [27]) . This oscillatory motion, which occurs intensely a few moments after opening, has important consequences, including influencing the trajectory of the capsule as it is coupled with the parachute. This dynamic response to the oscillations of the capsule can trigger a self-exciting mechanism of the capsule itself that can lead to uncontrolled vibrations and a possible mission failure.

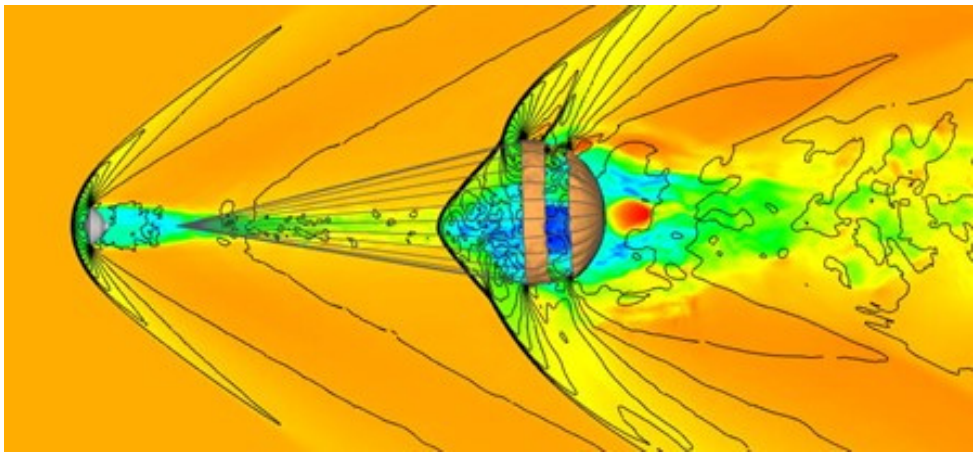

Figure 8: Supersonic parachute-capsule coupling

Traditionally, a supersonic parachute for extraterrestrial exploration applications consists of the parts show in figura 9:

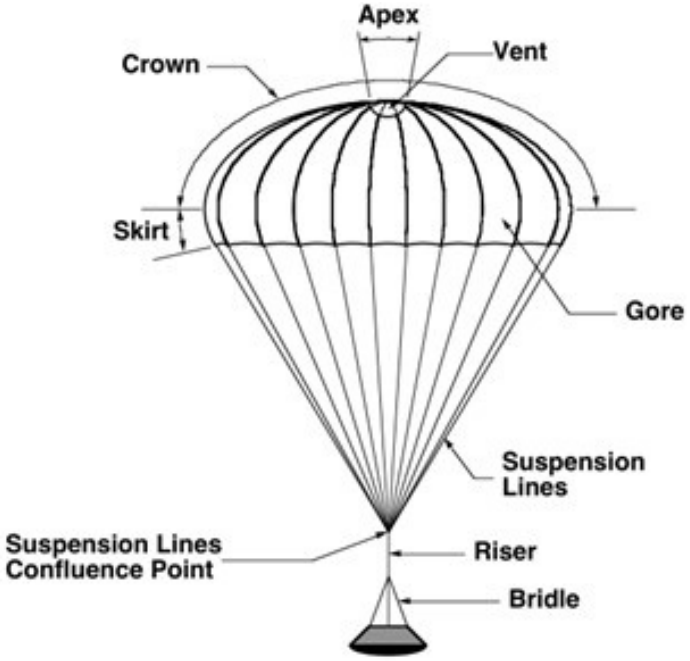

Figure 9: Supersonic parachute model for extraterrestrial exploration

The main performance parameters are as follows [18],[8]:

Nominal Area,S0

- area based on canopy constructed surface area;
- includes vent area and other open areas;
- used as reference area for aerodynamic coefficients.

Nominal Diameter, D0

$$D0 = \sqrt{4S_0)/\pi} \tag{1}$$

Constructed Diameter, Dc

- Maximum diameter of the parachute (measured along the gore radial seam) of the parachute

Conical Parachute Base Angle, μ

Vent Diameter, Dv

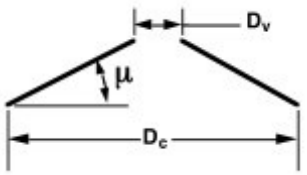

Figure 10: Supersonic parachute geometrical parameters/1

Vent Area, Sv

- constructed area of the vent;
- although related, the vent area and vent diameter (Dv) are not always related by the simple relationship between the area and diameter of a circle;
- Sv is typically $\simeq$ 1 % of S0.

Geometric Porosity, Δg

- ratio of total open areas (e.g., Vent Area) to the Nominal Area;
- usually expressed as a percentage.

Total Porosity, Δt

- the sum of the geometric porosity and an equivalent porosity due to fabric permeability;
- fabric permeability is converted to an "equivalent" open area of the parachute to determine the porosity due to fabric permeability;
- usually expressed as a percentage.

The geometric and total porosity have important effects on the performance of the parachute in terms of exerted resistance, stability, and peak of the maximum load endured.

Projected Area, Sp

- projected area of the inflated parachute;
- sometimes used as reference area for aerodynamic coefficients in parachutes.

Projected Diameter, Dp

$$Dp = \sqrt{4S_p)/\pi} \tag{2}$$

Suspension Line Length, Ls

$$L_S/L_D = 1 \quad \text{or} \quad 2 \tag{3}$$

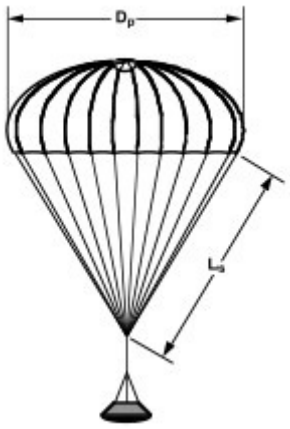

Figure 11: Supersonic parachute geometrical parameters/2

1.3.1 PARACHUTE TYPES [8]

There are two main type of spersonic parachute:

- solid fabric
- ribbed fabric

The second tipology is commonly used for interplanetary exploration missions.
A further classification is made based on the different type of sail used for the supersonic parachute:

Figure 12: Supersonic parachute classification

GUIDE SURFACE ("RIBLESS")

They are a type of parachute characterized by a low drag coefficient (CD0 $\simeq$ 0.3) and good stability. For this reason, they are used in situations where stability is a fundamental requirement. Also for subsonic applications they can be used but they are difficult to realize for this conditions.

CONICAL RIBBON

They have a moderate drag coefficient (CD0 $\simeq$ 0.5) and good stability. They are suitable for subsonic and supersonic applications. If made of Kevlar, they are very strong and can be opened at very high dynamic pressures.

DISK GAP BAND (DGB)

They are characterized by a drag coefficient ranging from 0.4 (low) to 0.7 (moderate) and provide good stability. Unlike other types of parachutes, the DGB design allows for modification of the Cd in favor or against stability by changing the "gap" and width of the characteristic strip of this type.
The DGB, like the conical ribbon parachute, is suitable for subsonic and supersonic applications, and thanks to its versatility, it has been used in the vast majority of Mars exploration missions.

RINGSAIL

They provide the highest drag coefficient (CD0 $\simeq$ 0.8), and to achieve optimal performance, their design is custom-made by varying the shape of the "sail" and its distribution of geometric porosity.

1.3.2 SUPERSONIC PARACHUTES FUNCTIONING

During the famous "7 minutes of terror" in which EDL sequence happens, for the parachute phase of the capsule descend the following steps take place:

DEPLOYMENT

Process by which the parachute is exposed to the airstream so that inflation can start.It starts with the parachute in its deployment bag within the capsule and ends with the parachute stretched-out, but not inflated, and completely out of its bag.
To deploy a supersonic parachute there are three principal methods:

- extractor rocket (rocket used to extract pilot or main parachute);
- pilot parachute;
- mortar (Used in all US missions to Mars).

For a good deployment the system has to satisfy some requirements as keep the parachute under tension, from tadling, prevents "dumping" of the canopy, minimize inertial deployments loads and be reliable. Even if the parachute in this phase is not open, this process generates forces that influences the descent

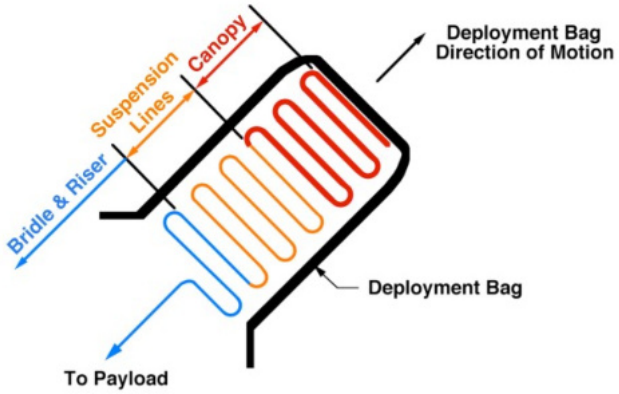

Figure 13: Parachute: deployment

of the capsule.In fact as the parachute bag re-accelerates to the entry vehicle velocity, inertial forces are generated. These inertial forces are known as snatch loads (figure 14):

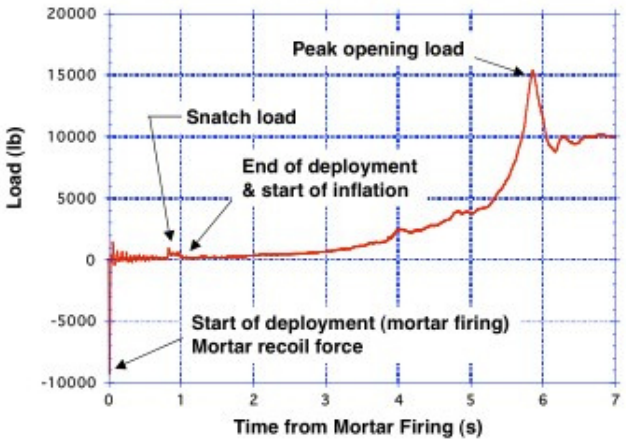

Figure 14: Snatch loads deployment

INFLATION

The process by which the parachute is filled or opened is called "parachute inflation".It starts when the parachute is completely out of its deployment bag, streaming behind the entry vehicle, and ends with its first full inflation. During this process, the surrounding air or fluid enters the parachute, filling its cavities and creating the necessary aerodynamic resistance for deceleration. Proper parachute inflation is crucial to ensure stable deployment and effective vehicle deceleration.
The process is represented in the figure 15: The inflation process of the parachute can be happen in the

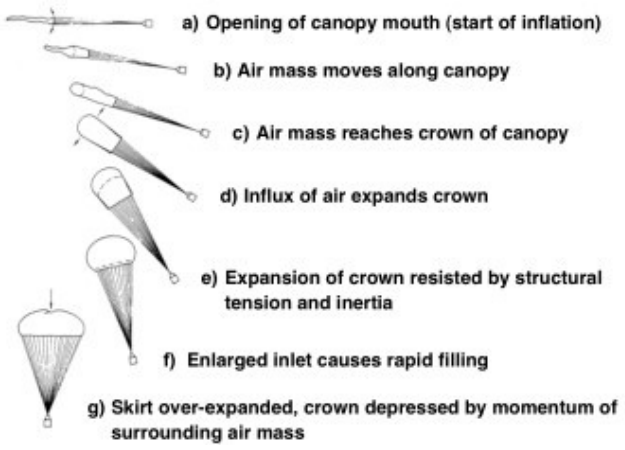

Figure 15: Parachute: inflation

subsonic regime (**Subsonic Inflation**) or in supersonic regime (**Supersonic Inflation**).At supersonic speeds, inflation is often modeled as occurring over a fixed time, proportional to the parachute diameter but independent of Mach number (in the range $1.5 \leq M \leq 2.5$).
Another classification for the inflation parachute process regards the instant when the peak opening load occurs.There is **Infinite-Mass Inflation** and **Finite-Mass Inflation**.
If inflation is of the infinite mass type there will be little deceleration and reduction in the dynamic pressure during inflation. In this case the peak opening load will occur at full inflation. It can happen when inflation occurs so rapidly that there is no time for significant deceleration of the entry vehicle during inflation. For these reasons parachute inflation in thin atmospheres at supersonic speeds is often of the infinite mass type. One example is Mars. On the other hand, the finite-mass inflation is when the payload has “finite-mass”. In this case there will be substantial deceleration, reduction in the dynamic pressure during the inflation and the peak opening load will not occur at full inflation.

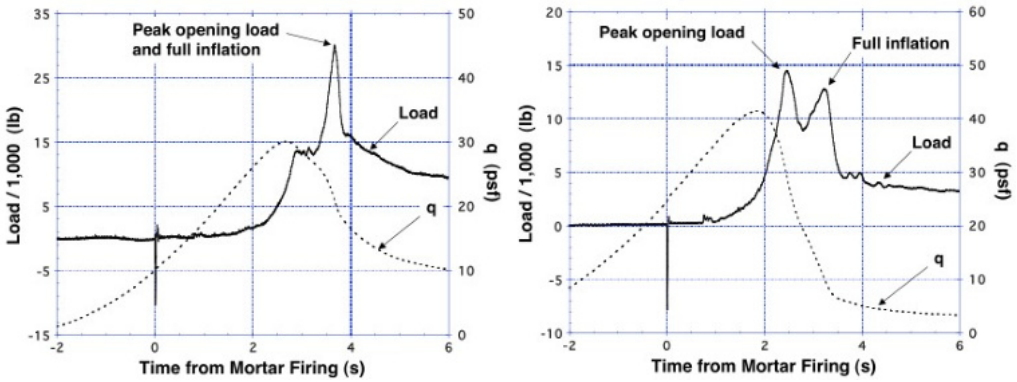

Figure 16: Infinite-Mass inflation and Finite-Mass inflation load comparision

1.4 EDL SEQUENCE IN THE PAST AND FUTURE INTERPLANETARY EXPLORATION MISSIONS

At the foundation of the simulations and study carried out in this master's thesis is a general analysis of the main space missions to Mars and other planets in the solar system of the world's leading space agencies (NASA, ESA, CNSA, and JAXA).
The objective was to gather reference information (dimensional sizes, activation parameters, basic assumptions, etc.) for both the design and simulation of the supersonic parachute and to compare the various strategies of the different agencies.
The missions that have been considered are the following:

- Tianwen-1 (CNSA)
- Exomars 2016 – 2028 (ESA)
- Mars Science Laboratory (NASA)
- Dragonfly Mission (NASA)

Tianwen-1 (CNSA)

Tianwen-1 [16] was the most recent Martian exploration mission, which included an orbiter and a rover, to reach Mars in May 2021 after the failure of the previous Chinese mission, Yinghuo-1.
Regarding the descent phase of the capsule and in particular the part related to the supersonic parachute, three different types were analyzed for this mission: the DGB parachute, Cross parachute, and Ringail parachute. The final choice favored the Disk-Gap-Band type, as it guarantees good stability and excellent performance during the inflation phase under supersonic conditions and low atmospheric density.
For the design and development, four different types of DGB were studied and tested, and their structural parameters are summarized in the table 2:

Table 2: Structural parameters of each parachute.

Parachute	**MPF DGB**	**Viking DGB**	**Hemisflo DGB**	**Triconical DGB**	**Tapered DGB**
Disk area rateo	0.384	0.53	0.53	0.53	0.53
Gap area ratio	0.1	0.12	0.12	0.12	0.12
Band area ratio	0.516	0.35	0.35	0.35	0.35
Number of gores	20	20	20	20	20
Ls/Do	1.7	1.7	1.7	1.7	1.7

The parachute models tested for this mission are rappresented in the figura 17[16]:

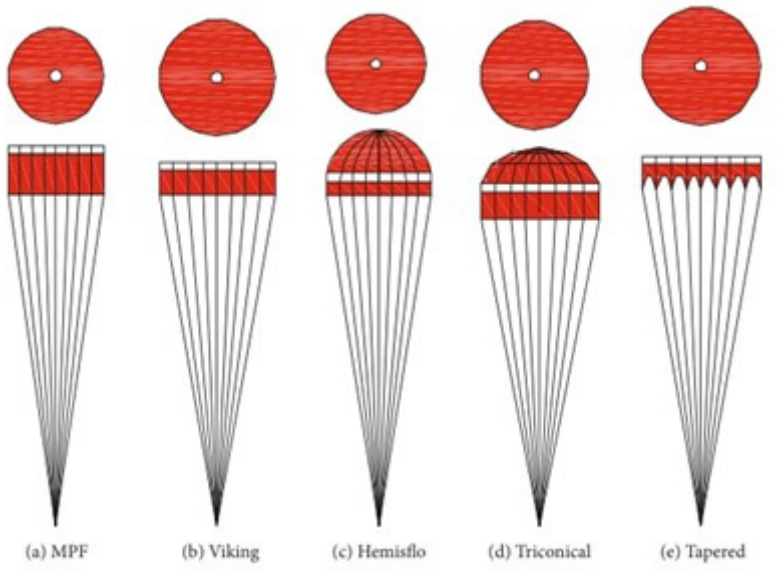

Figure 17: Structures of different DGB parachutes

The study and the comparison between different DGB parachutes to choice the best model for the mission, has permitted to define some general selection criteria utilize also for the simulation explain in this paper. First of all, to increase the parachute's coefficient of drag, the geometry of its disk must be modified by increasing its diameter. Regarding stability, the width of the parachute's "band" is very important. These two elements lead to the conclusion that the Tapered configuration is optimal.
Finally, by analyzing the results of the simulations, it was observed that the trend of CD decreases as the Mach number increases, except for the Hemisflo model which has an increasing trend from M = 0.9.

Exomars 2016-2028 (ESA-Roscosmos)

Before the success of the Chinese mission, there was the failure of the European Space Agency (ESA) mission in collaboration with the Russian space agency (Roscosmos), ExoMars [19]. This important joint space program is characterized by two missions: the first, launched in 2016, involves the Martian orbit insertion of the Trace Gas Orbiter (TGO) orbiter and the sending of the demonstration descent module, Schiaparelli, to test the entry, descent, and landing of the probe (which failed with the crash of the probe). Schiaparelli was built to demonstrate Europe's ability to perform the critical EDL phase in order to land on Mars. However, a few moments after the parachute opening, the capsule began to oscillate with angles that caused the saturation of the inertial measurement unit (IMU).
This had the catastrophic consequence of prematurely activating the final descent phase, subsequently causing the crash with the surface [29],[25],[24].
The main causes found after numerous investigations were:

- large movement of the parachute canopy due to the unstable flow motion;
- oscillation of forces due to the variation in resistance area of the parachute canopy.

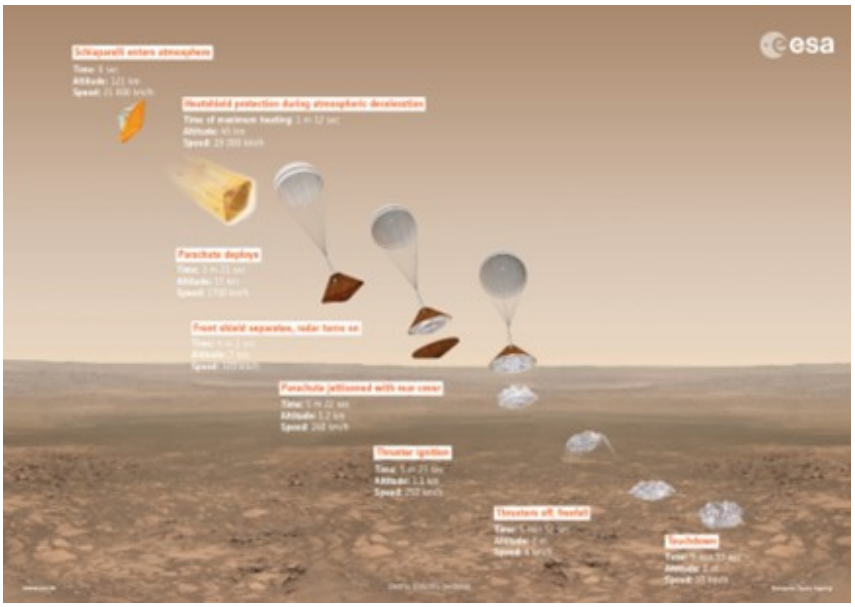

Figure 18: EDL Exomars 2016 mission

The second plan involves the launch of a larger capsule, but geometrically identical to Schiaparelli, containing the Rosalind Franklin rover for the search for life on Mars, whose launch is still to be scheduled (originally planned for 2022 but postponed to 2028).
It also involves the use of two parachutes: The first, a supersonic DGB type, is deployed at M $\simeq$ 2 and has the goal of slowing down the capsule to subsonic speed within 20 seconds. Subsequently the second parachute, a ringslot type equipped with a large sail, is deployed at M $\simeq$ 0.7. The use of a larger resistance area for the second parachute is made possible by the fact that the loads to be supported in subsonic regime are less intense, as they scale with the square of the velocity. However, it also requires a high geometric porosity.

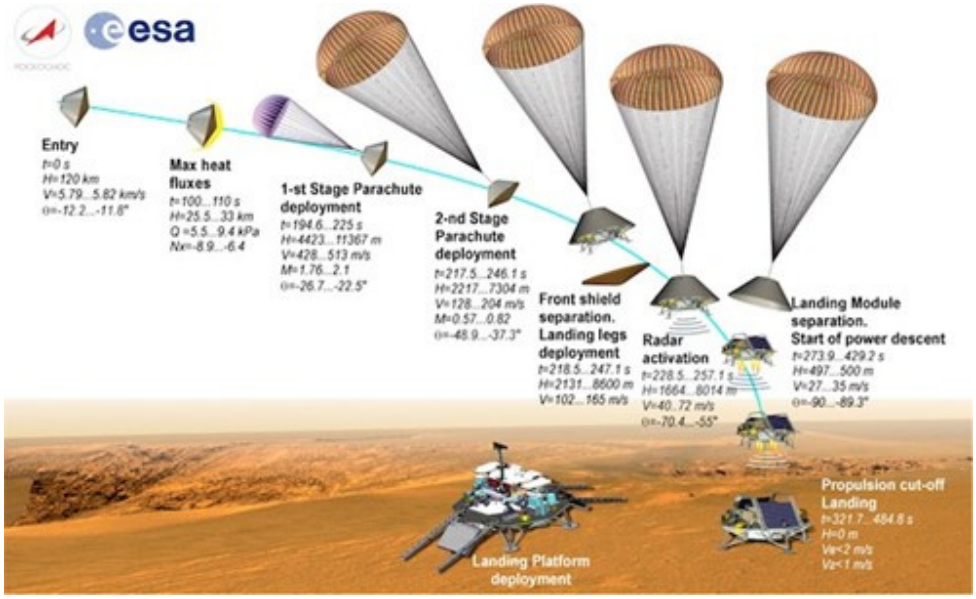

Figure 19: EDL Exomars 2022 mission

Mars Science Laboratory (NASA) - Dragonfly Mission (NASA)

The last two missions analyzed for this article were designed by the American space agency, NASA, and concern a Mars exploration mission (Mars Science Laboratory, MSL) and an exploration of Titan (Dragonfly), the largest satellite of Saturn.
MSL involved the sending of the Curiosity rover to Mars with the aim of investigating the possible presence of life. The launch took place in November 2011 and after 9 months, in August 2012, the landing on the Martian surface occurred after successfully executing the new EDL sequence, depicted in figure 20 [21]:

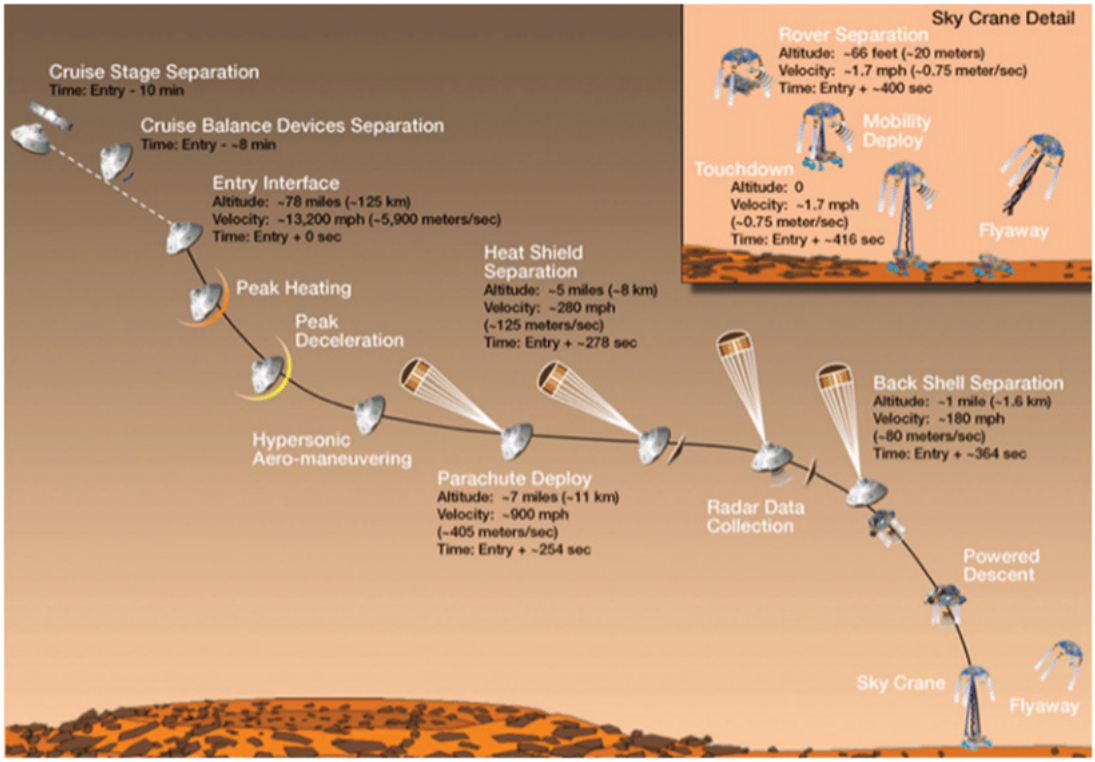

Figure 20: EDL Mars Science Laboratory mission

The entry, descent, and landing (EDL) phase start when the spacecraft reached the Martian atmosphere, about 125 kilometers above the surface, and ended with the rover touches the martian surface.
The EDL sequence for this mission included a combination of technologies inherited from past NASA Mars missions, as well as exciting new technologies. In fact, The sheer size of the rover (nearly 900 kilograms) precluded it from taking advantage of an airbag-assisted landing and used sky crane touchdown system. The new EDL architecture breaks down into four parts:

1. **Guided Entry**: The spacecraft was controlled by small rockets during descent through the Martian atmosphere, toward the surface,
2. **Parachute Descent**: Like Viking, Pathfinder and the Mars Exploration Rovers, was used to slowe the spacecraft a large parachute,
3. **Powered Descent**: Rockets controlled the spacecraft's descent until the rover separated from its final delivery system, the sky crane.
4. **Sky Crane**: the sky crane system lowered the rover to a "soft landing" - wheels down - on the surface of Mars.

In particular, to land the rover, a supersonic DGB parachute with a diameter of 16 meters and connection wires to the capsule longer than 50 meters was used. This parachute was designed to withstand opening in the Martian atmosphere at M = 2.2.
The last mission analyzed is the NASA mission called *Dragonfly* which is still under the development. That represents a new generation of interplanetary exploration mission that will send an nuclear power octocopter to the surface Titan (the biggest satellite of Saturn).
Unlike Mars exploration missions and the consolidated EDL sequence used for such missions, Titan represents a new challenge that requires the development of a new controlled descent system. In fact, its dense atmosphere, large-scale atmospheric height, and low gravity allow for a much slower entry and descent sequence, 100 minutes, compared to the "7 minutes of terror" characteristic of landing on Mars.
Focusing on the parachute phase, once the function of decelerating the heat shield has been performed, the pilot DGB parachute is ejected to further stabilize and decelerate the spacecraft. The opening takes place at around M=1.5.
Due to the density of Titan's atmosphere, this configuration remains active for about 80 minutes until the main subsonic parachute is opened at a certain altitude. After 17 minutes, the drone is released and begins the landing phase on the surface.
A representation of what has been described is visible in the following figure 21:

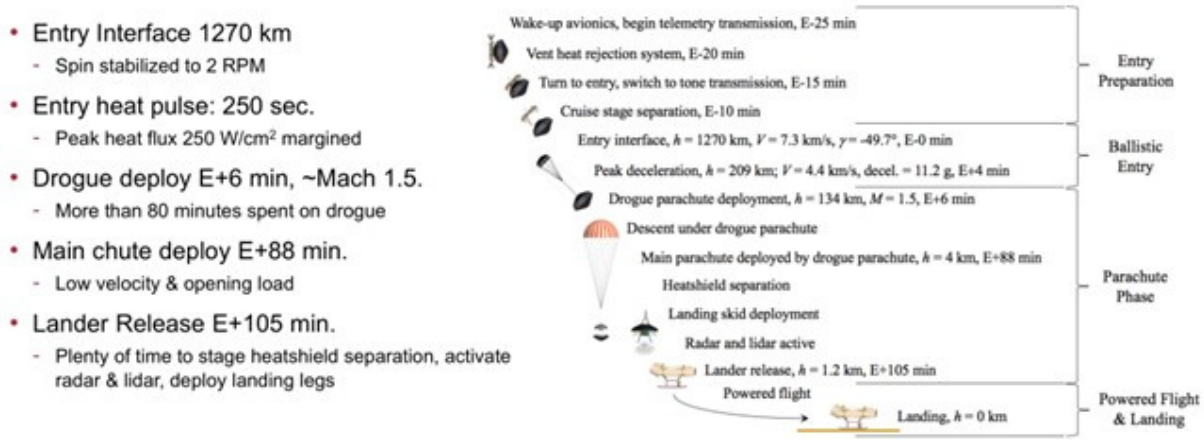

Figure 21: EDL Dragonfly mission

1.5 DISK GAP BAND (DGB) PARACHUTE

1.5.1 HISTORY AND DESIGN

A first design consideration, based on the analysis made on the past and future mission to Mars and other platens, that can be made is that for all major world space agencies, the type of parachute commonly used for interplanetary exploration applications in supersonic regime is the **Disk Gap Band** (DGB) parachute.
The main reasons for this choice are mainly reliability and effectiveness that they can offer both in supersonic and subsonic regime. In addition, they are characterized by a geometry that, with the modification of certain parameters, allows adapting performance to different scenarios that do not necessarily involve Mars.
To successfully land in the designed area on the surface and slow down the capsule during the descent phase, the supersonic parachute system is an integral part of the EDL sequence.
This type of parachute provides an aerodynamic drag force that allows the probe to decelerate from supersonic to subsonic velocity. As the name suggests, the base components of the DGB parachute are circular disk and an orthogonal cylindrical band, which are separated by an empty band as shown in the figure 22:

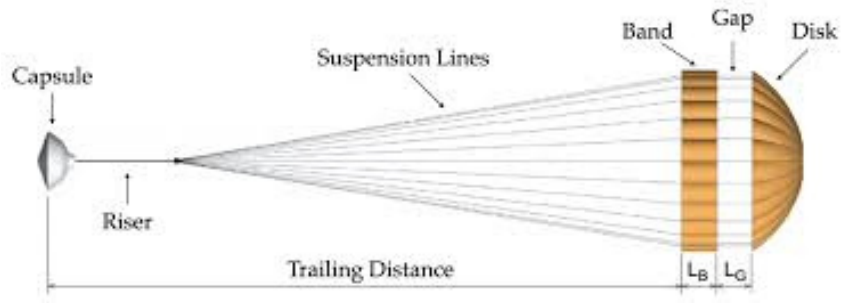

Figure 22: Disk Gap Band parachute

The DGB parachute was originally designed by Clint Eckstrom in the early 1960s for high-altitude rockets for meteorological applications.Its design was chosen to achieve good strength and stability, with a relatively simple geometry and low storage volume. In addition, at supersonic conditions, The disk needs to be partially permeable to the flow so that the parachute is stable.
To meet these designed requirements, Eckstrom understood that a geometrical porosity was necessary to increment the stability of the parachute and this target was obtained with the addition of the **vent** and the **Gap** between circular disk and an orthogonal cylindrical band.
The DGB parachute configuration has been commonly used in supersonic deceleration, which can be traced back to the 1970s with the beginning of the study for interplanetary exploration programs, and has been used in most of NASA's exploration missions.
Thanks to the **Planetary Entry Parachute Program (PEPP)**, the DGB configuration was studied by NASA through an experimental approach, obtaining data from tests carried out in low-density environments.

After the design years, the first important application for the DGB supersonic parachute were the Viking missions designed by NASA, the first to successfully land two lander on the surface of Mars.They development and qualification, in terms of parachute system, still represents the most extensive and documented reference study for the design of a Mars exploration mission that includes the EDL sequence and in particular the deceleration through the supersonic parachute.
The parachute design for the Viking missions was able to ensure excellent aerodynamic characteristics in supersonic conditions that were never simulated because they were difficult and expensive to duplicate in tests.
Moving on to an engineering analysis, one of the main uncertainties and critical points of this type of parachute regards the inflation phase in supersonic condition which influence accordingly the deceleration of capsule.In particular, it is typically a fluid-structure interaction problem.
The difficulty in studying the aerodynamic characteristics of the parachute is also present at low speeds, as its structural deformation is a non-linear and unpredictable phenomenon. For these reasons, the supersonic deceleration layout must be specifically designed to achieve high aerodynamic performance.
From the study of the previously presented missions, some design considerations have been derived that are useful during the design phase. It has been observed that in order to increase the drag coefficient (Cd), the parameter to consider is the diameter of the disk. Increasing the diameter allows for a larger area of resistance after deployment. Regarding the other fundamental characteristic, stability, the key role lies in the width of the orthogonal cylindrical band and specifically in its design. In fact, using a tapered band shape, as shown in figure 17:, provides greater stability. Finally, during the development phase, it is important to consider that the Mach number also greatly influences the performance and design of the parachute, especially during its opening.

1.5.2 EXPERIMENTAL STUDIES IN LITERATURE

Research in the field of supersonic parachutes for space applications over the past 60 years has led to significant advancements and is continuously evolving, as we will see in the following brief analysis available in the literature.
The performance and behavior of supersonic parachutes were first studied by NASA with the Mercury program. This initial study, conducted by Maynard in 1961 using wind tunnel testing [20], successfully identified the regime of maximum criticality at a Mach number of approximately 2. Knowledge of this value is crucial because at this Mach number, the parachute experiences strong oscillations that render the system unstable. Consequently, at higher Mach numbers, the drag coefficient rapidly decreases due to instability during inflation. The research also led to the identification of the cause of these oscillations, which is the turbulent flow that develops behind the capsule during descent.
Finally, it was demonstrated that the performance of the supersonic parachute, in terms of drag and stability, decreases when the shock wave ahead of the parachute moves upstream of the capsule.
With the aim of improving the performance of supersonic parachutes at high Mach numbers, the optimized design of the Disk Gap Band (DGB) for supersonic regime was studied by Eckstrome [11] within the NASA's PEPP program. During the development of the Viking missions, these analyses aimed to study the design for applications in the rarefied atmosphere of Mars through numerous high-altitude drop tests on Earth [3][4][22][23].
One of these studies, conducted by S. Steinberg [26], tested a scaled model of the Viking DGB parachute in a wind tunnel and found that the aerodynamic drag coefficient reaches its maximum value at a Mach number of approximately 1.4 while for higher Mach numbers the drag produced by the supersonic parachute decreases. This research also observed that a significant increase in aerodynamic drag is achieved by increasing the ratio between the cable length and the cap diameter (L/D)[7].

In 2003, Juan R. Cruz conducted studies on two models of supersonic parachutes based on the NASA Mars Exploration Rover (MER) and Mars Pathfinder (MPF) missions to determine the drag and stability coefficients. This study demonstrated that increasing the height of the circular band, detached from the disk, leads to a decrease in drag but a corresponding increase in stability. Additionally, it was one of the first studies to emphasize the importance of fabric porosity, in addition to geometric factors, in relation to parachute drag and stability.

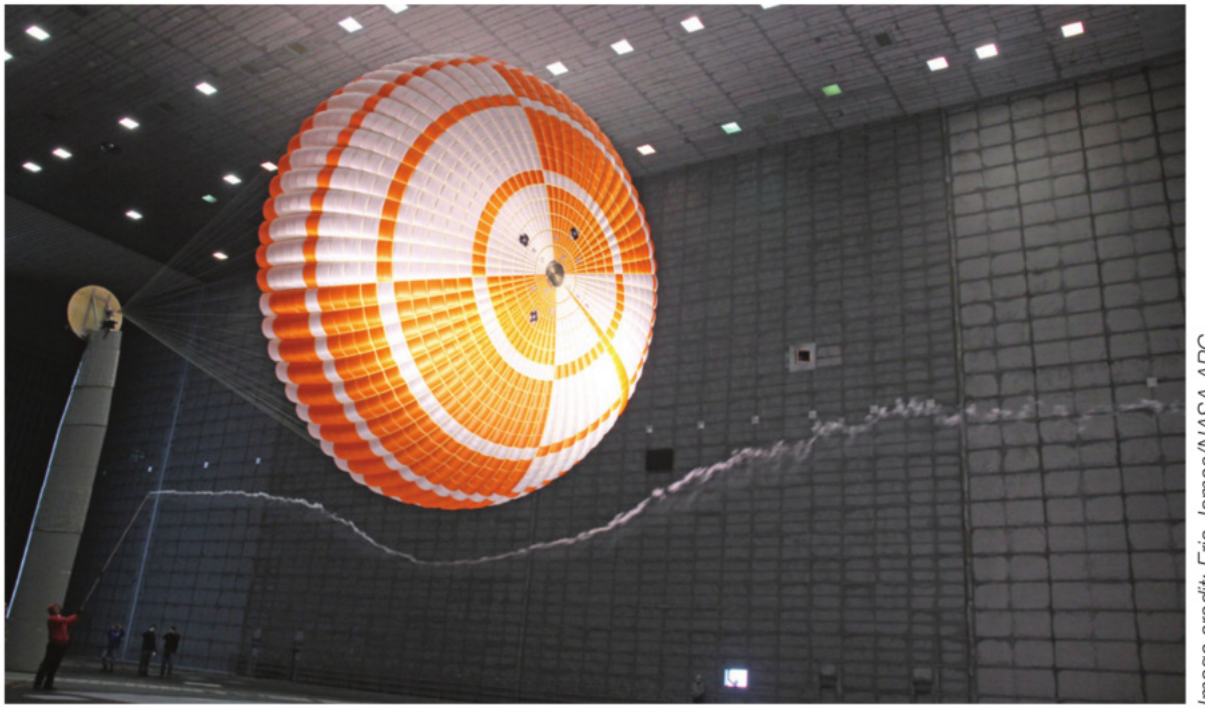

Figure 23: Example of DGB parachute test in wind tunnel

2 NUMERICAL SIMULATION AND MODELS

2.1 MARS ATMOSPHERE RECONSTRUCTION

Regarding the simulation part, the first step was to define the main parameters of the Martian atmosphere. Indeed, by utilizing the "Mars Climate Database"[2], temperature, density, and pressure values at specific altitudes were obtained (see the following table).

Table 3: Mars atmosphere data

Altitude [m]	Temperature [K]	Density [Kg/m3]	Pressure [Pa]
2.49e+04	1.77e+02	2.03e-03	6.89e+01
2.38e+04	1.77e+02	2.28e-03	7.76e+01
2.27e+04	1.78e+02	2.55e-03	8.73e+01
2.17e+04	1.80e+02	2.84e-03	9.81e+01
2.06e+04	1.82e+02	3.15e-03	1.10e+02
1.95e+04	1.84e+02	3.48e-03	1.23e+02
1.84e+04	1.87e+02	3.84e-03	1.38e+02
1.62e+04	1.94e+02	4.62e-03	1.72e+02
1.40e+04	2.01e+02	5.53e-03	2.13e+02
1.30e+04	2.04e+02	6.03e-03	2.36e+02
1.26e+04	2.05e+02	6.20e-03	2.44e+02
1.19e+04	2.07e+02	6.56e-03	2.61e+02
1.16e+04	2.09e+02	6.74e-03	2.69e+02
1.12e+04	2.10e+02	6.93e-03	2.78e+02
1.08e+04	2.11e+02	7.12e-03	2.88e+02
1.05e+04	2.12e+02	7.32e-03	2.97e+02
1.01e+04	2.13e+02	7.52e-03	3.07e+02
9.82e+03	2.14e+02	7.73e-03	3.17e+02
9.47e+03	2.15e+02	7.95e-03	3.27e+02
9.11e+03	2.16e+02	8.17e-03	3.38e+02
8.41e+03	2.17e+02	8.63e-03	3.60e+02
7.70e+03	2.19e+02	9.13e-03	3.83e+02
7.35e+03	2.20e+02	9.39e-03	3.95e+02
7.00e+03	2.20e+02	9.66e-03	4.08e+02
6.64e+03	2.20e+02	9.95e-03	4.21e+02
6.29e+03	2.21e+02	1.02e-02	4.34e+02
5.94e+03	2.21e+02	1.05e-02	4.48e+02
5.58e+03	2.21e+02	1.08e-02	4.62e+02
4.88e+03	2.22e+02	1.15e-02	4.91e+02
4.52e+03	2.22e+02	1.19e-02	5.07e+02
4.17e+03	2.22e+02	1.22e-02	5.23e+02
3.82e+03	2.22e+02	1.26e-02	5.39e+02
3.47e+03	2.23e+02	1.30e-02	5.56e+02
3.11e+03	2.23e+02	1.34e-02	5.73e+02
2.76e+03	2.23e+02	1.38e-02	5.91e+02
2.41e+03	2.24e+02	1.42e-02	6.10e+02
2.05e+03	2.24e+02	1.46e-02	6.29e+02
1.70e+03	2.24e+02	1.50e-02	6.48e+02
1.35e+03	2.24e+02	1.55e-02	6.68e+02
1.00e+03	2.23e+02	1.61e-02	6.89e+02

After loading these reference values into the Matlab code, the trends of each atmospheric parameter were obtained using the 'interp1' function, which performs linear interpolation. The results are depicted in the following figure:

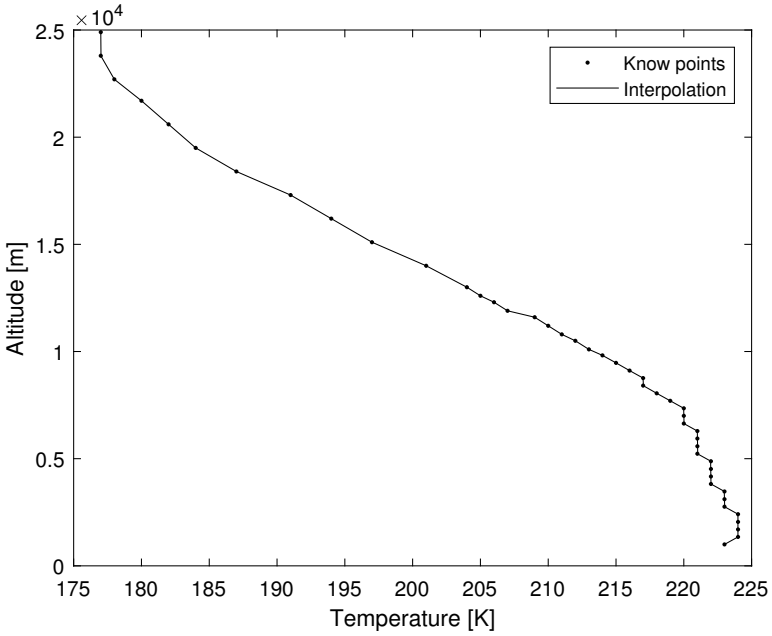

Figure 24: Mars altitude-temperature trend

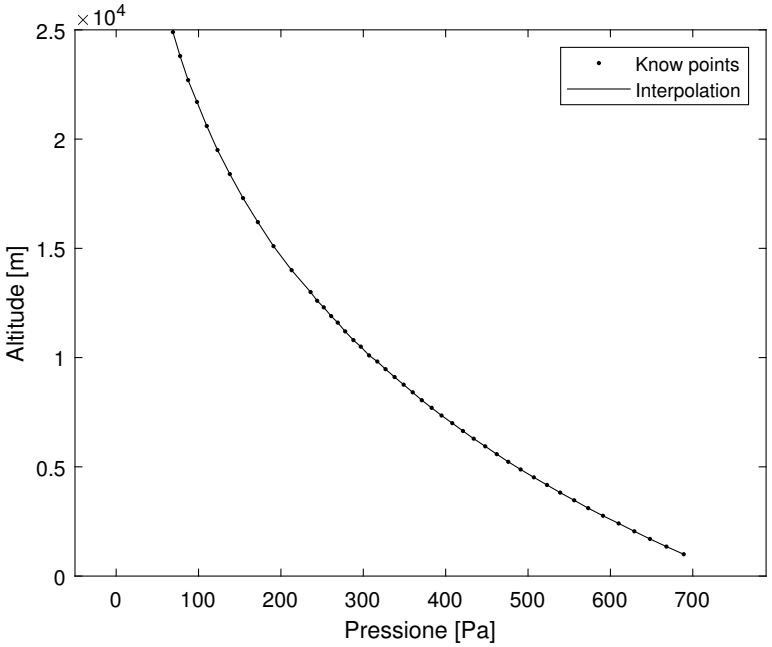

Figure 25: Mars altitude-pressure trend

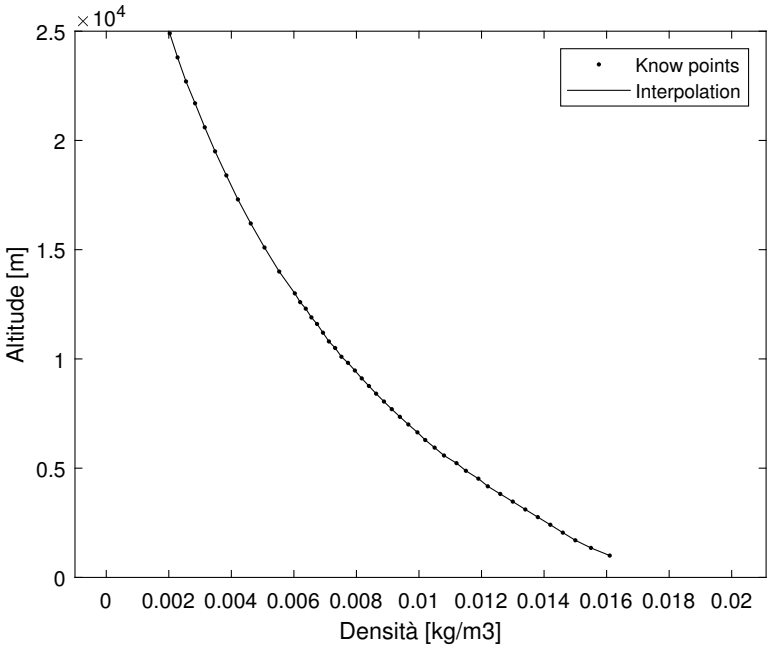

Figure 26: Mars altitude-density trend

Reconstructing the behavior of Martian atmospheric parameters is important as they influence the descent dynamics and the performance parameters of the supersonic parachute. In fact, as we will see later on and in the appendix where the code is presented, the dynamics of each simulated phase depend on the atmospheric parameters that affect variables such as drag force, dynamic pressure, coefficient of drag, etc. Therefore, knowledge of the characteristics of the Martian atmosphere is essential.

2.2 DESCENT ONE DIMENSIONAL MODEL

2.2.1 INTRODUCTION: INITIAL CONDITIONS

In this second chapter, initially, a preliminary study of the atmospheric descent phase on Mars using a supersonic parachute is presented, with the aim of analyzing its performance and becoming familiar with this system.
To develop this first part and delve into the intricacies of modeling and simulating parachute systems, we employ a one-dimensional approach. The one-dimensional model delevope in Matlab, in fact, allows us to simplify the complex dynamics of the parachute system while capturing the fundamental principles and behaviors that govern its performance.
This fisrt model for studying the behavior of the supersonic parachute in the Martian atmosphere, was divided in three principal parts:

1. **Capsule phase**: simulation of the descent where is considered only the capsule and its behavior in martian atmosphere.
2. **Parachute deployment and inflation phase**: simulation of the phenomenon of the deployment of the supersonic parachute.
3. **Parachute descent phase**: simulation of performance of the supersonic parachute.

for the second and third phases, the Disk Gap Band parachute has been chosen, a decision justified in the introductory part of the thesis.
The simulation model is characterized by simplifying assumptions and considerations:

- A one-dimensional model subject to the gravitational force (F_{P}), the drag force generated by the parachute (F_{D_P}), and the resistance force exerted by the capsule's heat shield (F_{D_C}).
- Coefficient of drag known at the initial stage (C_{D_0}).
- Diameter of the Disk Gap Band parachute is known at the initial stage (D_{0_P}).
- Velocity, altitude and Mach namber is know at the initial stage (V_0, H_0, M_0).
- Only the vertical components of the variables are considered. That is, both the capsule and the parachute have a zero angle of attack.

In particular, to verify the correct functioning of the code, the design values of the MSL and Perseverance missions by NASA have been taken as reference.
A presentation of the model for the simulation is show in the follow figure 27:

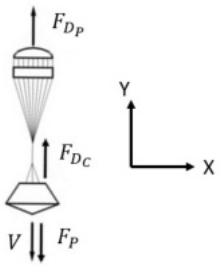

Figure 27: Simulation model

2.2.2 PRESENTATION MATLAB CODE SEQUENCE

Based on the initial conditions and the design of the supersonic DGB parachute, a simplified code was implemented in Matlab to simulate the trajectory of the capsule during descent in terms of velocity and acceleration, as well as the performance of the parachute regarding the resistance force exerted on the capsule. The following conceptual diagram explains the logical process of the simulated model:

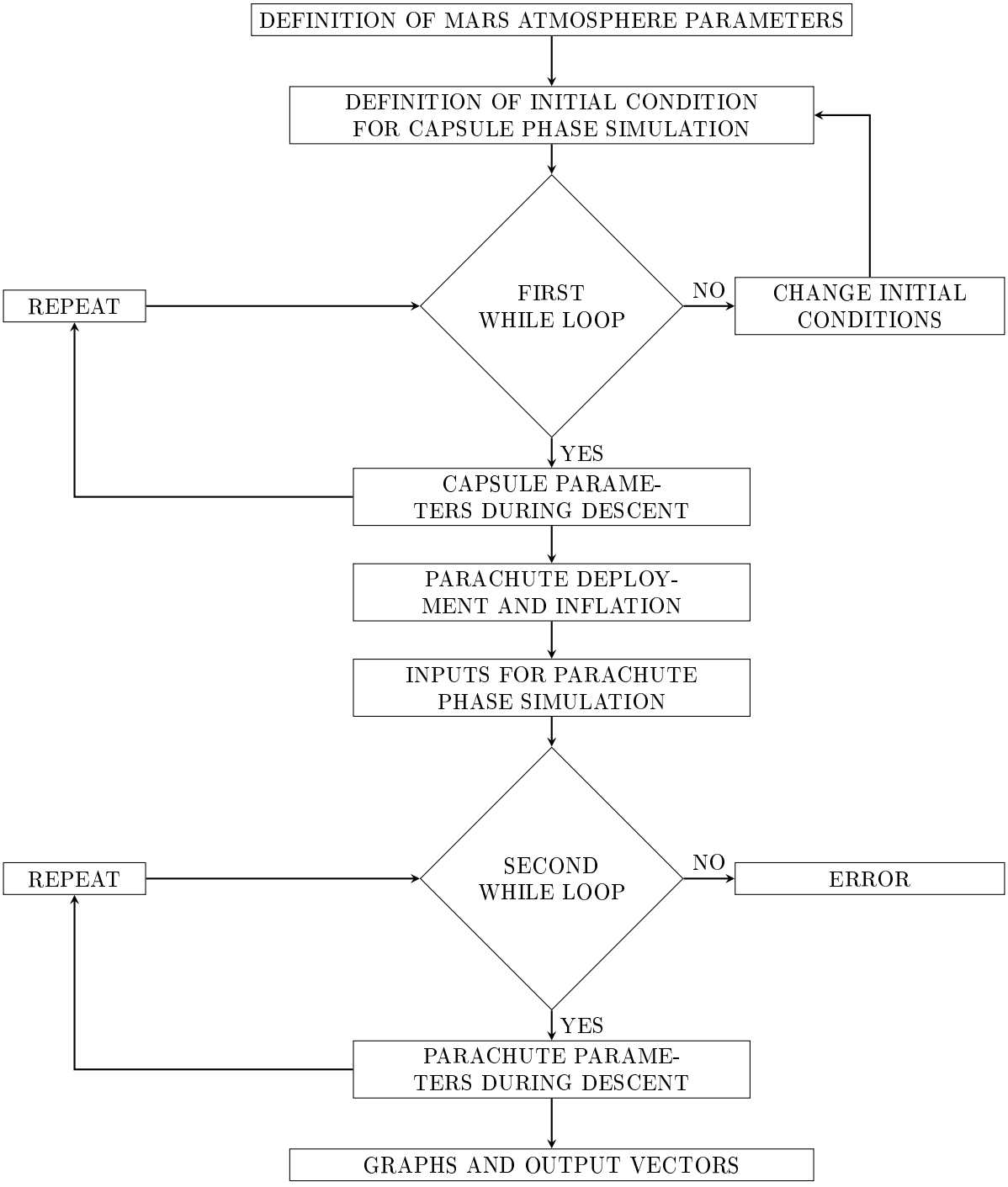

To verify the correctness of the code, a preliminary simulation based on the values of MSL missions was performed.

2.2.3 DESCENT PHASES: CAPSULE

Regarding the capsule phase of the simulation were considered the parameters of the MSL capsule represented in figure 28:

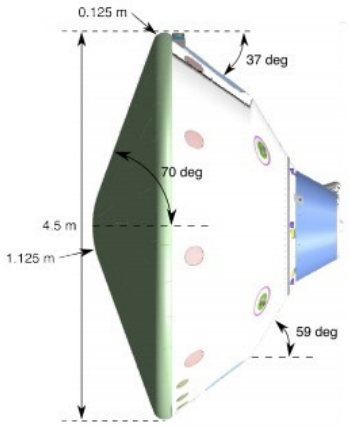

Figure 28: MSL capsule

Table 4: MSl capsule parameters

Diameter [m]	Drag Coefficient	Mass capsule [Kg]
4.5	1.53	3000

As said in the introduction of the chapter, this simplified simulation starts with the "Capsule phase" in which is simulated the performance of it in term of influence on the velocity, acceleration and drag force during the descent.
Regarding the dimensional data, they was taken from literature (see figure 7), while the drag coefficient of the capsule was estimated using the theory of the "planetary entry capsule"[14] explain in the follow pages.
Capsules and space probes have the highest entry velocities and these speeds are much higher than the local speed of sound (240 m/s at 60 km).They also correspond to Mach numbers ranging from 15 to 35 ("hypersonic").
During the hypersonic and supersonic descent phase, the aerodynamic and thermal forces acting on the capsule or space probe are extremely intense. These forces include the heating caused by high-speed air compression, as well as the drag force generated by air resistance.
To calculate the drag coefficient, it is necessary to first define the reference frame, called also Aerodynamics Coordinate System. It is represented in figure 28 for the most general configuration of “flyer” admitting a symmetry plane (“pitch” plane).
For geometry having an axis of symmetry, the natural choice of axis OX is along this “roll” axis, and orientation of the pitch plane can be chosen arbitrarily around it.
The incidence angle α is defined between the roll axis and the projection of the relative velocity vector on the pitch plane is positive when ω is positive, ranging from $-180°$ to $180°$. The sideslip angle β is the angle between the relative velocity vector and its projection on the pitch plane. It is positive when v is positive and ranges from $-90°$ to $90°$. For bodies of revolution, it is convenient to express the total angle of attack α and the windward meridian ϕ_ω.

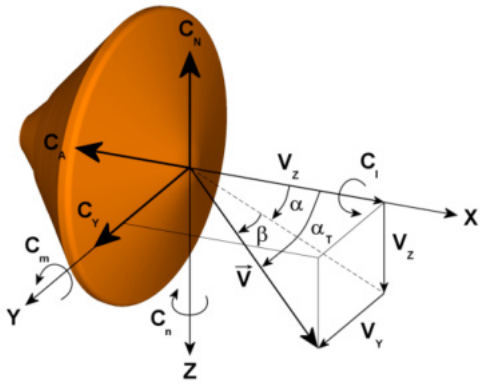

Figure 29: Aerodynamics Coordinate System [13]

Another important step before calculating drag coefficient is to introduce the aerodynamic coefficients. Their definition is related to the most natural reference frame which is the vehicle frame. The aerodynamic loads are calculated or measured along "longitudinal," "transverse," and "normal" axes (Ox, Oy, and Oz) then converted into dimensionless aerodynamic coefficients by "reference" forces and moments.
To define these reference forces and moments are use other reference parameters which are:

- Dynamic pressure:
$$\mathbf{q} = \frac{1}{2}\rho_\infty \cdot V_\infty^2 \tag{2.1}$$
- Reference area, **Sref**, defined as maximum cross section for ballistic vehicles
- Reference length, Lref, corresponding to overall to maximum diameter (case of space probes)

Thus the force and moment of references are $q \cdot S_{\text{ref}}$ and $q \cdot S_{\text{ref}} \cdot L_{\text{ref}}$.
Using this reference parameters we can define the static aerodynamics coefficients which are obtain starting from the components $\vec{X}_A, \vec{Y}_A, \vec{Z}_A$ of the aerodynamic force $\vec{R}_A$ and components (L, M, N) of the aerodynamic moment around the origin O. These coefficients are reported in the following table:

Table 5: Static Aerodynamics coefficients

Formula	Name	Symbol
$X_A = -A = -q \cdot S_{\text{ref}} \cdot C_A$	Axial force coefficient	C_A
$Y_A = q \cdot S_{\text{ref}} \cdot C_A$	Lateral force coefficient	Y
$Z_A = -q \cdot S_{\text{ref}} \cdot C_N$	Normal force coefficient	C_N
$L = q \cdot S_{\text{ref}} \cdot L_{\text{ref}} \cdot C_l$	Rolling moment coefficient	C_l
$M = q \cdot S_{\text{ref}} \cdot L_{\text{ref}} \cdot C_m$	Pitching moment coefficient	C_m
$N = q \cdot S_{\text{ref}} \cdot L_{\text{ref}} \cdot C_n$	Yawing moment coefficient	C_n

Thanks to these coefficients, drag coefficient can be define.
In general, talking about the drag in reentry phase, it use the aerodynamic frame relating to the air flow $(\{O_{xa}, O_{ya}, O_{za}\})$. This reference frame is obtained from the vehicle frame through a rotation $-\alpha$ around O_y, followed by a rotation β around O_{za} (see figure 29).
In this new reference frame, the axis O_{xa} is along the relative velocity $\vec{V_R}$ of the vehicle, and axis O_{za} is normal to $\vec{V_R}$ in the pitch plane.
The drag and the lift are the components, with opposite signs, of the aerodynamic force along O_{xa} and O_{za}. The side-slip force is along O_{ya}.In particular the drag coefficient of the capsule is define by:

$$C_D = (C_A \cdot \cos\alpha + C_N \cdot \sin\alpha) \cdot \cos\beta - C_Y \cdot \sin\beta \tag{2.2}$$

Taking into account the case studied, namely that of a Martian capsule, the objective is to decelerate a scientific payload or a human crew from an elliptic or hyperbolic outer atmosphere trajectory to a low supersonic velocity at a suitable altitude in order to initiate a soft landing.
To reach this requirements, deceleration must occur at the highest possible altitude, design a shallow trajectory (small path angle) and select a blunt aeroshell, which offers a low ballistic coefficient:

$$\beta = \frac{m}{S_{\mathbf{ref}} \cdot C_D}. \tag{2.3}$$

Hence, the aeroshell must have a shape that ensures a high value of the drag parameter $S_{\text{ref}} \cdot C_D$..
For all these reasons, The most usual shapes are:

- Sphere or spherical cap manned capsule
- Sphere–cone with high semiapex angle
- Sphere–cone with medium semiapex angle

The MSL capsule has as the shape the second type of the list.
Applying this theory to the model to be simulated and considering that the descent is completely vertical ($\alpha = 0$ and $\beta = 0$), the drag coefficient of the MSL capsule can be estimate as follow:

$$\cos(0) = 1 \tag{2.4}$$

$$\sin(0) = 0 \tag{2.5}$$

$$C_D = C_A \tag{2.6}$$

The value of axial force coefficient can be take from the following graph (figure 30) which represents Axial force coefficients in the continuous regime of a 70° sphere cone configuration similar to MSL:

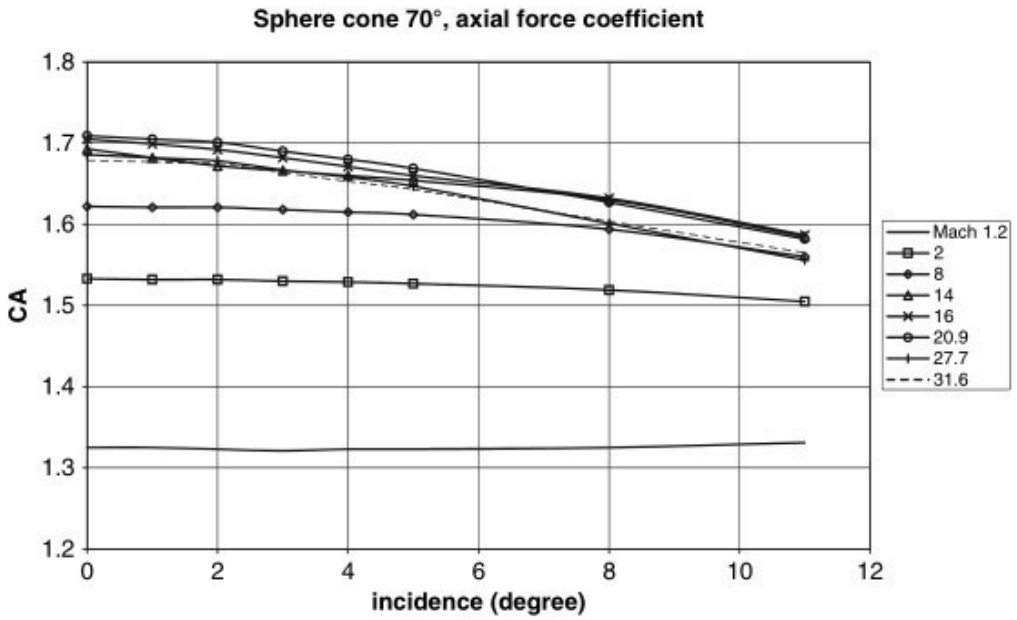

Figure 30: Axial force coefficients in the continuous regime of a 70° sphere cone configuration

$$from \quad 2.6 \qquad C_D = C_A = 1.53 \quad at \quad Mach = 2$$

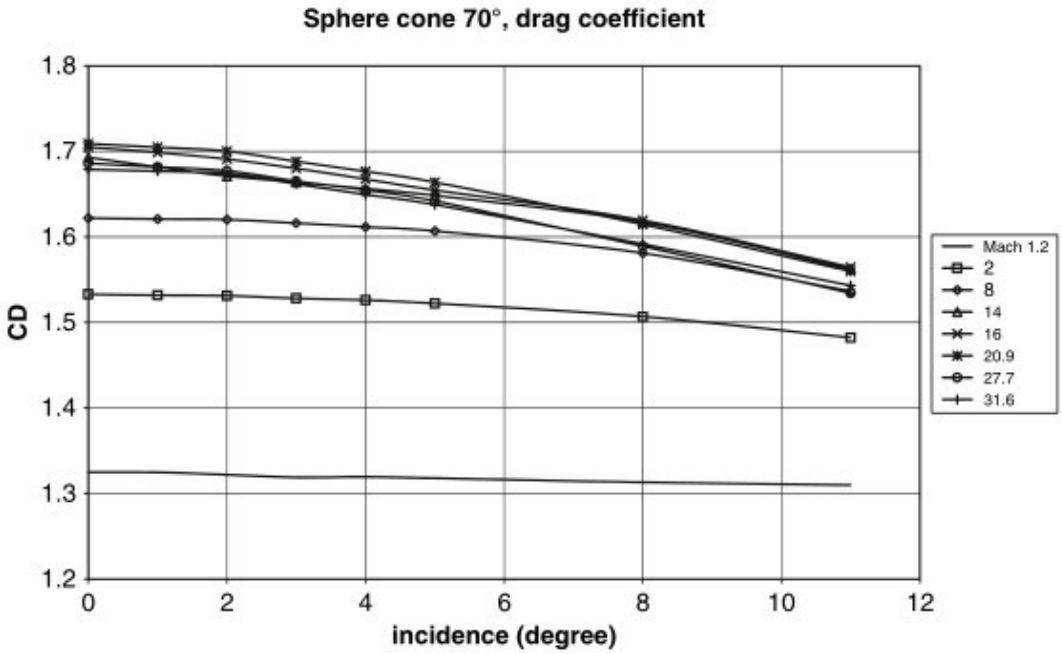

Figure 31: Drag coefficients in the continuous regime of a 70° sphere cone configuration

The results of capsule phase of the simulation were obtained following the logical flowchart wchich was implemented in Matlab:

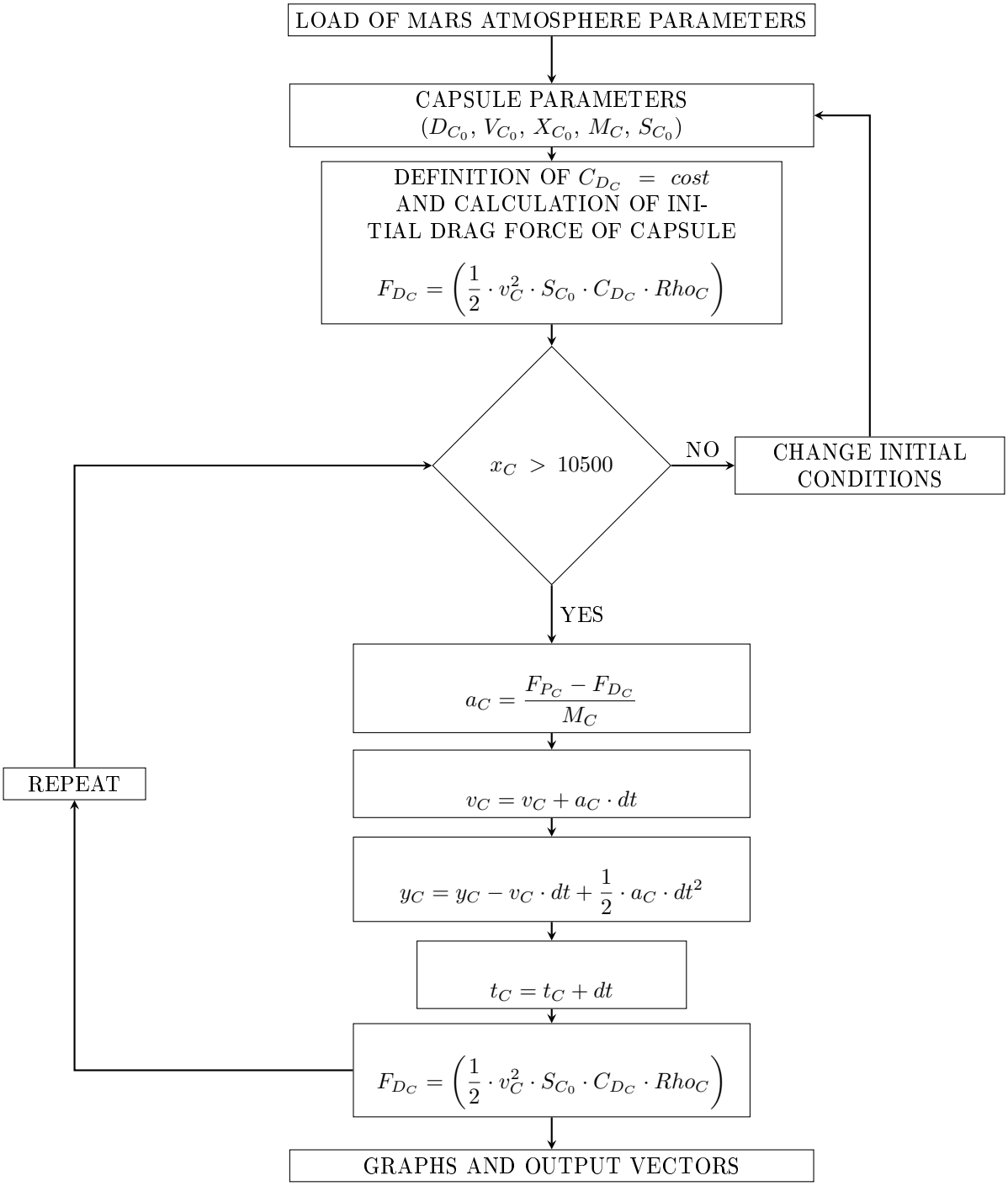

Taking the above flowchart as a reference, we can understand that in order to obtain the desired results, a method based on the assumptions described in the beginning of this chapter and basic considerations has been adopted. In other words it can be considered a simplified numerical model. This logical sequence of commands aims to determine the trajectory of the capsule in terms of velocity, altitude, acceleration, and the drag force experienced during descent.

Starting from the beginning, it has been decided to simulate the descent phase of the capsule starting from a fixed altitude (25 km), a known initial velocity (520 m/s). In addition, also the initial drag force

is known through the estimation of the resistance coefficient made previously.
After the definition of the starting parameters of the simulation, it was utilized a while loop control structure, in particular, as stopping condition for the iterations, it has been decided to set a known final altitude. This final altitude of 11 km derives from reports on a real NASA mission.
Inside of this loop of iterations, to estimate the capsule motion during the descent, the second Newton's law ($F = m \cdot a$) was taken as the starting point. This fundamental law of motion allows to determine the deceleration experienced by the capsule durinr the descent due to the function of the heat shield, which also protects the rover. Once this parameter has been estimated, using the laws of uniformly decelerated motion, other parameters of the capsule's motion such as position, velocity, and time have been calculated.
Finally, at each iteration, the calculation of the drag force on the capsule is updated to simulate the descent and the corresponding change of the atmospheric density.
The results of the simulation of the MSL capsule phase are reported in the following graphs:

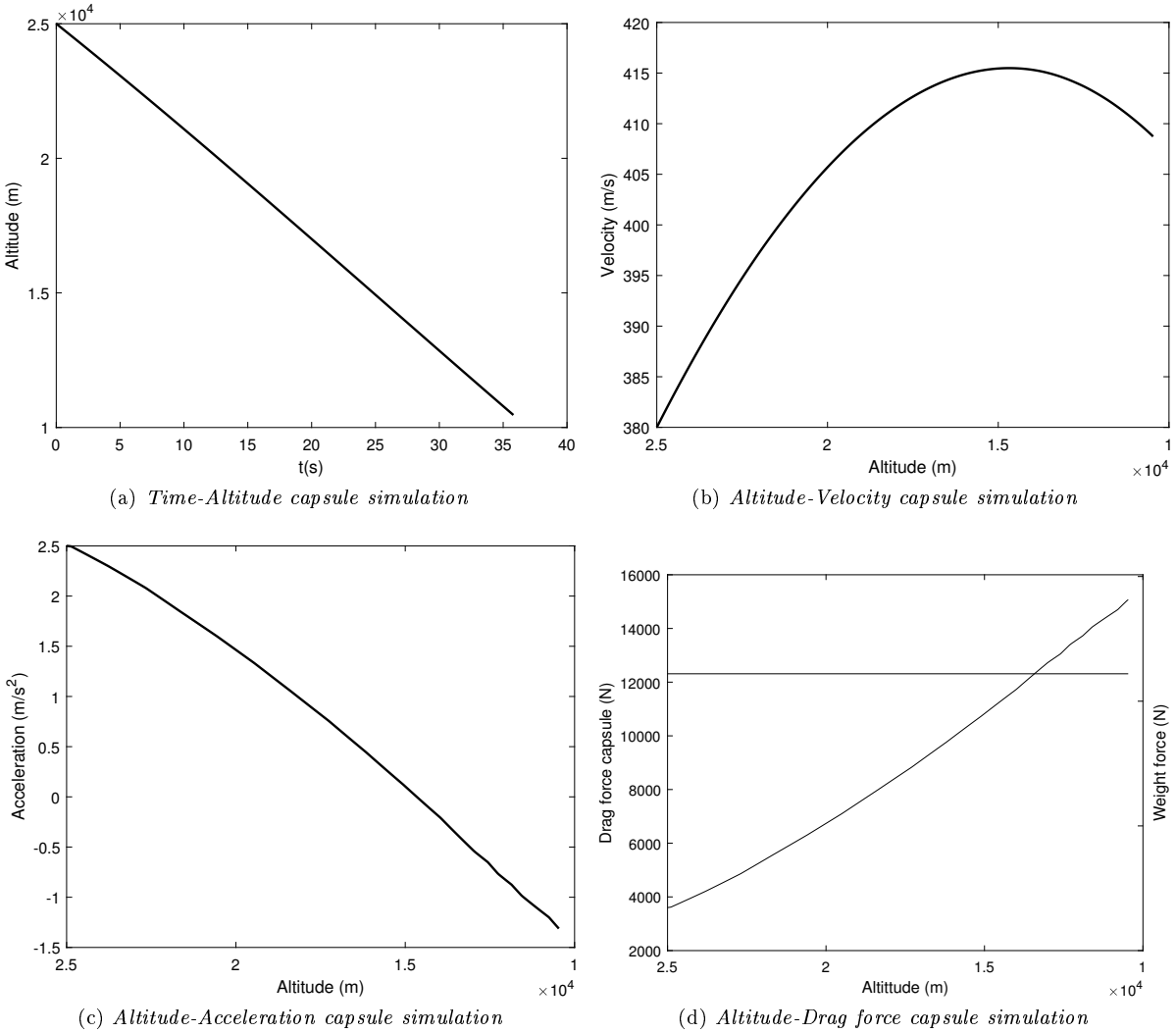

(a) *Time-Altitude capsule simulation*

(b) *Altitude-Velocity capsule simulation*

(c) *Altitude-Acceleration capsule simulation*

(d) *Altitude-Drag force capsule simulation*

Figure 32: Capsule simulation results

These initial results show how the altitude and velocity of the capsule follow a characteristic pattern of uniformly decelerated motion. In fact, the decelerating effect of the thermal shield can be observed in the graph representing the acceleration. It can be seen that as the altitude decreases and the atmospheric density of Mars increases, there is an increase in acceleration in the opposite direction of motion (de-

celeration). This phenomenon is explained by observing the behavior of the drag force exerted by the thermal shield, which increasingly opposes the motion of the capsule as the atmospheric density rises, consequently slowing it down.
Taking into account the basic assumptions and considerations made for this simplified simulation, in this initial part, the dominant parameters that influence the deceleration during the descent of the capsule are the density of Mars and the descent velocity. In fact, since the diameter of the capsule and its coefficient of drag are constant, the two previously mentioned parameters are interdependent and determine the deceleration of the capsule. It is also worth noting that initially, despite being subject to the drag force, the capsule experiences acceleration due to the fact that the weight force is greater than the opposing force to the motion.

2.2.4 DESCENT PHASES: PARACHUTE DEPLOYMENT AND INFLATION

In this first part of the subsection are simulated the events occurring from mortar firing ($t = t_{MF}$) to suspension lines stretch at ($t = t_{LS}$). In the other words, the time at the mortar firing is defined as the event at which the mortar recoil force starts. Instead, the time at suspension lines stretch is defined as the time at which canopy starts to emerge from the deployment bag.
To estimate the deployment time was used an empirical and simplified model based on data from previous missions [10].
Throw this model, the time at suspension lines stretch is calculated from the folloqing equation:

$$t_{LS} = t_{MS} + \frac{H_{TB} + L_R + L_S}{\bar{V}_{MF-LS}} \tag{2.7}$$

Regarding the parameters in formula 2.7, they are defined by the figure 33.
Instead $\bar{V}_{MF-LS}$ is the average deployment bag speed from mortar fire to suspension lines stretch. It is defined as:

$$\bar{V}_{MF-LS} = V_{Muzzle} \cdot [0.875 + (0.060 \cdot U[0,1) - 0.030] \tag{2.8}$$

$$V_{Muzzle} = 39\,\mathrm{m/s} + [4\,\mathrm{m/s} \cdot U[0,1) - 2\,\mathrm{m/s}] \tag{2.9}$$

Note that The quantity $U[0,1)$ is a random variable with uniform distribution in the interval between 0 (inclusive) and 1 (not inclusive).
At suspension lines stretch, the parachute "appears" in the simulation and its aerodynamic and inertial characteristics become active.

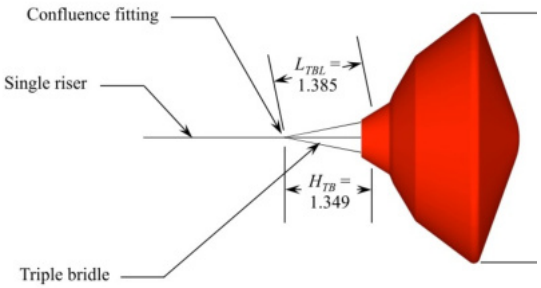

Figure 33: Dimensions capsule systems

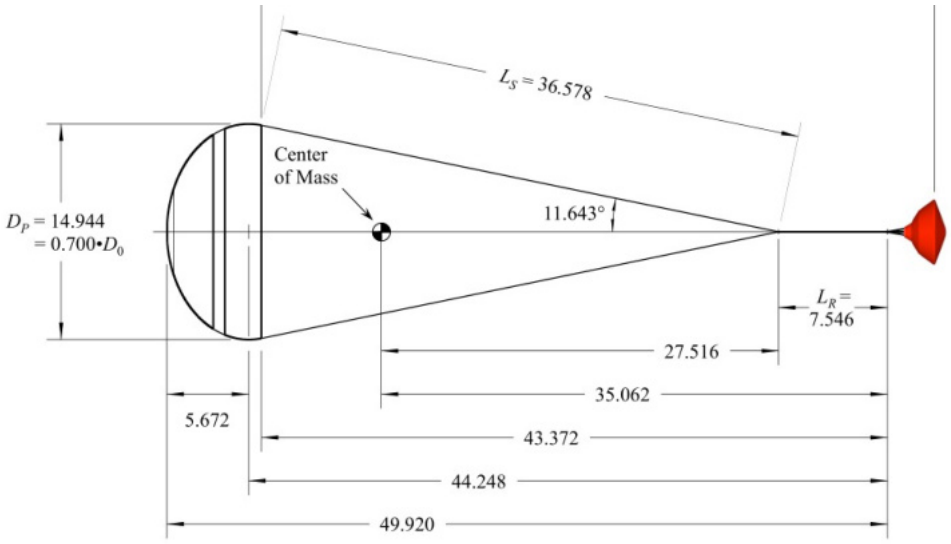

Figure 34: Dimensions parachute systems

Once the deployment has occurred and the state of line stretch has been reached, the inflation phase takes place.
The inflation phase represents the events occurring from suspension lines stretch up to, but not included, the first full inflation of the canopy ($t = t_{FI}$).The time at first full inflation is calculated from the equation 2.10:

$$t_{FI} = t_{LS} + \frac{D_o}{\bar{V}_{inf}} \tag{2.10}$$

where,

$$\begin{gathered} \bar{V}_{inf} = 29\,\mathrm{m/s} + [7\,\mathrm{m/s} \cdot U[0,1) - 3.5\,\mathrm{m/s}] \quad \text{is the average inflation speed} \\ D_o = \text{nominal parachute diameter} \end{gathered} \tag{2.11}$$

Once the deployment phase has been examined and the time required for the inflation process to reach the "first inflation" of the canopy has been estimated, the variation of the drag force generated by the parachute during this very short time interval has been analyzed [10].
In the analysis was simulated only inflation drag force because the forces and moments generated by the parachute during deployment are a small fraction of those encountered during inflation.
Because of this, parachute deployment forces (except for the mortar recoil force) and moments are assumed to be zero in the present model.
Instead parachute aerodynamic forces and moments during inflation are controlled by a time-dependent non-dimensional variable (K_I) which is used as multiplier for the parachute tangential, normal and pitching moment coefficients (C_T, C_N, C_{m_o}). In the present one dimensional model, only C_N in considered because the motion is only vertical. (K_I) is used during the time interval from (t_{LS}) to (t_{FI}) and defined by:

$$\begin{gathered} \text{for } t_{LS} \leq t < t_{FI} \text{ (Inflation) } K_I = C_X + \left(\frac{t - t_{FI}}{t_{FI} - t_{LS}}\right)^{n_I} \\ C_X = 1.407 \\ n_I = 4 \end{gathered} \tag{2.12}$$

CX is the opening load factor and nI is the exponent of the inflation prescribed area growth power function.

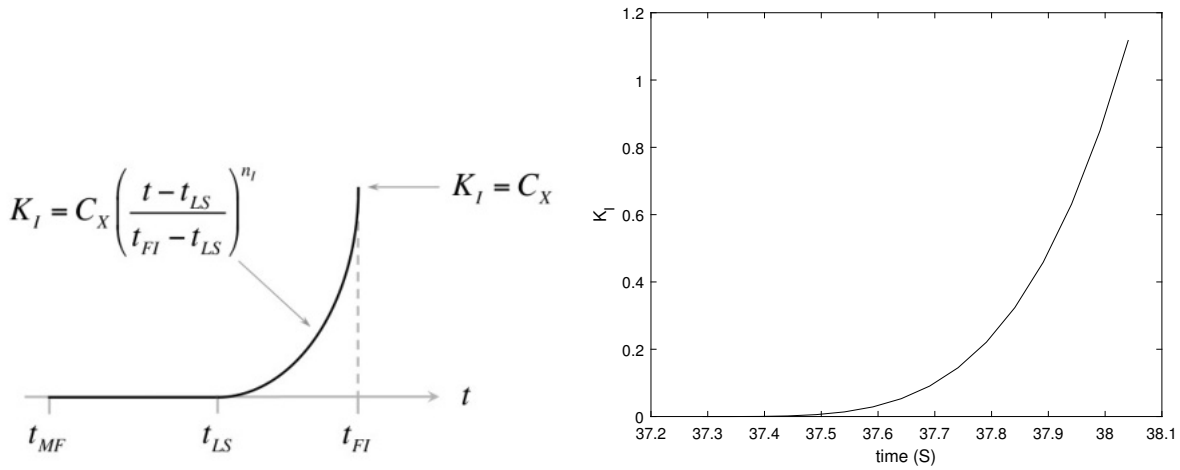

(a) *Reference K_I trend* (b) *Simulated K_I trend*

Figure 35: K_I trend comparision

The estimation of this factor allowed simulating the variation of the drag force during this important phase of the descent of the capsule on Mars, which is represents in the following figure:

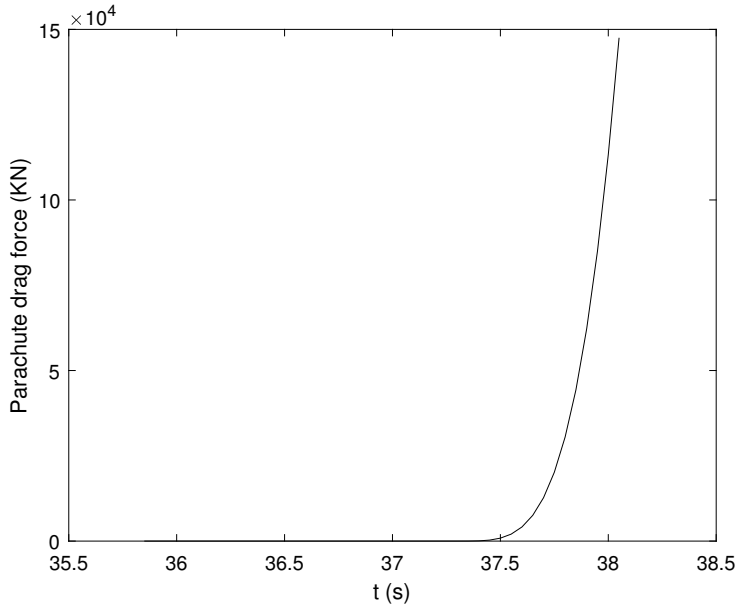

Figure 36: Opening parachute drag force during inflation

From the figure 36, it can be observed how, after an initial phase where only the capsule has a decelerating effect, there is a sudden and exponential increase, representing the parachute opening and the beginning of significant deceleration of the capsule.
Finally, the inflation process ends with the peak opening drag force.
In this model the first full inflation is assumed to be coincident with the inflation first peak force. The parachute aerodynamic force at first full inflation is calculated from the equation 2.13

$$F_{FI} = q_\infty C_X S_0 (C_T^2 + C_N^2)^{\frac{1}{2}} \tag{2.13}$$

where the values of the dynamic pressure, q_∞, C_T and C_N are those at t = t_{FI}.
Considering the one dimensional model simulated, $C_N = 0$ and $C_T = 0.55$.

C_N and C_T are the static aerodynamic coefficients in the model taken as reference for the simulation. They are specified as functions of the total angle of attack, $\alpha_{P,Tot}$.
The orientation of the forces and moments they represent are defined with respect to the total angle of attack plane:

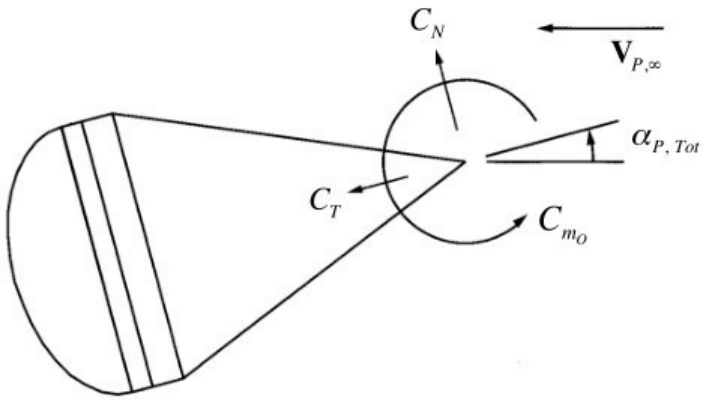

Figure 37: Parachute static aerodynamic coefficients.

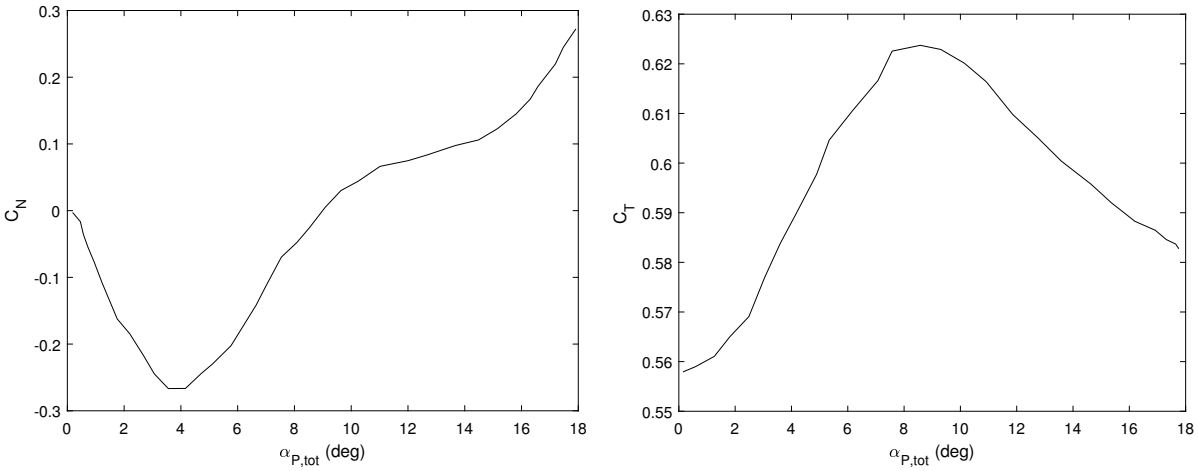

(a) C_N *Trend* (b) C_A *Trend*

Figure 38: Parachute static aerodynamic coefficients model

These parachute aerodynamic coefficients represents ad additional perturbation for the simuation and the $\alpha_{P,Tot}$ rappresents the random angle respect of the capsule and the motion direction that there can be during the inflation phase of the supersonic parachute.
In the present one dimensional simulation, vertical descent was simulated taking $\alpha_{P,Tot} = 0$ in order to have supersonic parachute and capsule along the same axis of motion.

2.2.5 DESCENT PHASES: PARACHUTE FULL INFLATED

The last event studied in this simulation concerns what happens after the inflation phase, namely the controlled descent of the capsule using the parachute system. During this time interval, two important phenomena occur that influence the parachute's performance: apparent mass and parachute area oscillations.

About the area oscillations phenomenon (see figure 39), previous flight with DGB parachutes indicates that for Mach numbers above 1.4, large parachute force oscillations occur after the first inflation peak force.

They are partially related to changes in the projected area of the parachute during this time interval, as the parachute undergoes collapse and re-inflation cycles, and are commonly referred to as area oscillations phenomenon. An important contributor to these area oscillations is interaction between the aeroshell wake and parachute flow fields.

In the present simulation was included a model to study this phenomenon and to improve the fidelity of the aeroshell dynamics results obtained from the simulation. The area oscillations model described here is synthetic, in the sense that it simulates area oscillations without modeling the underlying physics.

The area oscillations model calculates a Mach number- and time-dependent nondimensional parameter, $K_{AOM}(M,t)$, that is used as a multiplier for the parachute tangential, normal, and pitching moment coefficients (C_T, C_N, C_{m_o} respectively).However in the present simulations it is used as multiplier factor for parachute area S_0 in order to simulate the phenomenon.

Area oscillations phenomenon model [10] is used between the first full inflation, t_{FI} , and the time at which the Mach number is 1.4. The value of K_{AOM} was estimate using a function consisting of a randomized sinusoidal oscillatory term constrained as follows:

- by an exponential function to drive K_{AOM} to 1.0 as the Mach number approaches 1.4
- by limiting the upper value of K_{AOM}
- by limiting K_{AOM} to positive values

Due to the interactions between the area oscillations model and the elastic modes of the parachute system, it is possible to obtain unrealistic values of the Mach number at the center of mass of the parachute. This is caused by the rapid motion of the parachute, leading to nonphysical feedback with the area oscillations and Mach Efficiency Factor models that will be discussed in this chapter.

In other words, the dynamic behavior of the parachute can cause deviations from expected Mach numbers at its center of mass, introducing inaccuracies in the area oscillations and Mach Efficiency Factor models. Thus, is used the Mach number of the center of mass of the aeroshell, not that for the parachute center of mass. The model used in the calculation of K_{AOM} is given in the appendix.

The Mach number time history starts near parachute inflation first peak force. Note that the calculated values of K_{AOM} exhibits a random oscillatory behavior about a value of 1.0, its magnitude decreases with M , and becomes equal to one at M =1.4.

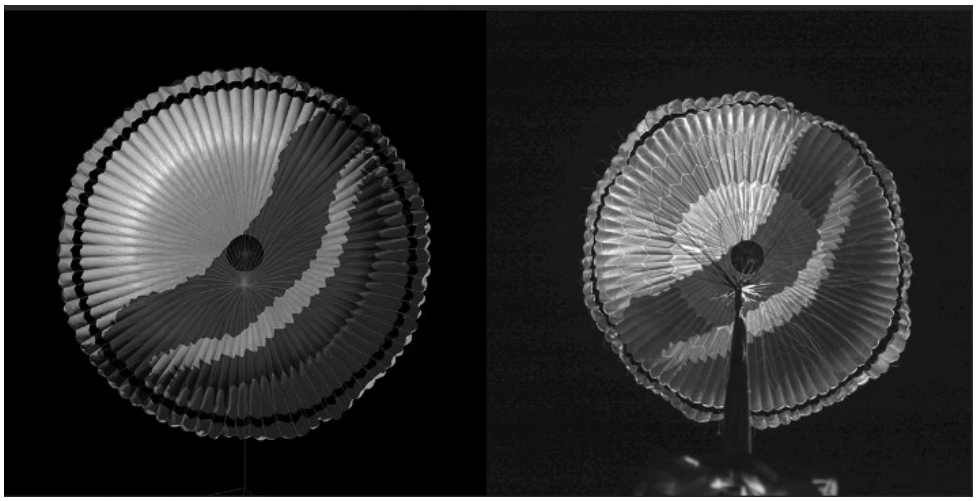

Figure 39: Area oscillations DGB supersonic parachute

Regarding the mathematical aspect of the model, it will be presented in the appendix section, while a graphical representation of reference model is shown in the following figure:

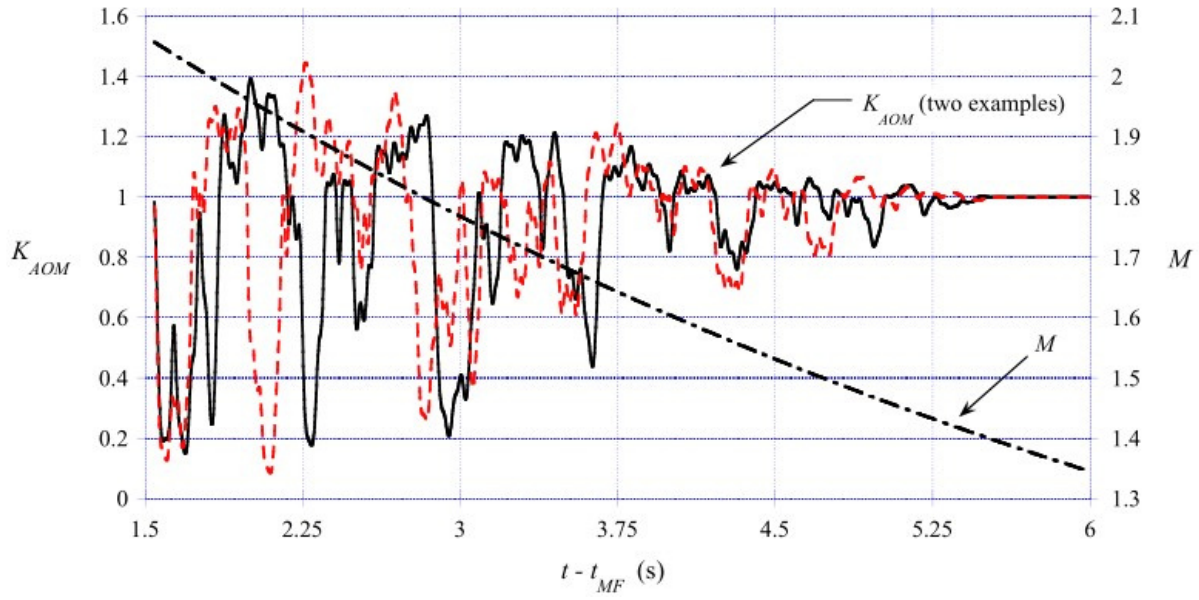

Figure 40: Reference K_{AOM} multiplier factor Model

The verification of the empirical model was performed using a MATLAB code containing a sequence of equations (see the appendix). In particular, the same time intervals and Mach values were considered for the simulation to achieve the most accurate comparison possible.
The obtained result is graphically shown in figure 41, where it can be seen that the amplitude of the frequencies is in agreement when compared to the reference model. The fact that the oscillations are different should not be taken into consideration as the model is based on random variables, making the phenomenon itself random. For this reason, the implemented model can be considered reliable based on these considerations. figure 42 depicts the model obtained from the one-dimensional simulation. In this case as well, considering the random component of the phenomenon, the result cannot be directly compared to the reference. However, it can be stated that the amplitudes of the frequencies obtained are

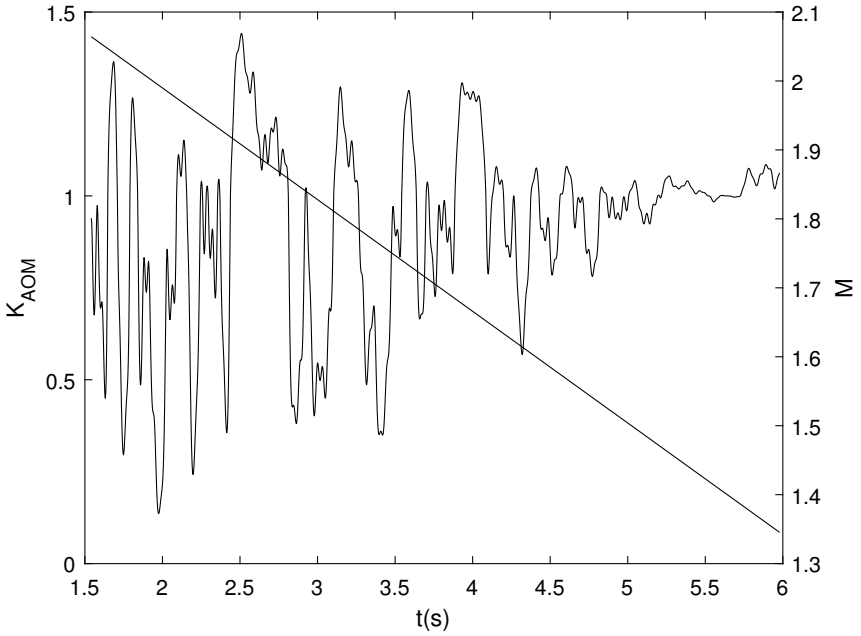

Figure 41: Verification K_{AOM} multiplier factor model

in agreement with the reference model. Regarding the different number of oscillations and, especially, the different time at which this phenomenon occurs (x-axis), the reason lies in the simulated model. In other words, considering that the model simulates a purely vertical descent and does not include all the factors influencing the descent to make the simulation realistic, it results in a different range of Mach numbers where the phenomenon occurs, and the transition from the initial Mach (M=1.7373) to the final Mach (M=1.4) is much faster than in the reference model. Consequently, the parachute area oscillations occur within 1.8 seconds.

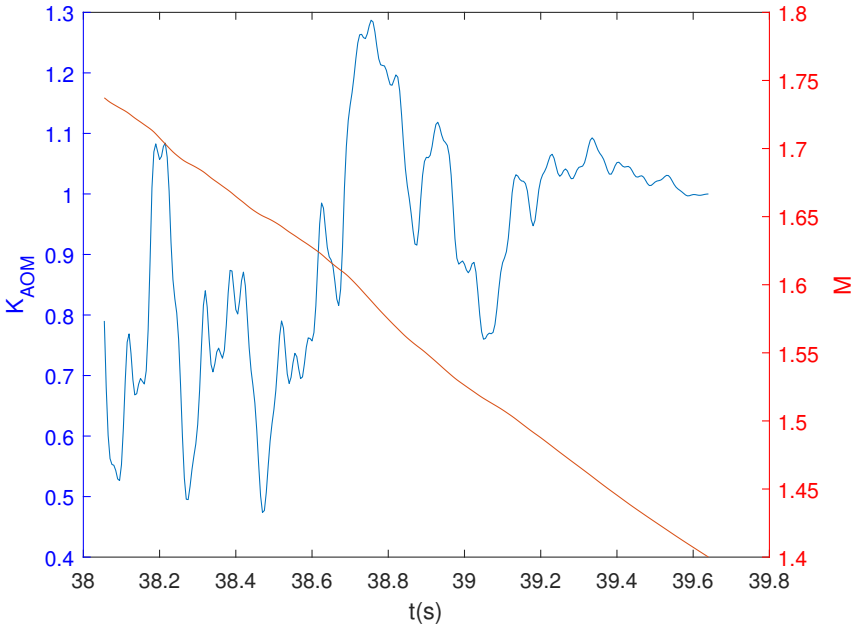

Figure 42: Multiplier factor K_{AOM} trend.

The other phenomenon considered that influences the descent of the capsule is the "apparent mass".
It is the term used to describe the mass of the fluid inside and around the parachute that generates aerodynamic forces proportional to the parachute's accelerations.
The model used to simulate "apparent mass" consists of a single point mass coincident with the physical center of mass of the parachute. The parameter m_{App} is dependent on the Mars atmospheric density at the parachute's center of mass,ρ_∞, and the parachute's nominal diameter, D_0.
The apparent mass is calculated from the following equation:

$$m_{App} = K_{App}\rho_\infty \pi D_0^3 \tag{2.14}$$

where K_{App} is the apparent mass coefficient,

$$K_{App} = \mathrm{T}[0, 0.035, 0, 070] \tag{2.15}$$

The parameter T[0, 0.035, 0.070] is a random number with triangular distribution whose lower limit is 0, its mode is 0.035, and its upper limit is 0.070. In the simulation the apparent mass is subject to the force of gravity. To counteract the force of gravity on the apparent mass an opposite buoyancy force vector, F_B , of magnitude:

$$F_B = m_{App} g_{Mars} \tag{2.16}$$

where g_{Mars} is the local acceleration of gravity acts on the parachute's center of mass.
This model becomes active when the parachute reaches its first full inflation, and remains active thereafter.

Like in the first part of the simulation, the "causal phase," the same logical procedure represented by the following flowchart was used for this phase of the simulation as well.

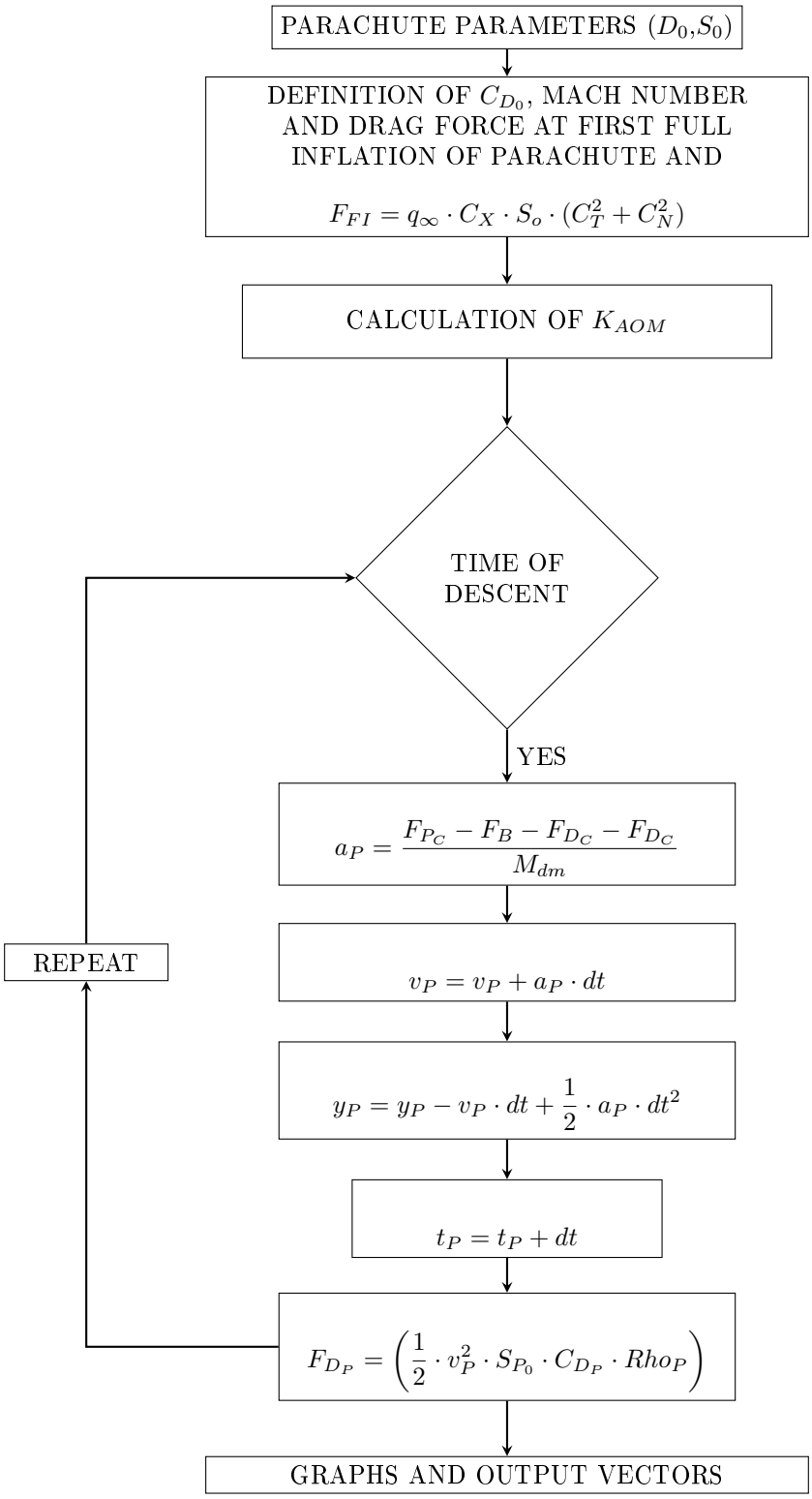

Specifically, the simulation of the supersonic parachute area oscillations phenomenon was implemented in the code as follows:

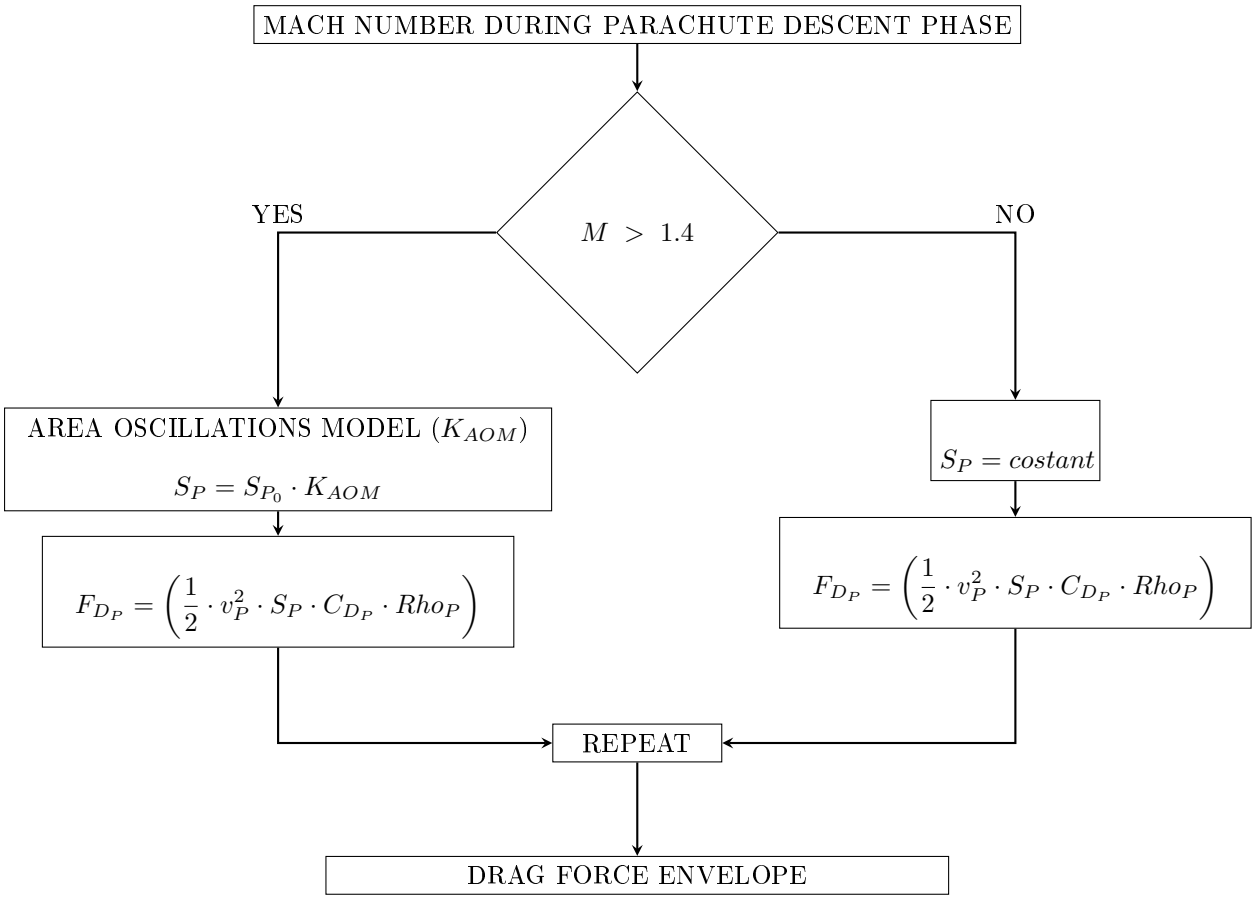

The parachute drag coefficient reference model is defined as functions of Mach number only. it was generated from an amalgamation of data from Viking wind tunnel tests, Viking BLDT flight tests, Phoenix Mars flight data and MSL-specific wind tunnel tests.
This model is rapprsented in the figure 43:

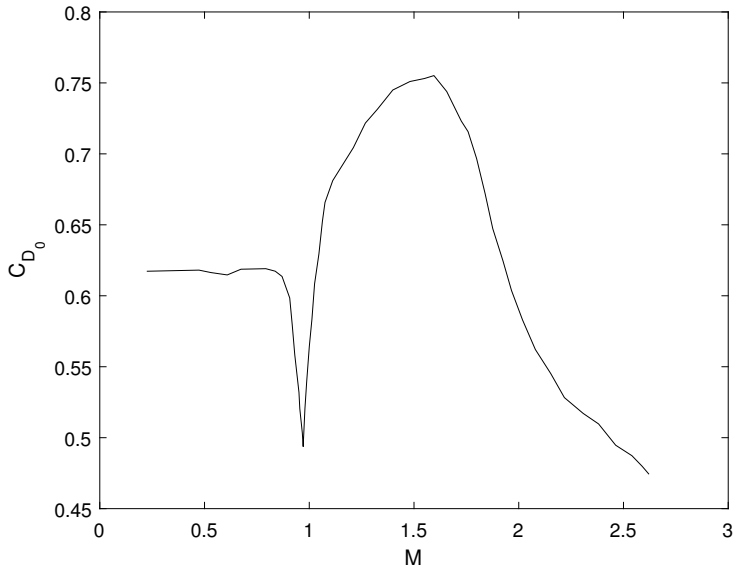

Figure 43: Nominal parachute drag coefficient model.

It assumes that C_{D_0} is independent of Mach number for $M \leq 0.8$ while a transonic drag dip occurs near M = 0.95.
This behavior has been observed in wind tunnel test and it is due to interaction between the aeroshell and parachute flow fields. Finally the drag coefficient increases and peaks at a Mach number of approximately 1.5, but then decreases again at higher Mach numbers. The last effect took in account in this phase of the simulation regards the "Mach Efficiency Factor (MEF)" [10].It is calculated by equation 2.17:

$$MEF = \frac{C_{D_0}\text{nominal}}{CD_0\text{nominal}|M = 2} \tag{2.17}$$

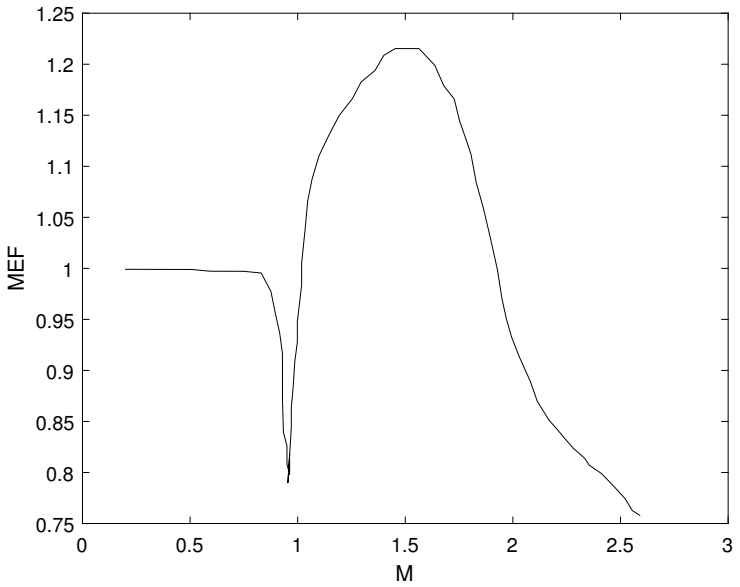

Figure 44: Mach Efficiency Factor (MEF) model.

2.3 DESCENT TWO-DIMENSIONAL MODEL

In the first part of second chapter the simulation was based on simplified one-dimensional models, considering only the motion along a single axis, typically the vertical direction. While the model provided valuable insights into the descent phase, they had limitations in capturing the complex dynamics of the spacecraft and the atmospheric interactions.

To overcome these limitations and achieve a more faithful representation of the parachute's behavior during descent, a transition was made to two-dimensional simulations, which consider both the motion along the x-axis (horizontal) and the y-axis (vertical).

The shift from a mono-dimensional model to a two-dimensional simulation was driven by the need to account for lateral forces, such as aerodynamic drag and lift, which significantly affect the trajectory and stability of the descending spacecraft.

By incorporating the motion along both axes, the simulation can capture the complex interactions between the spacecraft, the atmospheric conditions, and the resulting forces acting upon it.

The two-dimensional simulation also enables a more comprehensive assessment of critical events during descent, such as parachute deployment and inflation. The interaction between the parachute and the surrounding atmosphere, including the oscillations in the parachute area, can be captured more realistically, leading to improved predictions of the forces acting on the capsule and its subsequent behavior.

Overall, the transition from a one-dimensional model to a two-dimensional simulation is a significant advancement in accurately capturing the dynamics of the spacecraft and its interaction with the Martian atmosphere.

2.3.1 INITIAL CONDITIONS, HYPOTHESIS AND TRAJECTORY EQUATION

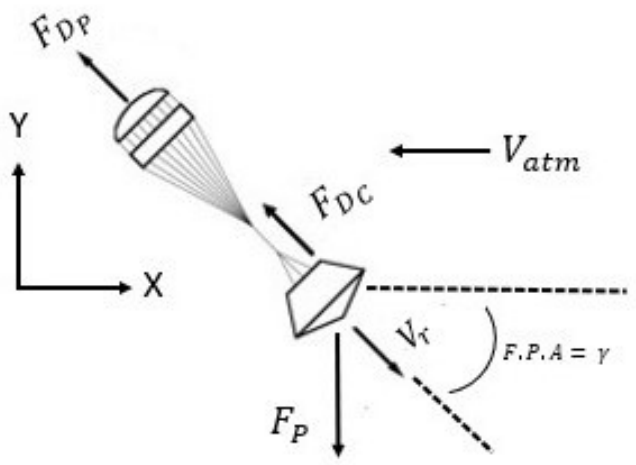

Figure 45: Simulation model

Figure 45 illustrates the two-dimensional simulated model. The bidimensionality is due to the flight path angle (F.P.A).

The flight path angle of a Mars entry capsule refers to the angle between the capsule's trajectory and the local horizontal plane as it enters the Martian atmosphere. It indicates the steepness or shallowness of the descent trajectory.

A positive flight path angle means that the capsule is descending at a shallower angle, while a negative flight path angle indicates a steeper descent. The specific flight path angle chosen for a Mars entry depends on various factors, including the mission objectives, desired landing site, atmospheric conditions, and the

capabilities of the entry system.
In general, it is an important parameter to consider during the entry phase, as it affects the amount of deceleration and the overall trajectory of the capsule as it passes through the Martian atmosphere. Controlling the flight path angle allows mission planners to optimize the entry trajectory and ensure a safe and targeted landing on Mars.
The transition to two-dimensionality also allows for the analysis of capsule verticalization during descent. In other words, in two dimensions, it is possible to simulate the variation of the flight path angle and visualize how the orientation of the capsule changes due to the action of the drag force experienced.
Then, an additional perturbation element was incorporated into the simulation to make it more realistic. As can be observed from the image, the velocity of the Martian atmosphere was taken into consideration. In particular, to simplify the simulation, the following assumption was made:

- Equatorial reentry on Mars, where the atmosphere rotates with the rotation of the planet.

With this hypothesi, the velocity of the atmosphere can be approximated as parallel to the x-axis and in the opposite direction of the capsule motion. It is defined by following equation:

$$V_{Atm} = \omega \cdot r \tag{2.18}$$

where r is the dustance from the center of Mars:

$$r = R_M \cdot h \tag{2.19}$$

In this case, the initial conditions for the capsule and parachute were based on the MSL (Mars Science Laboratory) mission by NASA.
By using the initial conditions from the MSL mission, such as the capsule's mass, dimensions, and initial velocity, as well as the parachute characteristics, the simulation sought to provide a more realistic representation of the dynamics and behavior of the descending capsule during the equatorial reentry on Mars. It's worth noting that the utilization of the MSL mission's initial conditions does not imply an exact replication of the mission or its specific trajectory. Instead, it serves as a reference and starting point for simulating a similar descent scenario on Mars, taking into account the unique characteristics and challenges of an equatorial reentry.
Regarding the equations used to simulate the trajectory of the capsule during the descent, even for two-dimensional models, the second law of Newton was used : $m \cdot a = \sum F$.
Then, by utilizing the flight path angle,(γ) which is defined as the angle of the motion direction with respect to the hypothetical plane of the horizon, the vertical ($\sin(\gamma)$) and horizontal ($\cos(\gamma)$) components of motion were derived.
In particular,the motion equations are presented in the following system of equations:

$$\begin{cases} m \cdot a_y = \sum F_y \\ m \cdot a_x = \sum F_x \end{cases} \tag{2.20}$$

from the system equations above a_y and a_x are extracted.
Once the components of acceleration are defined, it is possible to derive the components of velocity:

$$\begin{cases} v_y = v_y + a_y \cdot dt \\ v_x = v_x + a_x \cdot dt \end{cases} \tag{2.21}$$

and position of the capsule:

$$\begin{cases} y = y - v_y \cdot dt + \frac{1}{2} \cdot a_y \cdot dt^2 \\ x = x - v_x \cdot dt + \frac{1}{2} \cdot a_x \cdot dt^2 \end{cases} \tag{2.22}$$

To obtain the simulation of the trajectory and variations of the variables involved, iterations over time were performed using a while loop for these systems of equations.
In particular, the main variation concerns the drag force, which consequently affects all the other variables since they depend on it.
The variation of the drag force follows the law:

$$F_D = \left(\frac{1}{2} \cdot v^2 \cdot S \cdot C_D \cdot Rho \right) \tag{2.23}$$

$$\begin{cases} F_{D_x} = F_D \cdot \cos(\gamma) \\ F_{D_y} = F_D \cdot \sin(\gamma) \end{cases} \tag{2.24}$$

From equation 2.23 it can be observed how the variation of F_D is caused by the changes in atmospheric density, parachute drag coefficient, and system velocity during descent.
This simulation process has been implemented for each phase of the descent considering the different variable for each phase.
In fact, for the capsule phase the motion equation are:

$$\begin{cases} m_C \cdot a_y = F_P - F_{(D_C)_y} \\ m_C \cdot a_x = -F_{(D_C)_x} \end{cases} \tag{2.25}$$

while, for the phase with also supersonic parachute are:

$$\begin{cases} m_{DM} \cdot a_y = F_P - F_B - F_{(D_C)_y} - F_{(D_P)_y} \\ m_{DM} \cdot a_x = -F_{(D_C)_x} - F_{(D_P)_x} \end{cases} \tag{2.26}$$

Regarding the intermediate phase of the simulation about deployment and inflation of supersonic parachute, it follows the same numerical of the one dimensional model.
In this two-dimensional model, the capsule's verticalization during descent is also simulated. This is possible through simulating the variation of the F.P.A angle due to the change in descent velocity caused by resistance forces.
Specifically, this variation occurs in both the x and y directions of motion, allowing the evaluation of the new angle at each step using the following formulas:

$$\text{F.P.A} = \lambda = \arctan\left(\frac{-V_y}{V_x} \right) \tag{2.27}$$

At the end of the simulation, what we expect is a gradual variation from the initial angle to 90° in the last phase before reaching the final part of the Entry, Descent, and Landing (EDL) sequence.

2.4 PERTURBATION PHENOMENA CONSIDERED

For the two-dimensional model, like the one-dimensional model, several phenomena characterizing the descent of a capsule on Mars have been considered.
In particular, these are:

- Aerodynamic forces: The interaction between the capsule and the Martian atmosphere
- DGB supersonic parachute C_D database
- Gravity: The gravitational force exerted by Mars, which influences the capsule's motion and descent speed
- Parachute deployment: The deployment and dynamics of a parachute system used for slowing down the capsule during descent.
- Multiplier coefficient K_I model to simulate the parachute drag force during inlfation process until the first full inflation
- Parachute area oscillations model: calculation of multiplier factor K_{AOM}
- Apparent mass contribution during the descent with full inflated parachute
- Flight path angle variation to simulate the verticalization of the descent phase
- Perturbation due to mars atmospheric velocity along x-axis

Regarding the K_{AOM} model obteined for the 2D-simulation model, it is rappresented in the following figure:

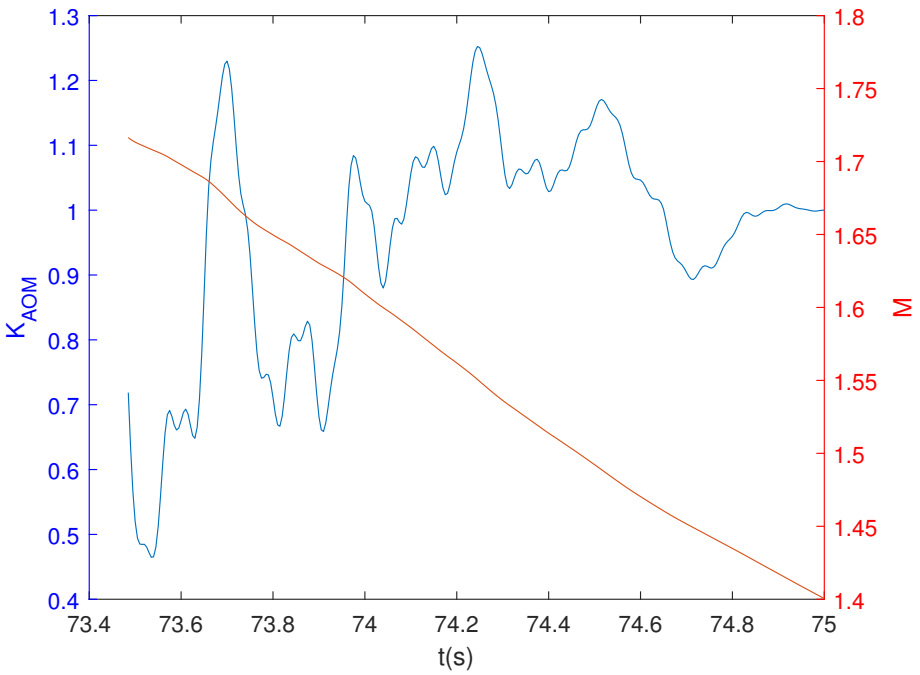

Figure 46: Multiplier factor K_{AOM} trend.

3 RESULTS AND CONSIDERATIONS

In this chapter, the considerations are made regarding the obtained results, particularly by comparing the data with the actual values from the MSL mission. This allows for the verification of the code's performance and the assessment of its level of reliability.
The targets values are contain in the following table [9]:

Table 6: Key events timing and states

Event	$\Delta t_{\mathbf{MF}}$ **(s)**	h **(m)**	γ **(deg)**	M	V **(m/s)**
Mortar fire / deployment	0.000	11000	/	1.752	405
Suspension lines Stretch	1.135	/	/	1.737	/
First full inflation	1.770	/	/	1.695	/
Back shell separation	110	1.600	-85.5	0.324	100

For the values of the drag force exerted by the parachute, the following reference values were used:

- $F_{FI} = 150$ KN and $F_{Design} = 289$ KN

3.1 ONE-DIMENSIONAL SIMULATION

The following graphs show the results, in terms of altitude, velocity, acceleration, and drag force, obtained from the simulation. In each of them, the three phases are separated by dashed vertical lines.

Altitude analysis

Figure 47a represents the variation in altitude (only vertical) of the capsule, starting from an initial altitude of 25 km and reaching a final altitude of 1600 m.
The different behaviors in the three simulated phases are clearly noticeable.
In the first part (capsule phase), where only the capsule is present, the descent is rapid, and the altitude decreases quickly. In the second phase (deployment and inflation phase), Figure 47b, we can observe how the behavior changes during the parachute deployment (from $t_{MF} = 35.80s$ to $t_{FI} = 38.03s$) and during the parachute inflation ($t_{IN} = 0.79s$).
Lastly, in the final descent phase (parachute descent phase), after the parachute is fully deployed and the phenomenon of parachute area oscillations occurs, there is a gradual and controlled decrease in altitude. This is because the capsule is slowed down by the parachute, in addition to the thermal shield.

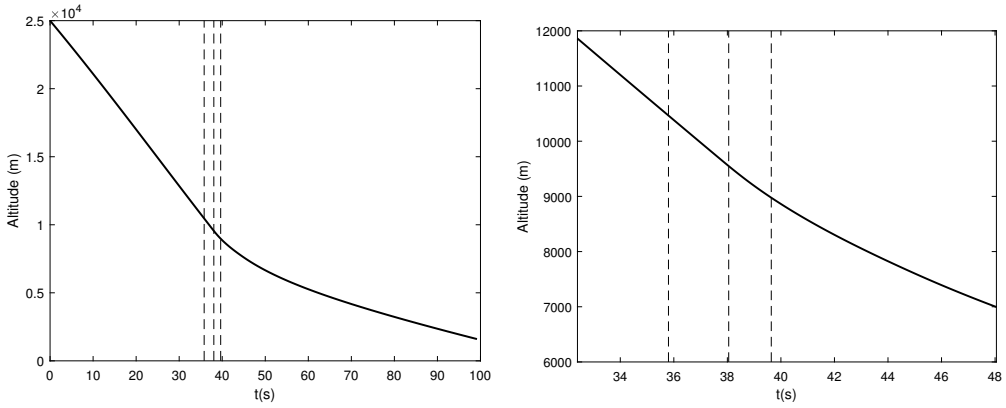

(a) *Total trend* (b) *Deplyment and Inlfation phase*

Figure 47: Vertical descent trajectory of Capsule

Velocity analysis

Figure 48a, the variation in the velocity of the capsule during descent through the Martian atmosphere is depicted. In other words, this graph illustrates the deceleration caused first by the capsule and then by the supersonic parachute.
In particular, it can be observed that in the initial part of the simulation, there is a slight acceleration of the capsule. This is due to the fact that the weight force acting on the capsule is greater than the drag force generated by the thermal shield, which fails to slow down the descent.
Subsequently, as the thermal shield begins to decelerate the capsule and reduce the system's velocity, the deployment, inflation, and stabilization phases of the parachute occur (Figure 43b). This brings the velocity to a steady-state value because the parachute is fully open and stable. The influence of the parachute's opening on the velocity is clearly visible as there is a drastic decrease in just a few seconds due to the deceleration generated by the parachute's drag.

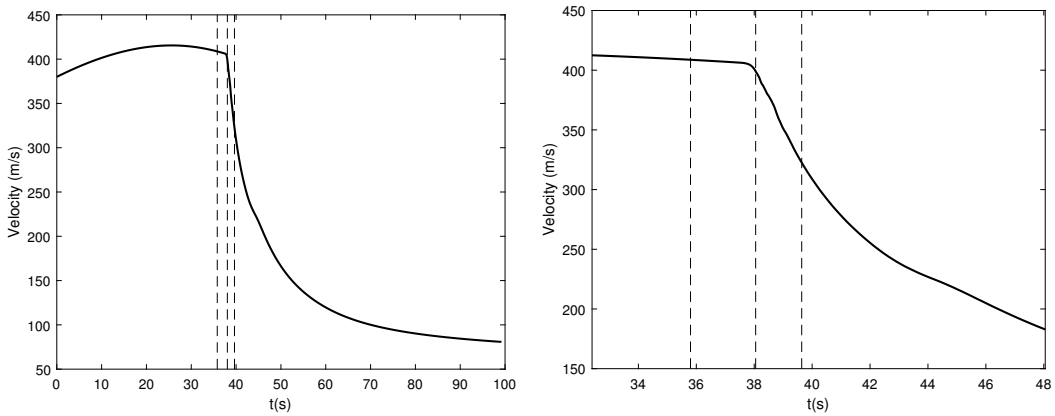

(a) *Total trend* (b) *Deplyment and Inlfation phase*

Figure 48: Vertical descent velocity of Capsule

Acceleration analysis

The trend of the acceleration generated in the opposite direction during descent is depicted in figure 49a. In these graphs, acceleration is negative because the capsule undergoes deceleration during descent, first due to the heat shield and then to the supersonic parachute once it is deployed. Specifically, it is immediately noticeable that during the deceleration phase caused by the heat shield, the acceleration follows a regular trend.
However, when the parachute deployment and inflation phase occurs, there is an initial exponential increase in deceleration, leading to the peak that represents full opening. Subsequently, figure 49b illustrates the phase of parachute area oscillation until reaching a steady value when the descent with the parachute is nominal.

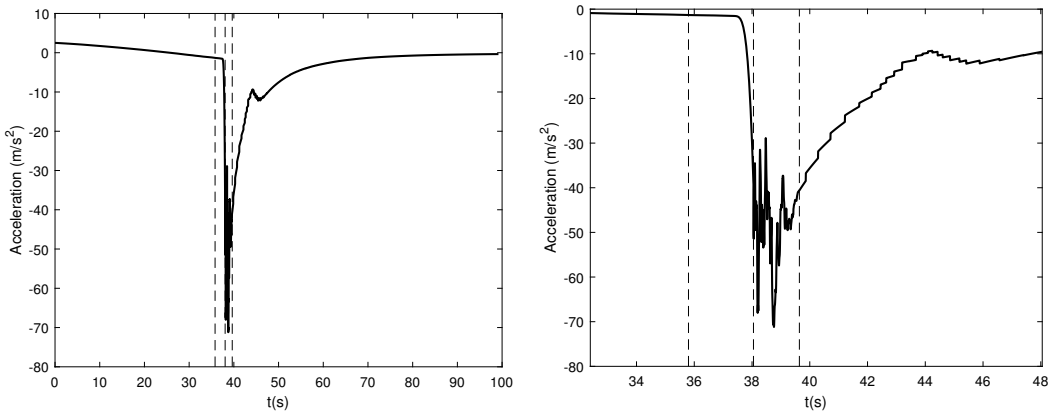

(a) *Total trend* (b) *Deplyment and Inlfation phase*

Figure 49: Vertical descent acceleration of Capsule

Drag force analysis

The final graphs, 49a and 50a, concerning the variation of the overall drag force experienced by the capsule during descent (due to the action of the heat shield and the parachute) support the previously mentioned considerations regars other parameters and their variations.
In fact, by analyzing both the time and vertical altitude trends, a clear change can be observed, primarily caused by the peak reached with the deployment of the supersonic parachute. This peak is responsible for the observed peak in acceleration and the change in the variations of velocity and altitude of the capsule. Furthermore, it can be observed how the drag force is influenced by the phenomenon of parachute area oscillations following the force peak, eventually reaching a steady value for the remainder of the descent.

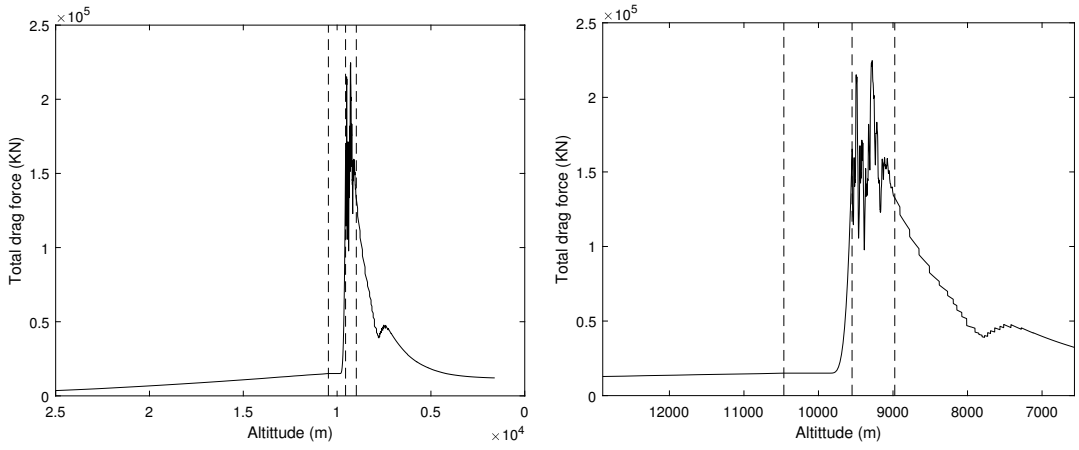

(a) *Total trand* (b) *Deplyment and Inlfation phase*

Figure 50: Total drag force (capsule and parachute)

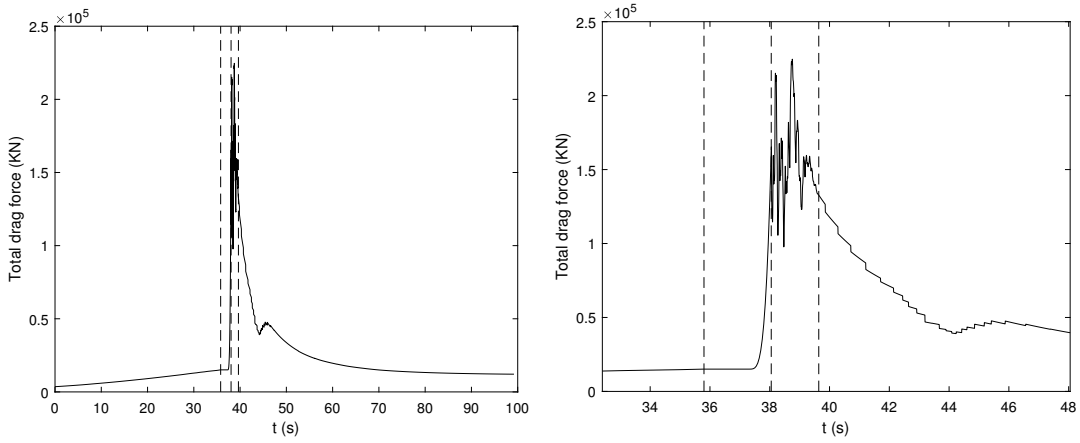

(a) *Total trand* (b) *Deplyment and Inlfation phase*

Figure 51: Total drag force (capsule and parachute)

The analysis of the results from the one-dimensional model cannot be compared to the realistic MSL model due to the simplified nature of the code.
However, the main objective of this initial analysis is to verify that the results reflect, at a physical level, the behavior that characterizes the descent of a capsule on Mars, considering all the perturbative phenomena taken into account.

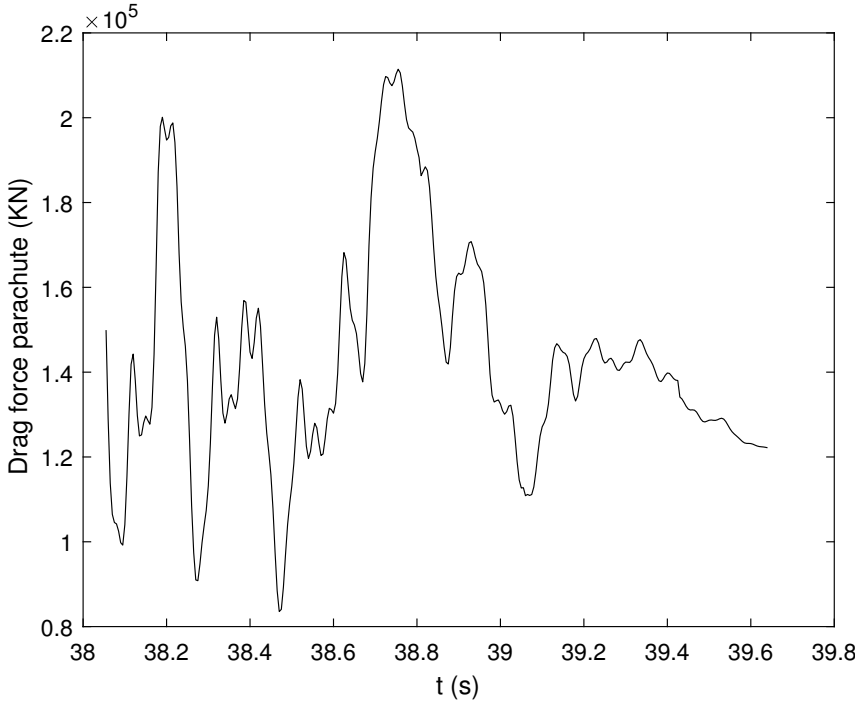

Figure 52: Variation of parachuet drag force during area oscillations phenomenon

From the figure 52, it can be clearly seen how the phenomenon of parachute area oscillations influences the drag force generated by the parachute.
The peak maximums and minimums on the graph simulate the opening and closing of the parachute canopy caused by the interaction with the airflow, which we will analyze in more detail when examining the results of the two-dimensional model.
To summarize the numerical results, the following table presents the values for the same parameters as

in Table 6, demonstrating the reliability of the implemented model.

Table 7: Simulation key results one-dimensional model

Event	$\Delta t_{\mathbf{MF}}$ **(s)**	h **(m)**	γ **(deg)**	M	V **(m/s)**
Mortar fire / deployment	0.000	10500	/	1.791	408.73
Suspension lines Stretch	1.441	/	/	/	/
First full inflation	2.235	/	/	1.737	/
Back shell separation	63.39	1.600	-90	0.344	80.76

Taking into account the simulated conditions and the underlying assumptions used, the obtained results allow us to consider the one-dimensional model reliable. As expected, the final reference altitude is reached in a shorter time (Δt = 63.39s) since the descent is purely vertical.
Regarding the drag force, the simulated value is:

- F_{FI} = 176.8 KN

The considerations made about the obtained results are confirmed by the simulation carried out considering the time interval, in which the simulated phases take place, equal to the reference time (Δ=110s). It is indeed observed that under these conditions, the capsule crashes to the ground ($h_f < 0$), confirming that with a vertical descent, the target is reached in a shorter time (see figure)

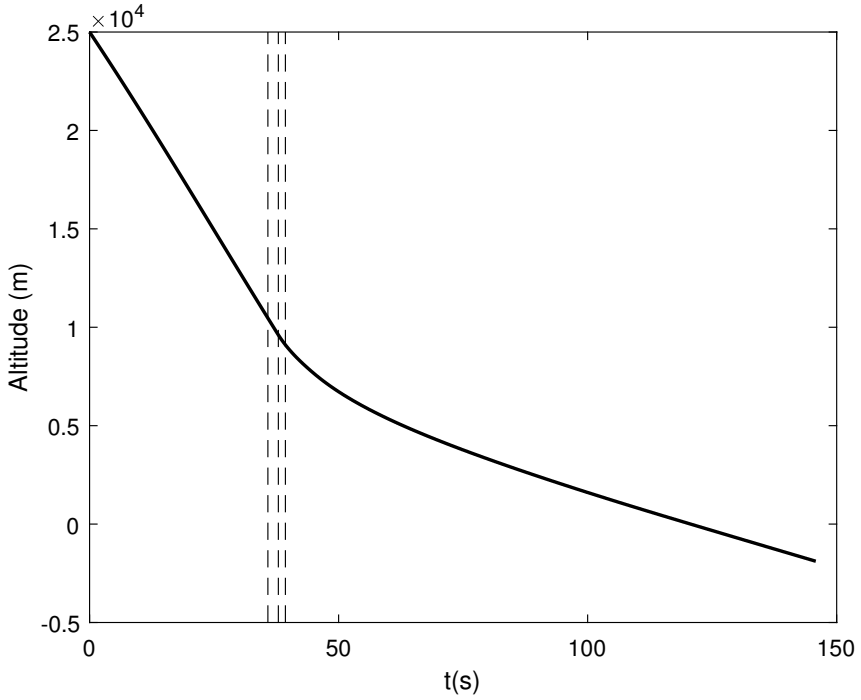

Figure 53: Total trend

3.2 TWO-DIMENSIONAL SIMULATION

The graphs depicting the results obtained from the two-dimensional simulation allow for a more accurate understanding of what happens during the descent of a capsule on Mars, particularly during the central phases of the Entry, Descent, and Landing (EDL) sequence.
In fact, studying the capsule's descent in a two-dimensional manner and considering all the factors that influence this descent enables a simulation that closely resembles reality, within the limits of computational power and the complexity of the code.
This approach helps simulate the behavior of the parachute and its role in the descent as faithfully as possible. Furthermore, these results allow the validation of the implemented code by comparing them with the data collected in the literature.

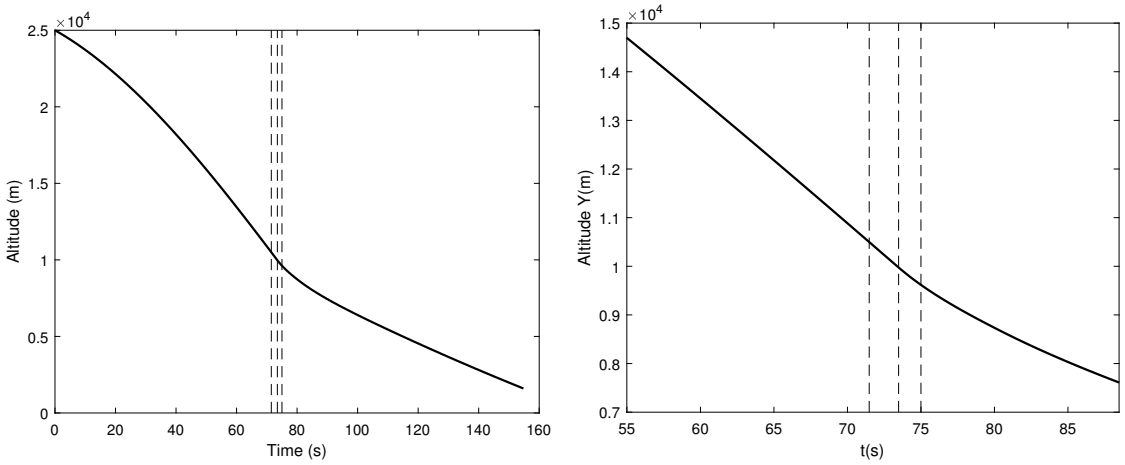

(a) *Total trend* (b) *Deplyment and Inlfation phase*

Figure 54: Vertical descent trajectory of Capsule

The first two graphs in figure 54 show the altitude variation of the capsule during the descent until the moment of parachute detachment and the beginning of descent using retro-rockets. In the figure 54a, we have an overall view, while in the figure 54b, we have a more specific representation of what happens during the deployment, inflation, and area oscillations phases of the parachute.
A first observation we can make is that the effect of the parachute on the descent can be seen in the slope of the altitude decrease over time, unlike the initial phase where the deceleration is solely due to the capsule's heat shield, which is likely to be lower than that provided by the supersonic parachute.
Indeed, this phenomenon is clearly visible in the left image where the transition from deceleration through the heat shield to the phase where the supersonic parachute is fully deployed highlights this concept.
The subsequent figures 55,56 and 57 represent the results obtained from the simulation regarding the vertical component of velocity, the vertical component of acceleration, and the total drag force exerted, first by the capsule and then by the supersonic parachute, for each of the three descent phases.
In all the graphs, the distinction between the three phases and the influence of the area oscillation phenomenon on the studied parameters are clearly visible. In particular, the reason for the initial increase in vertical velocity of the capsule and consequently positive acceleration is that the weight force is greater than the drag force exerted by the capsule. This is because the Flight Path Angle (FPA) is small at the beginning, and the capsule primarily experiences resistance in the horizontal component.

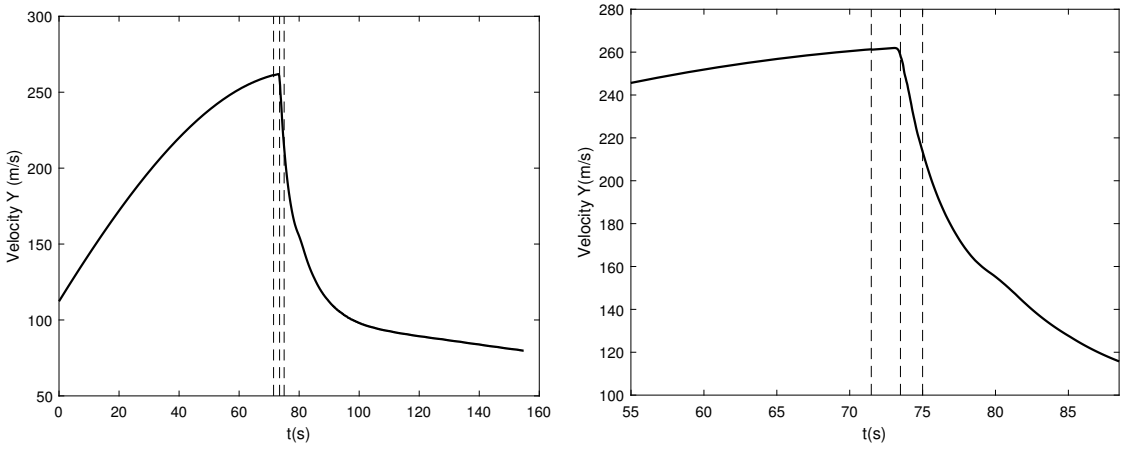

(a) *Total trend* (b) *Deplyment and Inlfation phase*

Figure 55: Vertical descent velocity of Capsule

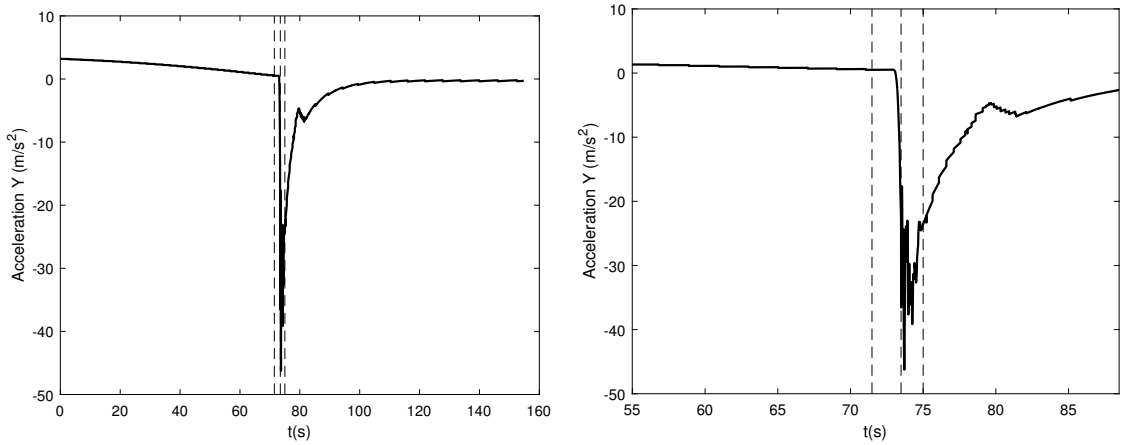

(a) *Total trend* (b) *Deplyment and Inlfation phase*

Figure 56: Vertical descent acceleration of Capsule

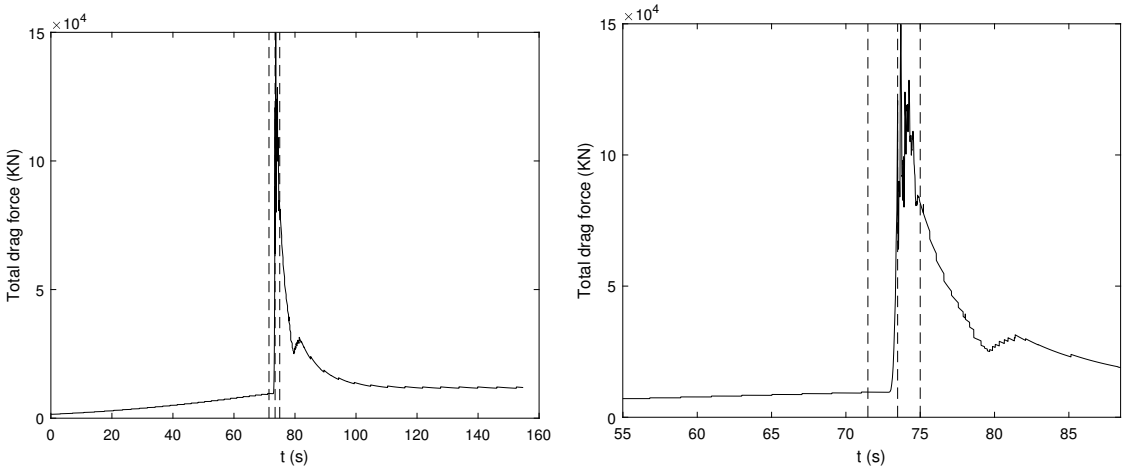

(a) *Total trand* (b) *Deplyment and Inlfation phase*

Figure 57: Total drag force (capsule and parachute)

The general overview of the capsule descent, considering its trajectory in the atmosphere, the relative velocity and relative acceleration, is shown in the following graphs:

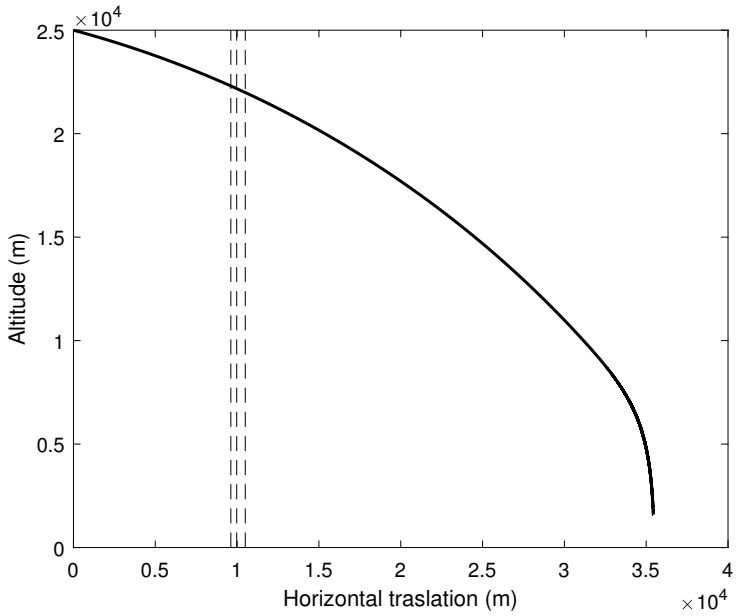

Figure 58: Total trajectory of capsule during descent

From figure 58 the verticalization of the trajectory can be observed after the parachute deployment, indicated by the first dashed line.
The trajectory in the final phase appears to be almost vertical, as expected. This nearly vertical orientation is necessary for the proper initiation of the final phase of the Entry, Descent, and Landing (EDL) sequence.

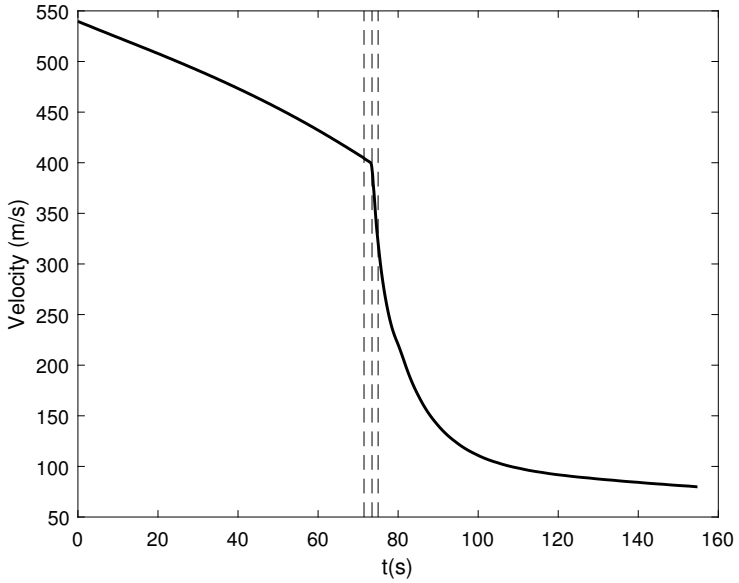

Figure 59: Capsule relative velocity during descent

Similarly, concerning the velocity, the deployment of the supersonic parachute DGB causes a sudden decrease due to the drag force exerted. Its action leads the capsule to reach a steady descent velocity before the separation.

The same consideration can be made for the relative decelleration obtained from the simulation due to the supersonic parachute.

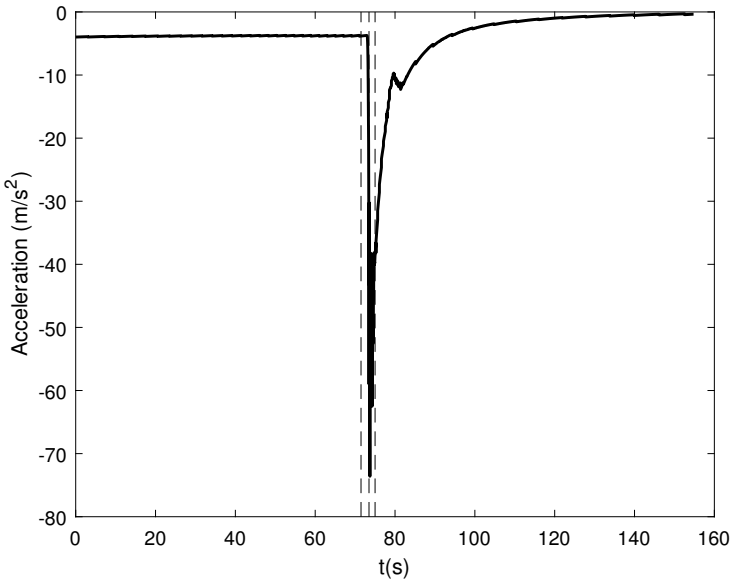

Figure 60: Capsule relative acceleration during descent

The verticalization observed in the overall trajectory of the capsule is well represented by the variation of the Flight Path Angle (FPA) shown in figure 61. It can be noticed that once the parachute deployment occurs, there is a faster change in the F.P.A due to the deceleration caused by the drag force, which vertically aligns the orientation of the capsule to a final angle close to -90deg.

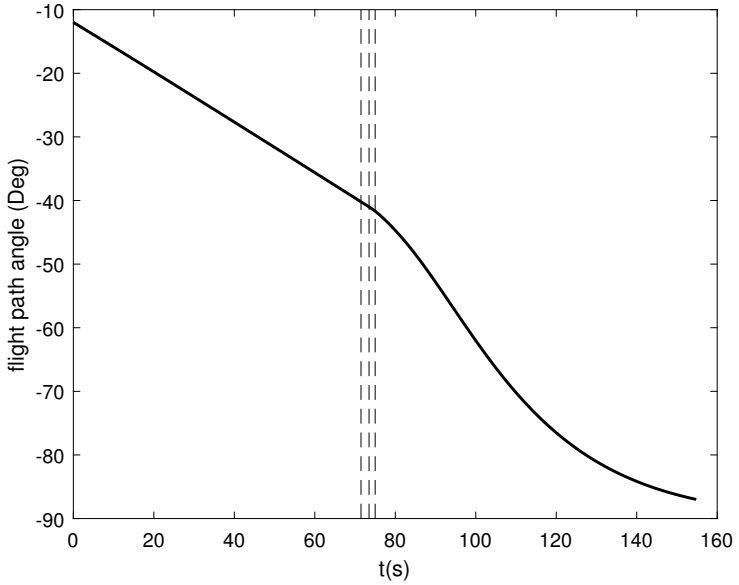

Figure 61: Flight path angle variation / verticalization of capsule

In the last two graphs, we can see respectively the variation of the drag force of the parachute during the inflation phase, and the behavior of the drag force due to the phenomenon of area oscillations.

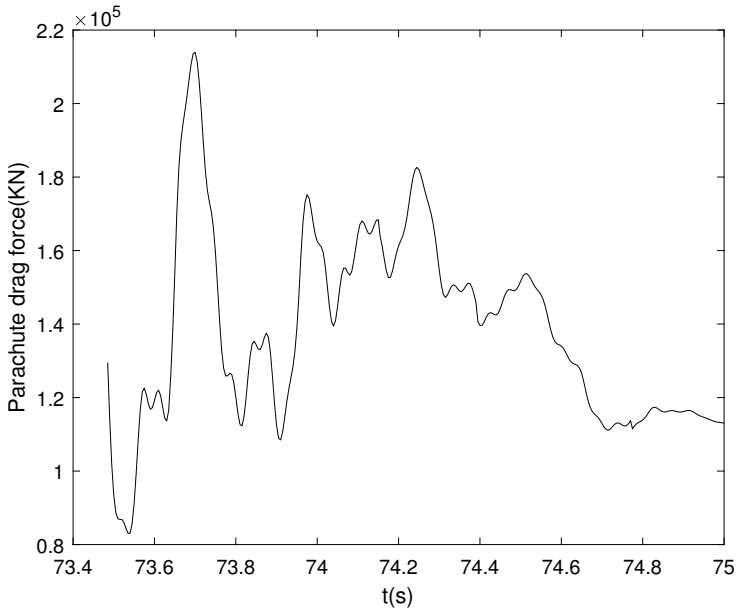

Figure 62: Parachute drag force influenced by K_{AOM} model

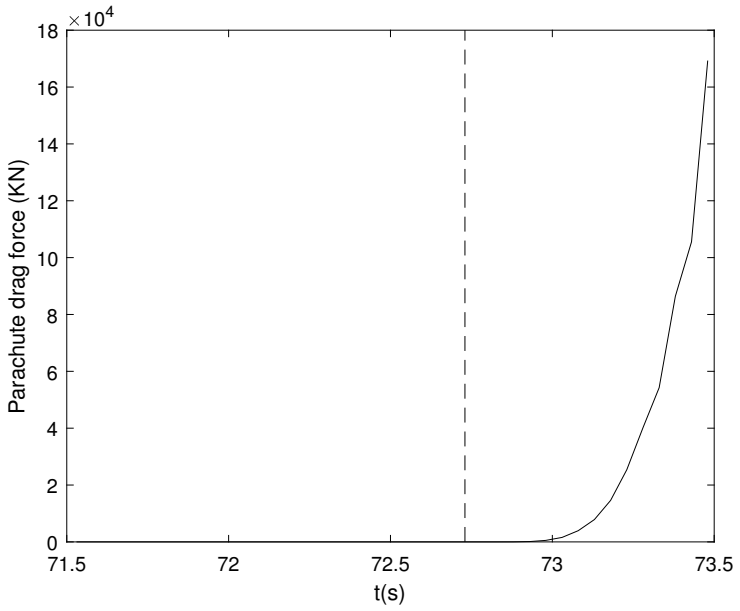

Figure 63: Parachute drag force during inlfation

Table 8: Simulation key results two-dimensional model

Event	$\Delta t_{\mathbf{MF}}$ **(s)**	h **(m)**	γ **(deg)**	M	V **(m/s)**
Mortar fire / deployment	0.000	10500	/	1.771	404.55
Suspension lines Stretch	1.294	/	/	/	/
First full inflation	1.981	/	/	1.716	/
Back shell separation	83.32	1.600	-86.95	0.340	79.75

Regarding the numerical results and the comparison with reference data, it can be observed that the two-dimensional simulation is closer to the reference model, especially in terms of the time required to reach the final altitude. As expected, the two-dimensional model provides a more realistic result compared to the one-dimensional model.

Taking into account that no drag coefficient database was used for the capsule, the dynamics of the capsule during descent were not simulated, and the contribution generated by lift was not considered, it can be concluded that the model is reliable.

Another factor contributing to the difference in results is the initial choice of Flight Path Angle (FPA). Since the exact value at 25 km is unknown, an initial estimate of -20° was assumed, which allows reaching the deployment phase with a velocity consistent with the reference model. However this value not allow to verify if the simulated F.P.A at the deployment event is correct and high probably influence especially the capsule phase.

The initial choice of the F.P.A is also justified by the following graph([17]):

The graph in figure 64, referring to the Perseverance 2020 mission (the most recent NASA mission for Mars exploration), justifies the assumption made in the selection of the initial angle.

In fact, for the capsule phase, the choice of an F.P.A of -12° is reliable, while at the DGB deployment, the FPA is around -22.5°. To achieve this, a code constraint has to be placed within the descent phase with the capsule, as the simulation level of this phase, for the consideration about capsule made before, does not allow reaching these values.

Without this constraint, the simulated F.P.A at deplyment is around -40deg and this is the reason why we obtain simulated results that are lower than the actual ones in terms of timing. In fact, the error propagates over time throughout the descent phase. With the implemented code, the best achievable case is an initial FPA of -2deg, with a corresponding capsule velocity of 1350 m/s. These values lead to an F.P.A at deployment of -26.5deg, with a corresponding Mach number of 2.15 (which approaches the parachute opening limit).

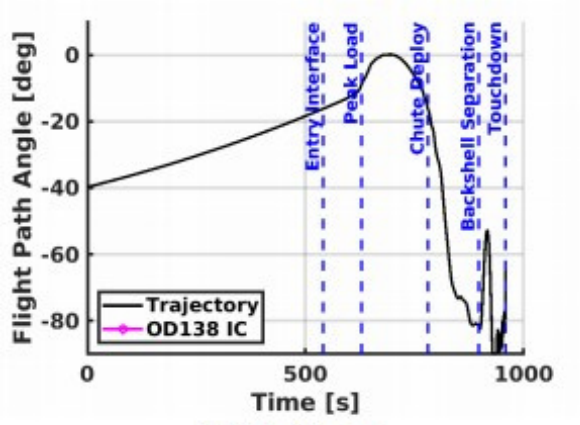

(b) Flight Path Angle

Figure 64: Perseverance F.P.A reference trend

To verify the statements about F.P.A, a simulation was performed without considering the initial descent phase of the capsule but setting the initial conditions for the supersonic parachute deployment phase according to the values used in Mars exploration missions.
From the simulation results (figure 65), it can be observed that the time interval between deployment and reaching the final altitude is now in agreement with the reference value, with the exception of an inherent error in the model itself, as the dynamics are not realistic. This demonstrates, firstly, the reliability of the code used and, secondly, the influence of the capsule's dynamics, particularly the F.P.A (Flight Path Angle), on the supersonic parachute descent phase. This aspect will be further discussed in the next chapter. By setting the supersonic parachute deployment conditions to an F.P.A of approximately -22.5° and a relative velocity of 405 m/s (corresponding to M=1.72, in accordance with NASA missions), it is observed that the time to reach the reference altitude is approximately 100 seconds, compared to an expected result of 110 seconds.

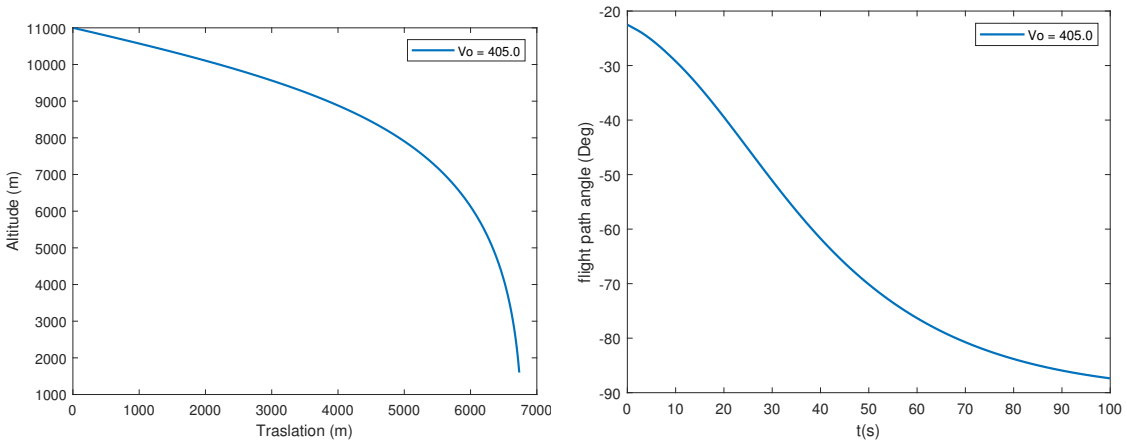

(a) *Trajectory* (b) *F.P.A variation*

Figure 65: Verification matlab code regarding supersonic parachute descent phase

Regarding the drag force, the simulated value obtained is:

- $F_{FI} = 171.1$ KN

3.2.1 MACH NUMBER LIMIT COMPARISON

From the initial Viking landing in 1976 onward, the deployment of a supersonic parachute has consistently been a pivotal moment in the Entry, Descent, and Landing (EDL) systems employed for Mars missions. Due to the criticality of the parachute deployment event, the potential failure of the parachute is a significant risk that is carefully considered in the design of Mars Entry, Descent, and Landing (EDL) systems.
Deployments at higher Mach numbers and dynamic pressures pose a greater risk of parachute failure, primarily due to three factors [28]:

- increased dynamic pressures lead to higher structural loads on the parachute
- higher Mach numbers result in intensified aerothermal heating of the parachute structure, potentially weakening the material
- DGB parachutes deployed above Mach 1.5 are prone to instability known as areal oscillations, characterized by partial collapses and vigorous re-inflations

In the case of high Mach number deployments, particularly in regions where heating is not the primary concern, the main focus is on the increased vulnerability to areal oscillations.
The qualification of the Viking parachute system allowed for successful deployment within the Mach range of 1.4 to 2.1, along with a corresponding dynamic pressure range of 250 to 700 Pa [5]. However, it should be noted that Mach 2.1 is not an absolute limit for the effective operation of DGB parachutes on Mars, and there is limited flight test data available beyond Mach 2.1 to assess the increased risk to the EDL system.
While experts in parachute technology agree that higher Mach numbers increase the likelihood of failure, there are differing opinions regarding the specific upper limit. For instance, Gillis [15] suggests a maximum Mach number of 2 for aerodynamic decelerators, while Cruz [6] places the upper range somewhere between two and three.
In this chapter, we conducted an analysis of the case involving the deployment of the supersonic parachute at higher mach number, followed by a comparison with the mission's nominal Mach deployment.
The values obtained by this simulation are reported in the table 9:

Table 9: Simulation key results of Mach number limit comparison

Event	$\Delta t_{\mathbf{MF}}$ **(s)**	h **(m)**	γ **(deg)**	M	V **(m/s)**
Mortar fire / deployment	0.000	10500	/	2.153	491.83
Suspension lines Stretch	1.438	/	/	/	/
First full inflation	2.231	/	/	2.046	/
Back shell separation	84.8	1.600	-86.05	0.353	82.93

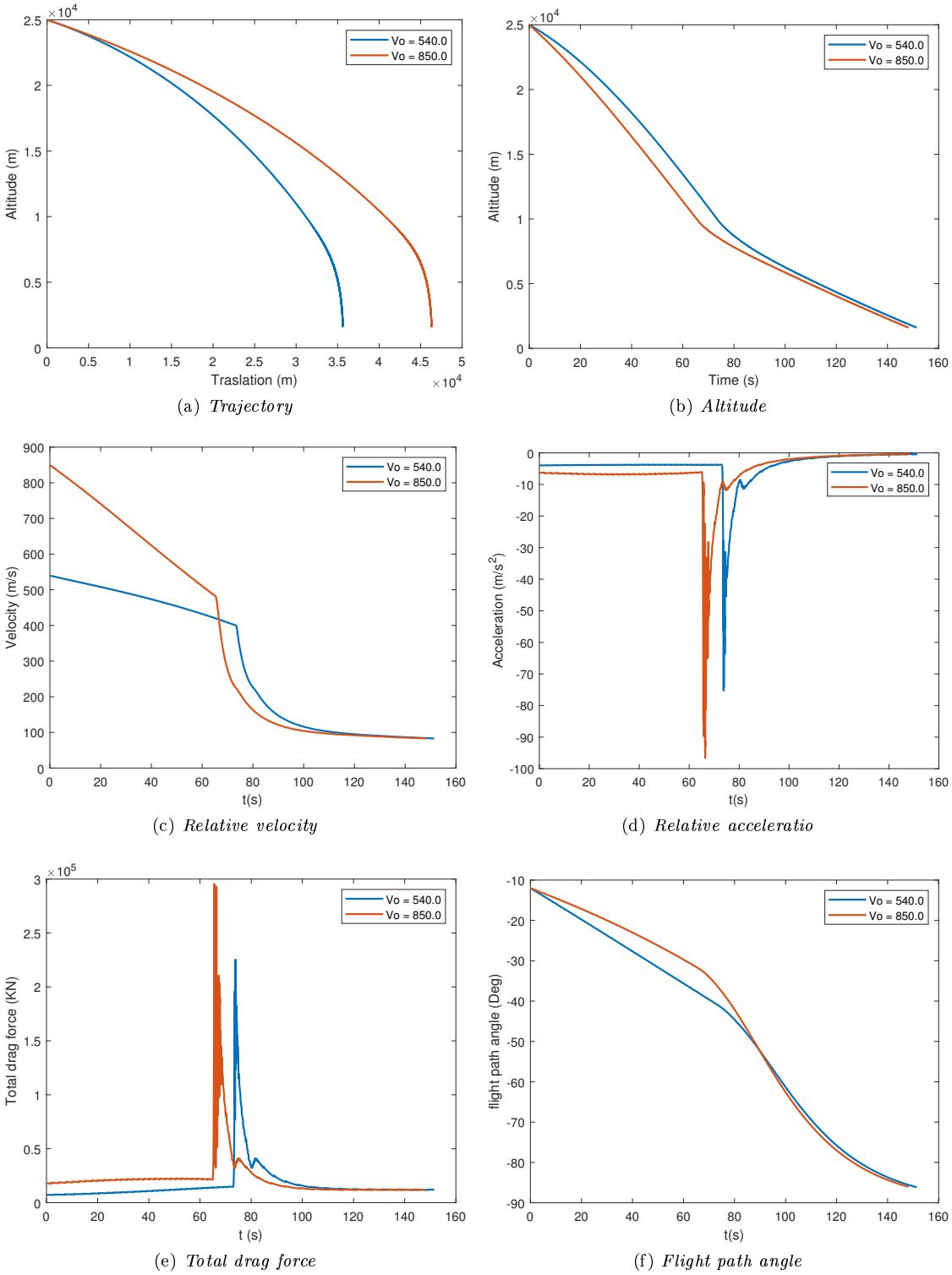

(a) *Trajectory* (b) *Altitude*

(c) *Relative velocity* (d) *Relative acceleratio*

(e) *Total drag force* (f) *Flight path angle*

Figure 66: Mission and limit Mach number scenarios comparision

In this section of the chapter, the results of the simulations comparing the mission scenario to the worst-case scenario for the selected supersonic parachute type are presented.

Starting from the analysis of the capsule's trajectory and altitude variation, it can be observed that a higher initial velocity leads to reaching the parachute deployment altitude in less time and that due to the drag force generated by the parachute, the horizontal displacement relative to the ground is greater. This initial analysis is supported by the total drag force generated during the descent in the two scenarios.

It can be seen that a higher mach number and a higher dynamic pressure at deployment result in a greater drag force exerted by the parachute, which greatly influences the descent trajectory.
This increased drag force exerted by the supersonic parachute on the capsule also has a significant impact on its velocity and deceleration. There is a more drastic decrease in velocity compared to the mission scenario, and the deceleration value is also higher.
Finally, regarding the flight path angle, it can be observed that the value obtained during deployment corresponds to a lower inclination and a subsequent steeper verticalization due to the greater forces at play. In the four graphs of figure 67, the comparison is made regarding the inflation phase and how

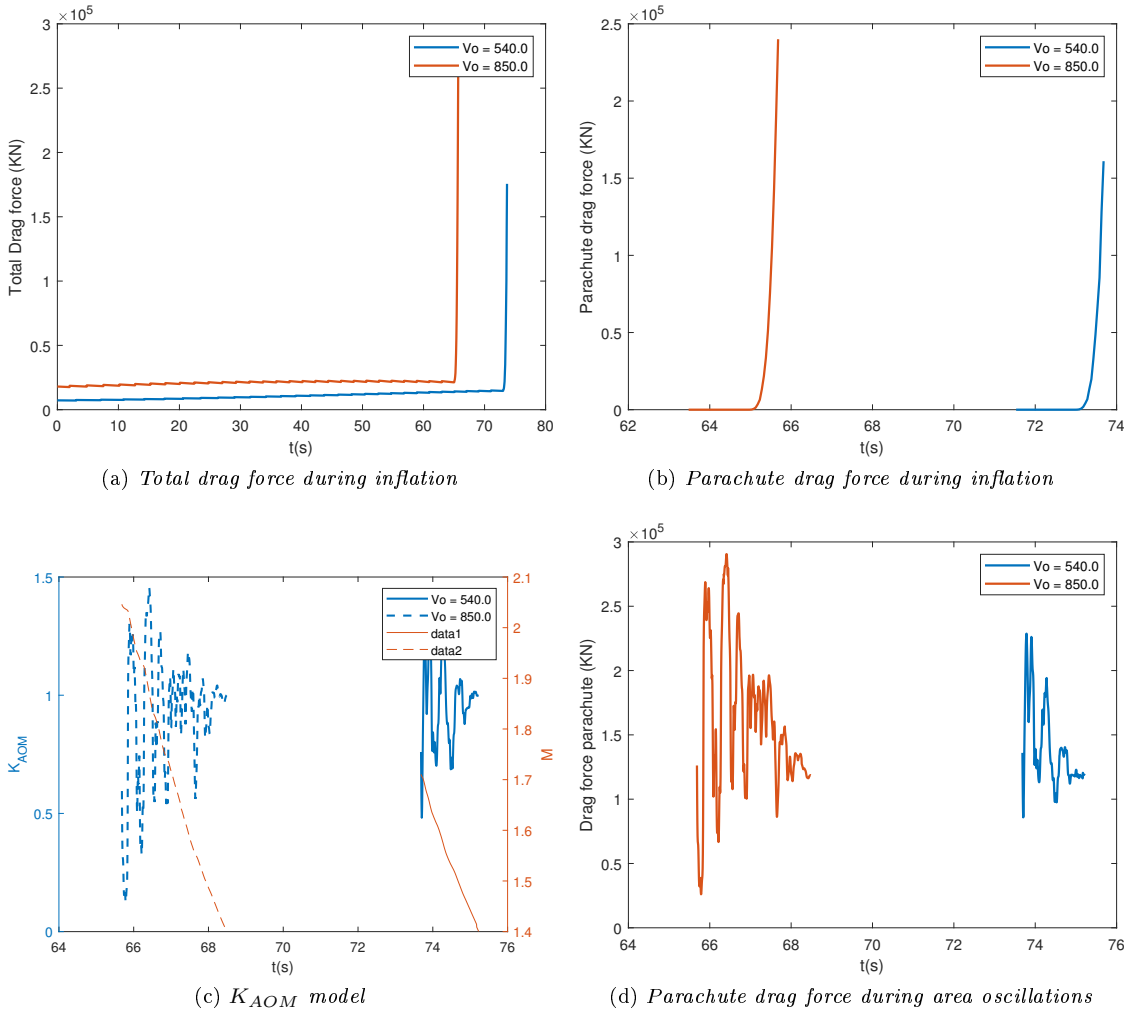

(a) *Total drag force during inflation*

(b) *Parachute drag force during inflation*

(c) K_{AOM} *model*

(d) *Parachute drag force during area oscillations*

Figure 67: Mission and limit Mach number scenarios comparision

the parachute drag force varies during the phenomenon of area oscillations. As expected, the simulated worst-case conditions in terms of Mach number and velocity result in a much greater force generated by the parachute compared to the mission scenario, confirming what was previously mentioned in the analysis of the capsule's descent. In particular, the obtained value is

- $F_{FI} = 238.80$ KN

. Regarding the area oscillation phenomenon, it can be observed that a higher Mach number in the first full inflation condition leads to a wider K_{AOM} pattern and, therefore, a more prolonged phenomenon. This is because the Mach range in which oscillations can occur is greater [2.04 - 1.4] compared to the mission range [1.72-1.4].

3.2.2 THE INFLUENCE OF PARACHUTE NOMINAL DIAMETER, MACH NUMBER VARIATION AND FLIGHT PATH ANGLE ON THE PERFORMANCE OF THE SUPERSONIC PARACHUTE

After simulating the behavior of the capsule during descent on Mars, taking the NASA MSL mission as a reference, several simulations were conducted regarding the performance study of the supersonic DGB parachute, varying parameters such as nominal diameter, initial capsule Mach, and flight path angle. Regarding the simulation with the variation of parachute nominal diameter the results are presented in the following table:

Table 10: Simulation key results of nominal diameter variation

D_0 (m)	M_{FI}	F_{FI} (KN)	t_{INF} (s)	$M_{\mathbf{final}}$(m/s)	$h_{\mathbf{final}}$ (m)	$\gamma_{\mathbf{final}}$ (deg)
10	1.7455	38.12	1.57	0.689	-4851.6	-77.22
15	1.730	84.32	1.95	0.472	-1203.4	-82.78
12	1.7269	120.90	1.86	0.401	248.6	-84.88
21.5	1.7026	167.65	2.26	0.349	1477.4	-86.52
24	1.6945	206.93	2.10	0.322	2214.0	-87.41
26	1.6927	242.34	2.14	0.303	2718.1	-87.94

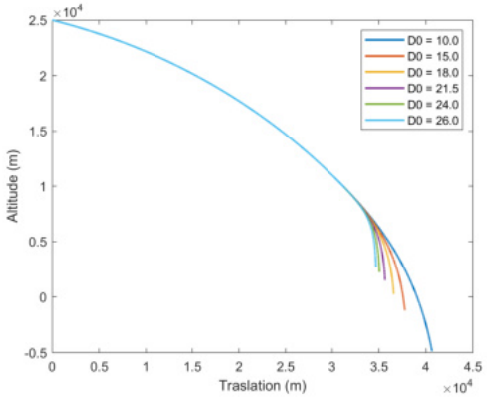

(a) *Trajectory*

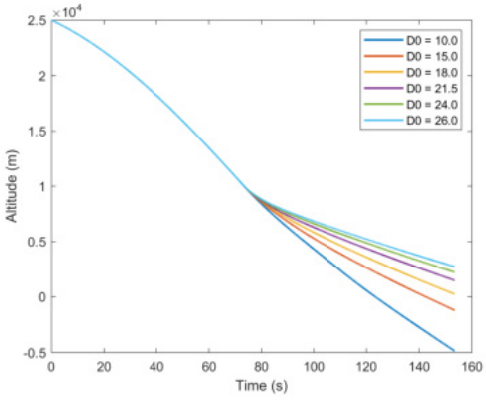

(b) *Altitude*

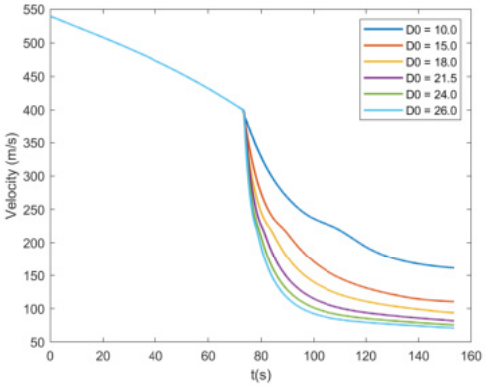

(c) *Relative Velocity*

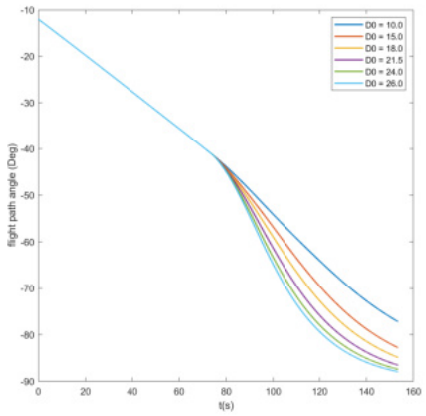

(d) *Flight Path Angle*

Figure 68: Parachute nominal diameter variation comparison

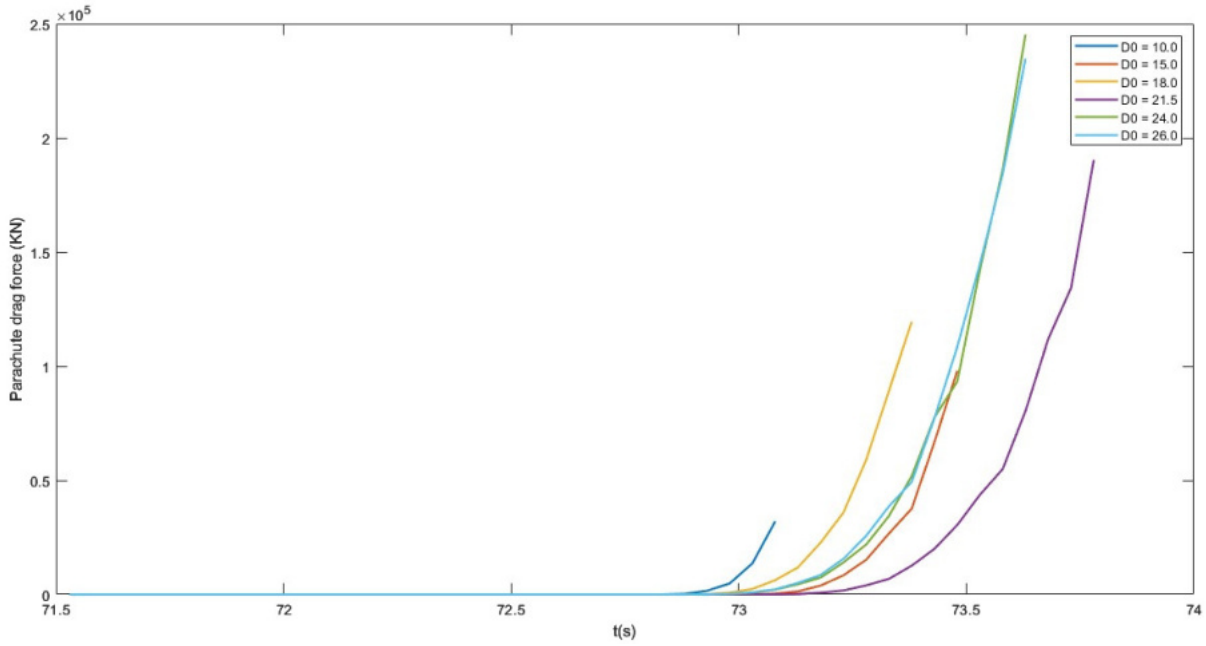

Figure 69: Parachute drag force during inflation comparison

Typical initial values were considered for a mission involving supersonic parachute deployment at Mach 1.7 and a descent phase duration of approximately 85 seconds (according to real values considered in the utilized code), resulting in a final altitude of around 1600 meters. Furthermore, to obtain these initial data, a flight path angle of -12 degrees was considered.

The graphs in figure 68,69 and numerical data (table10) obtained from the simulation emphasize how the choice of the nominal diameter of the parachute is critical and greatly influences the descent of the capsule.

In fact, simulating such a scenario, a supersonic parachute with a diameter that is too small could result in the capsule crashing onto the Martian surface, while one that is too large would not allow reaching the optimal altitude for the final phase of descent. This consideration is clearly seen in the trajectory and altitude graphs of the capsule. It is closely linked to the analysis of the drag force exerted by the parachute, as it is observed that as the diameter decreases, the force decreases, thus not providing sufficient deceleration to achieve the mission objectives. On the other hand, a diameter that is too large, exerting a high drag force on the capsule, would lead to excessive deceleration.

In general, the choice of diameter must be made in relation to the desired altitude to be reached, the time within which to reach it, as well as the mass of the capsule to be decelerated.

The influence of Mach number variation and flight path angle on the performance of the supersonic parachute is significant. The Mach number represents the relative velocity of the object compared to the speed of sound in the surrounding air. A change in the Mach number directly affects the pressure exerted on the object and the parachute.

As the Mach number increases, the compressibility of the air becomes a crucial factor. At supersonic speeds, the air gets compressed, creating shock waves around the object. These shock waves can affect the pressure exerted on the parachute, compromising its efficiency and ability to slow down the object.

Furthermore, the flight path angle, or angle of attack, influences the performance of the supersonic parachute. The flight path angle determines the direction and inclination of the airflow relative to the parachute. A higher flight path angle can increase the relative velocity and dynamic pressure on the object, putting the parachute under considerable strain.

Therefore, both Mach number variation and flight path angle need to be carefully considered in the design and performance analysis of supersonic parachutes to ensure they can operate effectively and safely in high-speed environments.
In this section are presented the results of simulations based on the variation of this two parameters. The goal is analyze how their variations influence the behavior of the capsule descent and evaluate the best design choices for this kind application.

MACH NUMBER VARIATION

Table 11: Simulation key results of Mach number variation

V_0 (m/s)	M_{MF}	F_{FI} (KN)	t_{INF} (s)	$M_{\mathbf{final}}$(m/s)	$h_{\mathbf{final}}$ (m)	$\gamma_{\mathbf{final}}$ (deg)
350	1.5302	126.64	2.16	0.346	1071.6	-87.37
450	1.6566	147.31	2.24	0.349	1264.0	-86.88
540	1.7710	168.90	1.89	0.351	1468.0	-86.46
650	1.9092	192.30	2.07	0.354	1629.1	-86.08
750	2.0323	214.24	2.21	0.358	1713.5	-85.80
850	2.1531	239.18	2.23	0.356	1833.6	-85.49

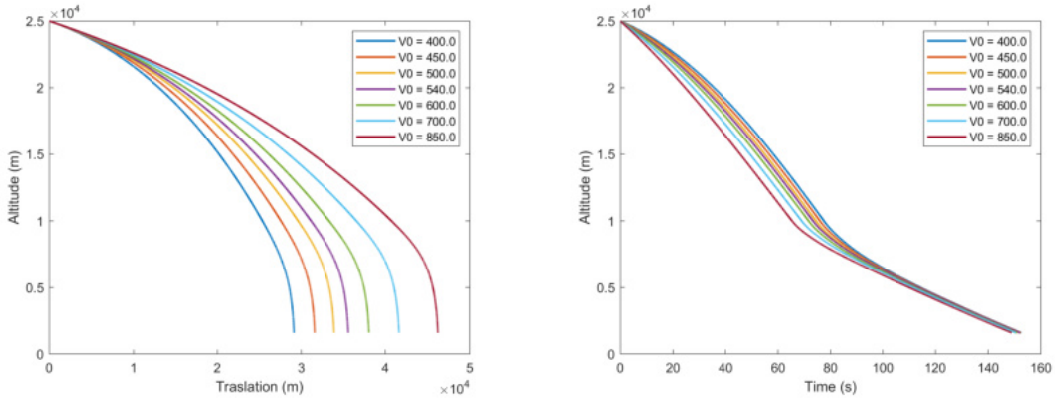

(a) *Trajectory* (b) *Altitude*

(c) *Relative Velocity* (d) *Relative Acceleration*

Figure 70: Initial Mach number variation comparison

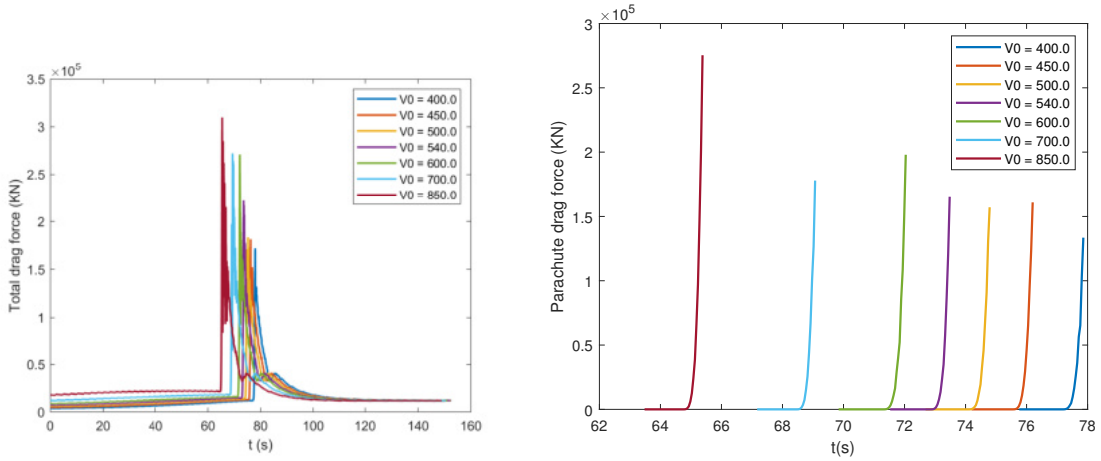

(a) *Total drag force* (b) *Parachute drag force during inflation*

Figure 71: Initial Mach number variation comparison

The simulation varying the Mach number was also conducted while keeping a constant flight path angle of -12 degrees and a descent time with the parachute according to realistic values for the chosen conditions. It can be observed from the graphs and numerical values that as the Mach number increases, the dynamic pressure on the parachute also increases, leading to a larger drag force. This increased drag force causes a more rapid decrease in velocity during descent, effectively slowing down the capsule at a faster rate. Consequently, the capsule reaches a higher altitude than the target due to the greater deceleration.
On the contrary, the simulation shows that a too low opening Mach number does not provide enough drag force to decelerate the capsule as desired. This results in a lower final altitude, increasing the risk of a ground impact or crash.
The relationship between Mach number and drag force is a key factor in determining the descent characteristics and final altitude achieved during the parachute deployment. Proper consideration of the Mach number and its impact on the drag force is crucial in designing and optimizing the parachute system for a successful mission.

FLIGHT PATH ANGLE VARIATION

Table 12: Simulation key results of flight path angle variation

γ_0 (m/s)	M_{MF}	F_{FI} (KN)	t_{INF} (s)	M_{final}(m/s)	h_{final} (m)	γ_{final} (deg)
-2	1.6874	152.19	2.12	0.351	14558.5	-86.55
-8	1.7331	160.46	2.10	0.352	1470.5	-86.49
-12	1.7710	166.58	2.18	0.350	1438.9	-86.47
-16	1.8124	174.01	1.87	0.350	1406.7	-86.53
-20	1.8552	183.69	1.91	0.349	1324.9	-86.61
-30	1.9580	200.78	1.97	0.345	994.65	-86.98
-40	2.0443	222.33	1.98	0.340	613.63	-87.45

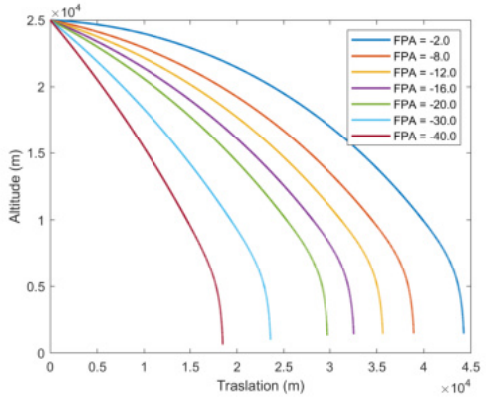

(a) *Trajectory*

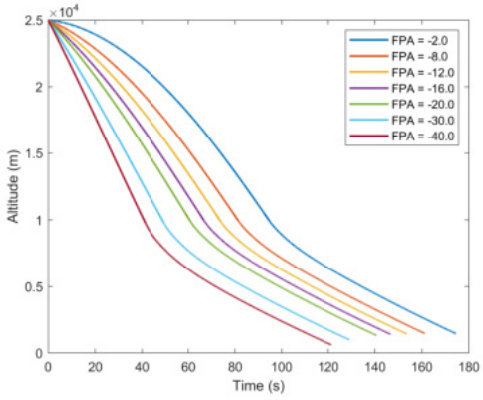

(b) *Altitude*

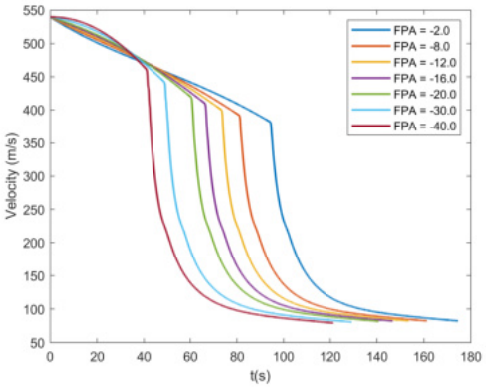

(c) *Relative Velocity*

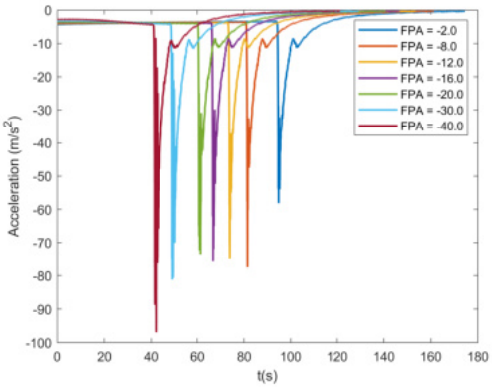

(d) *Relative Acceleration*

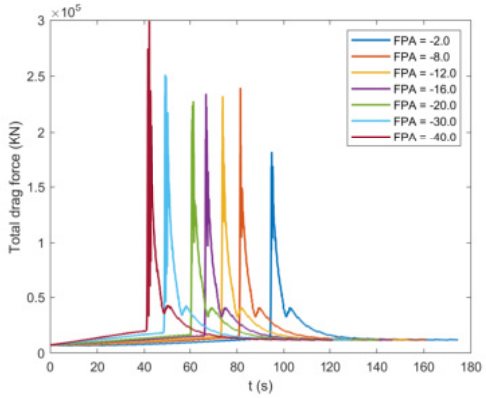

(e) *Total drag force*

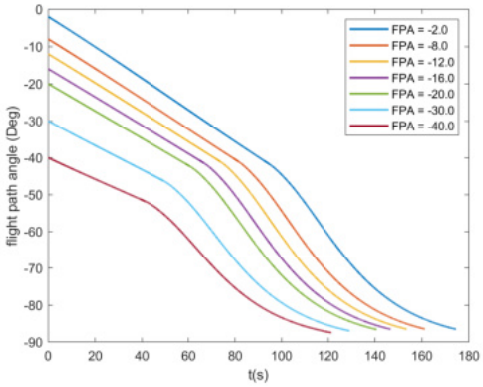

(f) *Flight Path Angle*

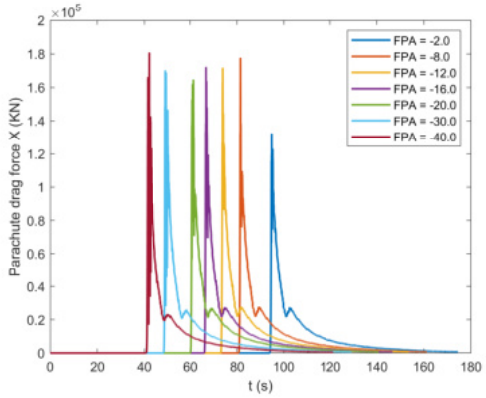

(g) *Parachute drag force X*

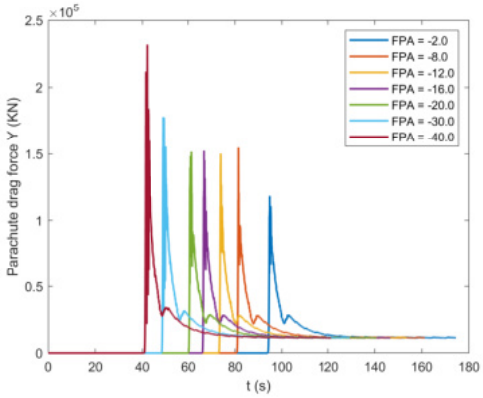

(h) *Parachute drag force Y*

Figure 72: Initial flight path angle variation comparison

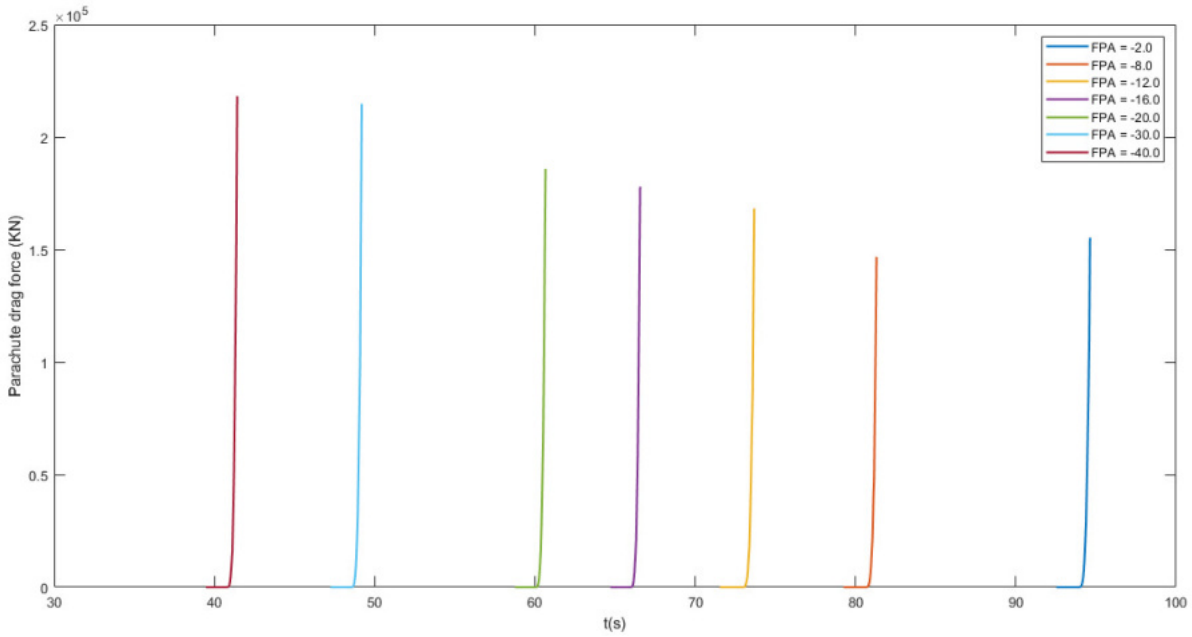

Figure 73: Parachute drag force during inflation comparison

The last simulation conducted focused on the influence of the flight path angle on the analyzed performance during descent. It is important to note that the analysis takes into account the fact that the dynamics of the capsule do not guarantee a faithful simulation of this phase, and therefore, the obtained flight path angle values at parachute opening may not be realistic. However, it allows for a quantitative result of the optimal target to be achieved under these conditions.

The significance of the flight path angle lies in its impact on the stability of the parachute and the descent speed. As evident from the velocity graphs, lower values of the flight path angle result in a lower Mach number at parachute opening, while higher values yield higher Mach numbers due to increased verticalization. Consequently, this phenomenon leads to higher drag forces exerted by the parachute for larger angle values and lower forces for smaller angle values.

Linked to this consideration of the relationship between force and flight path angle, it can be observed that the components of the drag force are also influenced. Smaller angles correspond to more horizontal motion of the capsule, resulting in larger x-component values of the force comparable to those obtained at higher velocities. In other words, the more horizontal the motion of the capsule, the more the supersonic parachute acts to decelerate the motion in that direction. Conversely, as the direction of capsule motion becomes more vertical, the y-component of the force becomes larger.

This observation is related to the fact that a more pronounced verticalization occurs for a more horizontal trajectory of the capsule, as shown in the flight path angle graph.

In conclusion, the flight path angle plays a crucial role in parachute performance during descent, influencing stability, drag forces, and the overall dynamics of the capsule.

4 CONCLUSIONS

4.1 ACTIVITIES CARRIED OUT

The work presented in this master's thesis focused on studying the performance of the DGB supersonic parachute used in the most critical phase of the EDL (Entry, Descent, and Landing) sequence, famously known as the "7 minutes of terror," which is employed in the majority of Mars exploration missions. Specifically, by analyzing past missions, a code was implemented to simulate the one-dimensional and two-dimensional behavior during the activation of the supersonic parachute for decelerating the capsule. This implementation model successfully simulated the descent trajectory of a Martian capsule containing a rover for an exploration mission, taking into account the adopted assumptions and simplifications.Through this simulation, the main factors influencing the parachute deceleration phase were analyzed with the aim of identifying the key parameters for optimizing the design choice.
In support of this, considerations were made regarding the best selection for certain design parameters based on simulations considering variations in descent conditions.
Overall, this study allowed for an understanding of what occurs during the most intense moments of the descent through the Martian atmosphere before landing, as well as an analysis of the performance of the supersonic parachute, specifically the DGB type.
In conclusion, it should be emphasized once again that the use of random phenomena within simulations necessarily leads to results that can vary with each simulation run. Therefore, a detailed comparison on a number-to-number basis cannot be performed. As mentioned earlier, the objective was to simulate and obtain results consistent with past missions in order to learn the key parameters that influence the performance of the supersonic parachute used in the Entry, Descent, and Landing (EDL) sequence.

4.2 FUTURE PERSPECTIVES

The simulation level achieved in this master's thesis can be considered acceptable and satisfactory, yet it still require further development and implementation.
Firstly, the first important improvement to implement is the dynamics of the capsule in order to obtain the most realistic results possible. This involves introducing a 6-degree-of-freedom model and studying the orientation of the capsule during descent.
Regarding the descent phase with the supersonic parachute, the addition of design characteristics such as geometric porosity, parachute weight, material properties, but above all the implementation of additional deployment models, would allow for a more detailed simulation of its performance. Furthermore the introduction of the Martian wind model would represent a further necessary step to ensure better results.
Finally, to achieve a study and a simulation model useful for the design of Mars exploration missions and beyond, it is necessary to compare different types of supersonic parachutes with respect to specific design parameters, considering various simulation scenarios.

5 APPENDIX

5.1 AREA OSCILLATIONS MATHEMATICAL MODEL

The equations used in the calculations to obtain the area oscillations multiplier, K_{AOM} , as described in section 2.1.5 are given below [10].
The variable M is the Mach number. The variable M_{FI} is the Mach number at first full inflation.
the values of MFI and M used in the area oscillations model should be those for the center of mass of the aeroshell, not those of the parachute's center of mass. The model should not be used for Mach numbers higher than M_{Init}.

Table 13: Constants used in the area oscillations model.

Costants	Value
n_{AOM}	3
K_{HF_1}	0.20
K_{HF_2}	0.15
w_{Min}	0.524 rad\s
M_{Init}	2.057
M_{Final}	1.40
E_{Max}	0.59
τ_{High}	1.08
τ_{Low}	1.08

$$\lambda = \frac{\ln(2)}{M_{\text{Init}} - M_{\text{Final}}}$$

$$K_{HF_1} = 15.9474 - 6.5617 M_{FI}$$

$$K_{HF_2} = 2.43032 + 0.787402 M_{FI}$$

$$R_i = \text{independent } U[0,1) \text{ for every } i = 1 \text{ to } 6$$

$$R_s = \frac{1}{M_{\sum_{i=1}^{6} R_i}}$$

$$K_i = R_s R_i \text{ for every } i = 1 \text{ to } 6$$

$$\omega_i = \pi\{U[0,1) + (i-1)\} + \omega_{Min} \text{ for every } i = 1 \text{ to } 6$$

$$\psi_i = 2\pi U[0,1) \text{ for every } i = 1 \text{ to } 6$$

$$\omega_{HF_1} = \pi\{7U[0,1) + 6\} + \omega_{Min} \text{ for every } i = 1 \text{ to } 6$$

$$\omega_{HF_2} = \pi\{7U[0,1) + 13\} + \omega_{Min} \text{ for every } i = 1 \text{ to } 6$$

$t_{shift} = t - t_{FI}$ where t is the lowest value of $t > t_{FI}$ for which

$$\left\{ \sum_{i=1}^{6} K_i \sin^{n_{\text{AOM}}}[\omega_i (t - t_i) + \psi_i] \right\} = 0$$

and its derivatice

$$\left\{\sum_{i=1}^{6} K_i \sin^{n_{\mathrm{AOM}}}[\omega_i(t-t_{FI})+\psi_i]\right\} = 0$$

$$n_{\mathrm{AOM}} \sum_{i=1}^{6} \omega_i K_i \sin^{n_{\mathrm{AOM}-1}}[\omega_i(t-t_{FI})+\psi_i]\cos[\omega_i(t-t_{FI})+\psi_i] < 0$$

All constants have been determined, and the calculations proceed as a function of time for t $> t_{FI}$.

$$S_6(t) = \left\{\sum_{i=1}^{6} K_i \sin^{n_{\mathrm{AOM}}}[\omega_i(t-t_{FI})+\psi_i]\right\} = 0$$

$$T_2(t) = S_6(t) - K_{HF_1} \sin^{n_{\mathrm{AOM}}}[\omega_{HF_1}(t-t_{FI})] - K_{HF_2} \sin^{n_{\mathrm{AOM}}}[\omega_{HF_2}(t-t_{FI})]$$

If $T_1(t) > 0$ then

$$T_2(t) = 1 + K_{\mathrm{High}} T_1(t) \left\{\exp\left[\lambda(M - M_{\mathrm{Final}})\right] - 1\right\}$$

$$T_3(t) = 1 + E_{\mathrm{Max}} \left(1 - \exp\left\{-\tau_{\mathrm{High}}\left[T_2(t) - 1\right]\right\}\right)$$

else

$$T_2(t) = 1 + K_{\mathrm{Low}} T_1(t) \left\{\exp\left[\lambda(M - M_{\mathrm{Final}})\right] - 1\right\}$$

$$T_3(t) = \exp\left\{\tau_{\mathrm{Low}}\left[T_2(t) - 1\right]\right\}$$

endif

perform the above conditional evaluation and appropriate calculations at every time step

If $M \leq M_{Final} > 0$ then

$$K_{\mathrm{AOM}}(t) = T_3(t)$$

else

$$K_{\mathrm{AOM}}(t) = 1$$

endifperform the above conditional evaluation and appropriate assignment at every time step

5.2 MATLAB BI-DIMENSIONAL CODE

MARTIAN ATMOSPHERIC PARAMETERS AND CAPSULE/PARACHUTE PARAMETERS DATABASE

```
%IMPORT MARTIAN ATMOSPHERIC PARAMETERS DATABASE
AM = readtable('AM25.csv'); % CSV DATABASE DOCUMENT

% ATMOSPHERIC PARAMETERS EXTRAPOLATION
H = table2array(AM(:, 'H'));        % ALTITUDE
T = table2array(AM(:, 'T'));        % TEMPERATURE
Rho = table2array(AM(:, 'Rho'));    % DENSITY
P = table2array(AM(:, 'P'));        % PRESSION

% CREATION ATMOSPHERIC DATABASE WITH LINEAR INTERPOLATION [25km to 1km]
Hi = H(1):-Passo:H(end);                    % ALTITUDE
Ti = interp1(H,T,Hi,'linear');              % TEMPERATURE
Rhoi = interp1(H,Rho,Hi,'linear');          % DENSITY
Pi = interp1(H,P,Hi,'linear');              % PRESSION

% LOAD CD_0 DGB SUPERSONIC PARACADUTE DATABASE
load Cd0_nominal
Cd_0_MSL=Cd0_nominal(:,2)'; % CREATION CD_0 VECTOR
M_MSL=Cd0_nominal(:,1)';    % CREATION M VECTOR

% LOAD CN DGB SUPERSONIC PARACADUTE DATABASE
load C_N_nominal
CN_MSL=C_N_nominal(:,2)';   % CREATION CN VECTOR
alpha_CN=C_N_nominal(:,1)'; % ALPHA ANGLE VECTOR

% LOAD CT DGB SUPERSONIC PARACADUTE DATABASE
load C_T_nominal
CT_MSL=C_T_nominal(:,2)';   % CREATION CT VECTOR
alpha_CT=C_T_nominal(:,1)'; % ALPHA ANGLE VECTOR

%  LOAD MEF DGB SUPERSONIC PARACADUTE DATABASE
load MEF
MEF_MSL=MEF(:,2)'; % CREATION mMEF VECTOR
M_msl=MEF(:,1)';   % CREATION M VECTOR

% LOAD CA CAPSULE DATABASE
load CA
CA_C=CA(:,2)'; % CREATION CA VECTOR
Incidence=CA(:,1)'; % ANGLR OF INCIDENCE
```

CAPSULE PHASE DESCENT SIMULATION

```
% DEFINITON OF GEOMETRICAL CAPSULE PARAMETERS

% CALCULATION OF INITIAL CD CAPSULE COEFFICIENT
alpha_incidence=0; % ANGLE OF ATTACK NULL
[~,indiceincidence]=min(abs(Incidence-alpha_incidence));
Cd0_c=CA_C(indiceincidence);

% DEFINITION OF INITIAL ATMOSPEHERIC VELOCITY
r0=Y0_c+R_M;
V0_a=omega*r0;

% INITIALIZATION VECRTORS AND SIMULATION PARAMETERS (VELOCITY, ALTITUDE, DRAG FORCE)
% DESCENT SIMULATION

while Yc > 10500

% ACCELERATION ALONG X AND Y DIRECTION
acy= 1/M_c*(Fp_c - Fdrag_cy);
acx= 1/M_c*(-Fdrag_cx);
AAi=sqrt(acx^2+acy^2);

% VELOCITY ALONG X AND Y DIRECTION
Vi_cy = Vi_cy + (acy * dt);
Vi_cx = Vi_cx + (acx * dt);
Vi= sqrt(Vi_cy^2+Vi_cx^2);

% VARIATION OF FLYGHT PATH ANGLE
FPA_rad= atan(-Vi_cy/Vi_cx);
FPA_grad= FPA_rad * (180 / pi);

% POSITION ALONG X AND Y DIRECTION
Yc=Yc - (Vi_cy*dt) + ((1/2)*acy*dt^2);% ay<0
Xc=Xc + (Vi_cx*dt) + ((1/2)*acx*dt^2); % ax<0
X=sqrt(Yc^2+Xc^2);

% ATMOSPEHERIC VELOCITY VARIATION
r=R_M+Yc;
Va=omega*r;

% RELATIVE VELOCITY CALCULATION
Vr=sqrt((Vi_cx-Va)^2+Vi_cy^2);

% TIMESTEP
t_c = t_c+ dt;
```

```
% CALCULATION OF NEW VALUE OF DENSITY AND ESTIMATION OF CASPULE DRAG FORCE
[~,indexc]=min(abs(Hi-Yc));
Rho_ic=Rhoi(indexc);
Fdrag_c=((1/2)*(Vr)^2*S0_c*Cd0_c*Rho_ic);
Fdrag_cy=abs(Fdrag_c*sind(FPA_grad));
Fdrag_cx=abs(Fdrag_c*cosd(FPA_grad));

end
```

SUPERSONIC PARACHUTE DEPLOYMENT AND FIRST FULL INFLATION

```
% DETERMINATION OF INFLATION MULTIPLIER COEFFICIENT (KI)

% DEPLOYMET AND INFLATION SIMULATION

while t_cp < t_FI

% ACCELERATION ALONG X AND Y DIRECTION
acpy = 1/M_c*(Fp_c - Fdrag_CPy);
acpx= 1/M_c*(- Fdrag_CPx);

% VELOCITY ALONG X AND Y DIRECTION
Vi_cpy = Vi_cpy + (acpy * dt_cp);
Vi_cpx = Vi_cpx + (acpx * dt_cp);
Vicp= sqrt(Vi_cpy^2+Vi_cpx^2);

% VARIATION OF FLYGHT PATH ANGLE
FPA_rad_cp= atan(-Vi_cpy/Vi_cpx);
FPA_grad_cp= FPA_rad_cp * (180 / pi);


% POSITION ALONG X AND Y DIRECTION
Ycp=Ycp - (Vi_cpy*dt_cp) + ((1/2)*acpy*dt_cp^2);% ay<0
Xcp=Xcp + (Vi_cpx*dt_cp) + ((1/2)*acpx*dt_cp^2); % ax<0
X_CP=sqrt(Ycp^2+Xcp^2);


% ATMOSPEHERIC VELOCITY VARIATION
r_cp=R_M+Ycp;
Va_cp=omega*r_cp;

% RELATIVE VELOCITY CALCULATION
Vr_cp=sqrt((Vi_cpx-Va_cp)^2+Vi_cpy^2);

% CALCULATION OF NEW VALUE OF DENSITY AND ESTIMATION OF CASPULE/PARACHUTE DRAG FORCE
[~,indexc_p]=min(abs(Hi-Ycp));
```

```
Rho_icp=Rhoi(indexc_p);

% DEPLOYMENT
if t_cp < t_LS

Fdrag_c2=((1/2)*(Vr_cp)^2*S0_c*Cd0_c*Rho_icp);
Fdrag_c2y=abs(Fdrag_c2*sind(FPA_grad_cp));
Fdrag_c2x=abs(Fdrag_c2*cosd(FPA_grad_cp));

% INFLATION
else

Fdrag_c2=((1/2)*(Vr_cp)^2*S0_c*Cd0_c*Rho_icp);
Fdrag_c2y=abs(Fdrag_c2*sind(FPA_grad_cp));
Fdrag_c2x=abs(Fdrag_c2*cosd(FPA_grad_cp));

% IMPLEMENTATION OF KI MODEL FOR PARACHUTE INFLATION DRAG FORCE
dinamic_pressure=0.5*Rho_icp*Vr_cp^2;
k_Ip=Cx*((t_cp-t_LS)/(t_FI-t_LS))^n_I;

% DEFINITION RELATIVE RANDOM ANGLE BETWEEN PARACHUTE AND CAPSULE
lower_a=0;
mode_a=8;
upper_a=12;
dist=makedist("Triangular",lower_a, mode_a, upper_a);
alfa_p_t=random(dist,1);
%phi_p_t=360*U01-180;
[~,indexalpha]=min(abs(alpha_CT-alfa_p_t));
C_T_n=CT_MSL(indexalpha);
C_N_n=CN_MSL(indexalpha);

Fdrag_cp=dinamic_pressure*S0p*k_Ip*sqrt((C_T_n)^2+(C_N_n)^2);
Fdrag_cpy=abs(Fdrag_cp*sind(FPA_grad_cp));
Fdrag_cpx=abs(Fdrag_cp*cosd(FPA_grad_cp));

end

% DENITION OF TOTAL DRAG FORCE (CAPSULE AND PARACHUTE)
Fdrag_CPy= Fdrag_c2y + Fdrag_cpy;
Fdrag_CPx= Fdrag_c2x + Fdrag_cpx;

% TIMESTEP
t_cp = t_cp+ 0.05;

end
```

SUPERSONIC PARACHUTE FULL INFLATED DESCENT PHASE

```
% CALCULATION OF OPENING PEAK FORCE DURING INLATION WITH q_inf,CT,CN at t=T_FI
F_FI=q_inf*S0*Cx*sqrt((CT^2)+(CN^2));

% DEFINITION OF APPARENT MASS COEFFICIENT
lower_app=0;
mode_app=0.035;
upper_app=0.070;
dist_app=makedist("Triangular",lower_app, mode_app, upper_app);
K_app=random(dist_app,1);

% FULL INFLATED PARACHUTE SIMULATION

while Yp > 1600

% CALCULATION OF APPARENT FORCE
[~,index_rho]=min(abs(Hi-Yp));
Rho_app=Rhoi(index_rho);
m_app=K_app*pi*Rho_app*(D0^3);
F_B=m_app*g_M; %lungo Y

% ACCELERATION ALONG X AND Y DIRECTION
apy = 1/M_dm*(Fp- F_B - Fdrag_Py);
apx= 1/M_dm*(- Fdrag_Px);
AAip=sqrt(apx^2+apy^2);

% VELOCITY ALONG X AND Y DIRECTION
Vi_py = Vi_py + (apy * dt_p);
Vi_px = Vi_px + (apx * dt_p);
Vip= sqrt(Vi_py^2+Vi_px^2);

% VARIATION OF FLYGHT PATH ANGLE
if FPA_grad_p > -90 && FPA_grad_p < 0

FPA_rad_p= atan(-Vi_py/Vi_px);
FPA_grad_p= FPA_rad_p * (180 / pi);

else

FPA_grad_p= -90;
FPAAp=[FPAAp,FPA_grad_p];

end

% POSITION ALONG X AND Y DIRECTION
```

```
Yp=Yp - (Vi_py*dt_p) + ((1/2)*apy*dt_p^2);
Xp=Xp + (Vi_px*dt_p) + ((1/2)*apx*dt_p^2);
X_P=sqrt(Yp^2+Xp^2);


% ATMOSPEHERIC VELOCITY VARIATION
r_p=R_M+Yp;
Va_p=omega*r_p;

% RELATIVE VELOCITY CALCULATION
Vr_p=sqrt((Vi_px-Va_p)^2+Vi_py^2);

% CALCULATION OF NEW VALUE OF DENSITY AND ESTIMATION OF CASPULE/PARACHUTE DRAG FORCE
[~,indexcc_p]=min(abs(Hi-Yp));
Rho_iccp=Rhoi(indexcc_p);
Fdrag_c3=((1/2)*(Vr_p)^2*S0_c*Cd0_c*Rho_iccp);
Fdrag_c3y=abs(Fdrag_c3*sind(FPA_grad_p));
Fdrag_c3x=abs(Fdrag_c3*cosd(FPA_grad_p));

[~,indexp]=min(abs(Hi-Yp));
Rho_ip=Rhoi(indexp);

% DEFINITION OF MEF FACTOR AND PERTURBATED PARACHUTE DRAG COEFFICIENT
[~,indexxp]=min(abs(M_MSL-M_pp));
Cd0_p=Cd_0_MSL(indexxp);
MEF_p=MEF_MSL(indexxp);
Cd0_P=Cd0_p*MEF_p;

% IMPLEMENTATION OF K_AOM MODEL FOR AREA OSCILLATIONS SIMULATION
if M_pp >= 1.4

output1=Function_K_AOM2(M_pp,tp,t_shift,t_FI,Wi,FHI,Ki,n_AOM,K_HF1,K_HF2,w_HF1,w_HF2,K_
kaom=output1;
S0_p=S0*kaom;
Fdragp=((1/2)*Vr_p^2*S0_p*Cd0_P*Rho_ip);
Fdragpy=abs(Fdragp*sind(FPA_grad_p));
Fdragpx=abs(Fdragp*cosd(FPA_grad_p));

%TIMESTEP
tp = tp + dt_p;

% AFTER AREA OSCILLATIONS MODEL (K_AOM=1)
else

S0_p=S0*1;
Fdragp=((1/2)*Vr_p^2*S0_p*Cd0_P*Rho_ip);
```

```
Fdragpy=abs(Fdragp*sind(FPA_grad_p));
Fdragpx=abs(Fdragp*cosd(FPA_grad_p));

% TIMESTEP
tp = tp + dt_p;

end

% CALCULATION OF SOUND VELOCITY AND MACH
gamma=1.3;
RCo2=189; %J/(mol*K)
[~,indexvspp]=min(abs(Hi-Yp));
Ti_cpp=Ti(indexvspp);
c_M_pp=sqrt(gamma*RCo2*Ti_cpp); %sound velocity on mars atmosphere
M_pp=Vr_p/c_M_pp;
Mpp=[Mpp,M_pp];

% DENITION OF TOTAL DRAG FORCE (CAPSULE AND PARACHUTE)
Fdrag_Py= Fdrag_c3y + Fdragpy;
Fdrag_Px= Fdrag_c3x + Fdragpx;

end
```

BIBLIOGRAPHY AND WEBOGRAPHY

[1] https://mars.nasa.gov/mars2020/spacecraft/overview/.

[2] http://www-mars.lmd.jussieu.fr/mars/access.html.

[3] Richard J Bendura, Lucille C Coltrane, and Earle K Huckins III. Performance of a 19.7 meter diameter disk gap band parachute in a simulated martian environment. Technical report, 1968.

[4] Richard J Bendura, Reginald R Lundstrom, Philip G Renfroe, and Stewart R LeCroy. Flight tests of viking parachute system in three mach number regimes. 2: Parachute test results. Technical report, 1974.

[5] Robert D Braun and Robert M Manning. Mars exploration entry, descent and landing challenges. In *2006 IEEE Aerospace Conference*, pages 18–pp. IEEE, 2006.

[6] Juan Cruz and J Lingard. Aerodynamic decelerators for planetary exploration: past, present, and future. In *AIAA Guidance, Navigation, and Control Conference and Exhibit*, page 6792, 2006.

[7] Juan Cruz, Raymond Mineck, Donald Keller, and Maria Bobskill. Wind tunnel testing of various disk-gap-band parachutes. In *17th AIAA Aerodynamic Decelerator Systems Technology Conference and Seminar*, page 2129, 2003.

[8] Juan R. Cruz. Parachutes for planetary entry systems. pages 100–200.

[9] Juan R Cruz, David Way, Jeremy Shidner, Jody L Davis, Richard W Powell, Devin Kipp, and Douglas S Adams. Reconstruction of the mars science laboratory parachute performance and comparison to the descent simulation. In *AIAA Aerodynamic Decelerator Systems (ADS) Conference*, page 1250, 2013.

[10] Juan R Cruz, David Way, Jeremy Shidner, Jody L Davis, Richard W Powell, Devin Kipp, Douglas S Adams, Anita Sengupta, Allen Witkowski, and Mike Kandis. Parachute models used in the mars science laboratory entry, descent, and landing simulation. In *AIAA Aerodynamic Decelerator Systems (ADS) Conference*, page 1276, 2013.

[11] Clinton V Eckstrom and John S Preisser. *Flight Test of a 30-foot Nominal Diameter Disk-gap-band Parachute Deployed at a Mach Number of 1.56 and a Dynamic Pressure of 11.4 Pounds Per Square Foot*. National Aeronautics and Space Administration, 1967.

[12] Karl T Edquist, Brian R Hollis, Artem A Dyakonov, Bernard Laub, Michael J Wright, Tomasso P Rivellini, Eric M Slimko, and William H Willcockson. Mars science laboratory entry capsule aerothermodynamics and thermal protection system. In *2007 IEEE Aerospace Conference*, pages 1–13. IEEE, 2007.

[13] KT Edquist, PN Desai, and M Schoenenberger. Aerodynamics fort he mars phoenix entry capsule. *AIAA Guidance, Navigationand Control ConferenceandExhibit, AIAA2008G7219*, 2008.

[14] Patrick Gallais. *Atmospheric re-entry vehicle mechanics*. Springer Science & Business Media, 2007.

[15] CL Gillis. Deployable aerodynamic decelerators for space missions. *Journal of Spacecraft and Rockets*, 6(8):885–890, 1969.

[16] Mingxing Huang, Wenqiang Wang, and Jian Li. Analysis and verification of aerodynamic characteristics of tianwen-1 mars parachute. *Space: Science & Technology*, 2022.

[17] Christopher D Karlgaard, Mark Schoenenberger, Soumyo Dutta, and David W Way. Mars entry, descent, and landing instrumentation 2 trajectory, aerodynamics, and atmosphere reconstruction. *Journal of Spacecraft and Rockets*, 60(1):199–214, 2023.

[18] Theo W. Knacke. Parachute recovery systems design manual. pages 400–600, MARCH 1991.

[19] John Lingard, John Underwood, Shane Glynn, Dominique Franqueville, Patrick Arfi, Olivier Bayle, Francesco Potenza, and Stefano Portigliotti. Exomars parachute system. In *20th AIAA Aerodynamic Decelerator Systems Technology Conference and Seminar*, page 2975, 2009.

[20] Julian D Maynard. *Aerodynamic characteristics of parachutes at Mach numbers from 1.6 to 3.* National Aeronautics and Space Administration, 1961.

[21] Manish Mehta, Anita Sengupta, Nilton O Renno, John W Van Norman, Peter G Huseman, Douglas S Gulick, and Mark Pokora. Thruster plume surface interactions: Applications for spacecraft landings on planetary bodies. *AIAA journal*, 51(12):2800–2818, 2013.

[22] RD Moog, RJ Bendura, JD TlMMONS, and RA Lau. Qualification flight tests of the viking decelerator system. *Journal of Spacecraft and Rockets*, 11(3):188–195, 1974.

[23] H Murrow, C Eckstrom, and D Henke. Development flight tests of the viking decelerator system. In *4th Aerodynamic Deceleration Systems Conference*, page 455, 1973.

[24] Nasaspacecraft. https://www.nasaspaceflight.com/2023/01/dragonfly-edl-overview/.

[25] J Santos, Aaron Brandis, Helen Hwang, Ali Gulhan, Thomas Thiele, and Frank Siebe. Overview of dragonfly entry aerosciences measurements (dream). In *2021 Fall Meeting of OPAG website*. Lunar Planetary Institute, 2021.

[26] Sy Steinberg, PAUL M SIEMERS III, and Robert G Slayman. velopment of the viking parachute configuration by wind-tunnel investigation. *Journal of Spacecraft and Rockets*, 11(2):101–107, 1974.

[27] University of South Carolina USC. https://sites.usc.edu/hptcl/supersonic-parachutes/.

[28] David Way. On the use of a range trigger for the mars science laboratory entry, descent, and landing. In *2011 Aerospace Conference*, pages 1–8. IEEE, 2011.

[29] Michael J Wright, Jeffrey A Herath, Helen H Hwang, James M Corliss, Aaron M Brandis, Dave Buecher, Doug Adams, and Ralph Lorenz. The dragonfly entry and descent system. In *International Planetary Probe Workshop (IPPW) 2019*, number ARC-E-DAA-TN70623, 2019.